



JAN KOCHANOWSKI UNIVERSITY

DOCTORAL SCHOOL

FACULTY OF NATURAL SCIENCES

PHYSICAL SCIENCES

Shahriyar Jafarzade

Phenomenology of light mesons with $J = 2, 3$

Doctoral dissertation written under the supervision of

Prof. dr. hab. Francesco Giacosa

Kielce 2023

This doctoral thesis was prepared within the research project 'Development Accelerator of Jan Kochanowski University in Kielce,' No. POWR.03.05.00-00-Z212/18, co-financed by the European Union funds under the European Social Fund.

Abstract

In this thesis, I present the results for light mesons with $J = 2, 3$

$$J^{PC} = 2^{++} = \{a_2(1320), K_2^*(1430), f_2(1270), f_2'(1525), G_2(???)\},$$

$$J^{PC} = 2^{--} = \{\rho_2(???), K_2(1820)/K_2(1770), \phi_2(???), \omega_2(???)\},$$

$$J^{PC} = 3^{--} = \{\rho_3(1690), K_3^*(1780), \phi_3(1850), \omega_3(1670), G_3(???)\},$$

within an effective hadronic model, the so-called extended Linear Sigma Model (eLSM). This model is based on the approximate chiral symmetry of QCD. Qualitative agreement between model results and PDG as well as LQCD data is obtained. Various predictions for the radiative decays can be tested in e.g., GlueX and CLAS12 experiments at Jefferson Lab.

After applying the chiral model for well-established spin-2 mesons (with $J^{PC} = 2^{++}$), I move on to their chiral partners (the axial-tensor mesons with $J^{PC} = 2^{+-}$), where the resonances are still missing. Large decay widths are predicted in the chiral model as well as in LQCD simulations.

Furthermore, I describe the decays of the spin-2 tensor glueball $G_2(???)$ within the eLSM, which can be helpful in future experimental searches e.g., BESIII and LHCb experiments. Some isoscalar tensor resonances of PDG with a mass of around 2 GeV are studied, and at present, the best tensor glueball candidate turns out to be the broad resonance $f_2(1950)$.

In the case of the ground-state spin-3 mesons ($J^{PC} = 3^{--}$), our chiral model is limited to the $SU(3)$ flavor symmetry because of the yet unknown chiral partners ($J^{PC} = 3^{+-}$). The effective model results are in good agreement with the PDG data and LQCD results, and the

predictions for the radiative decays can be interesting for photoproduction experiments such as GlueX and CLAS12. Additional estimates for the decay ratios of the $G_3(???)$ tensor glueball with $J^{PC} = 3^{--}$ are also presented.

The role of the glueball spectrum at non-zero temperature is explored within the Glueball Resonance Gas model below the critical temperature of the pure Yang-Mills sector of the QCD phase diagram. It turns out that the latest glueball spectrum from LQCD can well describe the pressure up to almost the critical temperature.

Phenomenologia lekkich mezonów z $J=2,3$

Streszczenie

W niniejszej rozprawie przedstawiam wyniki dla lekkich mezonów z $J = 2, 3$

$$J^{PC} = 2^{++} = \{a_2(1320), K_2^*(1430), f_2(1270), f_2'(1525), G_2(???)\},$$

$$J^{PC} = 2^{--} = \{\rho_2(???), K_2(1820)/K_2(1770), \phi_2(???), \omega_2(???)\},$$

$$J^{PC} = 3^{--} = \{\rho_3(1690), K_3^*(1780), \phi_3(1850), \omega_3(1670), G_3(???)\},$$

w ramach efektywnego modelu hadronowego, tzw. rozszerzonego liniowego modelu Sigma. Model ten oparty jest na przybliżonej symetrii chiralnej QCD. Uzyskano jakościową zgodność pomiędzy wynikami modelu a danymi PDG oraz LQCD. Liczne przewidywania dla rozpadów radiacyjnych mogą być przetestowane w przyszłych eksperymentach, m.in. GlueX i CLAS12 w Jefferson Lab.

Po weryfikacji działania modelu chiralnego na dobrze poznanych mezonach o spinie 2, przechodzę do sektora ich chiralnych partnerów (mezony aksjalne tensorowe o $J^{PC} = 2^{++}$), gdzie rezonansów wciąż brakuje. Duże szerokości rozpadów zostały przewidziane zarówno w modelu chiralnym jak i w symulacjach LQCD.

Ponadto opisuję brakujący glueball tensorowy $G_2(???)$ o spinie 2, w ramach modelu chiralnego, który może być użyteczny m. in. dla eksperymentów BESIII i LHCb. Badane są niektóre izoskalarne tensorowe rezonanse, zestawione w PDG, o spinie 2 i masie około 2 GeV. Dotychczasowe wyniki pokazują, że najlepszym kandydatem na glueball tensorowy okazuje się być szeroki rezonans $f_2(1950)$.

W przypadku mezonów w stanie podstawowym o spinie 3 ($J^{PC} = 3^{--}$), nasz model chiralny ma ograniczenia symetrii zapachu SU(3) ze względu na ciągle niepoznanych partnerów chiralnych ($J^{PC} = 3^{++}$). Wyniki modelu efektywnego pozostają w zgodzie z danymi PDG i wynikami LQCD. Przewidywania dla rozpadów radiacyjnych mogą być interesujące dla eksperymentów opartych na fotoprodukcji, tj.

GlueX i CLAS12. W pracy przedstawiono również dodatkowe oszacowania dla stosunków rozpadów gluaballa tensorowego $G_3(???)$ o $J^{PC} = 3^{--}$.

Rola spektrum glueballi w niezerowej temperaturze jest badana w ramach modelu Glueballowego rezonansowego gazu w obszarze poniżej krytycznej temperatury czystego sektora Yang-Millsa na diagramie fazowym QCD. Okazuje się, że najnowsze widmo glueballi z LQCD może dobrze opisywać ciśnienie prawie do samej temperatury krytycznej.

Acknowledgements

There are a lot of people who deserve my thanks, but some are particularly important.

First and foremost, I am thankful to Francesco Giacosa, my supervisor, working with me on Refs [1–4], sharing his insights with me, and providing me a lot of support throughout my Ph.D. studies.

Robert Pisarski’s acceptance of my doctoral internship, his hospitality, our work on Instantons, and his continuing support of me are all things for which I am thankful.

I am thankful to Adrian Königstein for collaboration in [1], Milena Piotrowska, Arthur Vereijken in [2,3] and Enrico Trotti in [4]. I appreciate Shahin Mamedov and Zeynab Hashimli’s cooperation on the holographic QCD.

Special thanks to Wojciech Broniowski and Stanislaw Mrówczyński, two of my teachers, for their support and advice. I am grateful for the interesting discussions that I had with Maciej Rybczynski, Subhasis Samanta, Vanamali Shastry, and Leonardo Tinti. Haradhan Adhikary, Ali Bazgir, Valeria Renya, Uzair Shah, Regina Stachura, Enrico Trotti and many others from the Institute of Physics deserve special acknowledgment. Enrico Trotti taught me how to cook, and I’m grateful that he was a kind flatmate.

I want to express my gratitude to my teachers Azar Ahmadov, Gurban Ahmedov, Emil Akhmedov, and Ilmar Gahramanov for their guidance until my doctoral studies. Special thanks to Ilmar Gahramanov, who inspired me to become a physicist and provided me with unending support during my undergraduate years.

My mother Gulshan, sister Arasta, and wife Zeynab have a lot to be thankful for.

Contents

1	Introduction	1
1.1	QCD: a brief recall	1
1.2	Conventional mesons	3
1.3	Open problems with $J = 2, 3$ mesons	6
1.4	Publications	8
1.5	Main Results	10
1.6	Organization of the thesis	11
2	Linear Sigma Model and its extension	13
2.1	Introduction	13
2.2	Chiral symmetry and its breakings	14
2.3	Decay process of $\rho \rightarrow \pi\pi$ within effective model	19
2.4	Conventional mesons within nonets	22
3	Spin-2 mesons	29
3.1	Introduction	29
3.2	Spin-2 eLSM	31
3.3	Masses of (axial-)tensor mesons	38
3.4	Results for $J^{PC} = 2^{++}$ mesons	42
3.4.1	Decay channel $T \rightarrow P^{(1)} + P^{(2)}$	42
3.4.2	Decay channel $T \rightarrow V_1 + P$	45
3.4.3	Decay channel $T \rightarrow \gamma + P$	46
3.4.4	Decay channel $T \rightarrow \gamma + V_1$	47
3.4.5	Decay channel $T \rightarrow V_1^{(1)} + V_1^{(2)}$	49
3.5	Results for $J^{PC} = 2^{--}$ mesons	51
3.5.1	Decay channel $A_2 \rightarrow V_1 + P$	51
3.5.2	Decay channel $A_2 \rightarrow A_1 + P$	55
3.5.3	Decay channel $A_2 \rightarrow T + P$	56
3.6	Conclusion	57

4	Spin-2 Glueball	59
4.1	Introduction	59
4.2	Chiral Lagrangians for G_2	60
4.3	Results for the decay ratios	62
4.4	Discussion	67
4.5	Conclusions	70
5	Spin-3 mesons	73
5.1	Introduction	73
5.2	Effective model	74
5.3	Results for $J^{PC} = 3^{--}$ mesons	79
5.3.1	Decay channel $W_3 \rightarrow P^{(1)} + P^{(2)}$	80
5.3.2	Decay channel $W_3 \rightarrow V_1 + P$	81
5.3.3	Decay channel $W_3 \rightarrow \gamma + P$	84
5.3.4	Decay channel $W_3 \rightarrow T + P$	86
5.3.5	Decay channel $W_3 \rightarrow B_1 + P$	87
5.3.6	Decay channel $W_3 \rightarrow A_1 + P$	90
5.3.7	Decay channel $W_3 \rightarrow V_1^{(1)} + V_1^{(2)}$	91
5.4	Spin-3 Glueball	93
5.4.1	Effective Lagrangians for G_3	94
5.4.2	Decay channel $G_3 \rightarrow V_1 + P$	95
5.4.3	Decay channel $G_3 \rightarrow \gamma + P$	96
5.4.4	Decay channel $G_3 \rightarrow V_1 + A_1$	96
5.4.5	Decay channel $G_3 \rightarrow B_1 + P$	97
5.4.6	Decay channel $G_3 \rightarrow B_1 + A_1$	98
5.5	Conclusions	99
6	Glueball Resonance Gas model	103
6.1	Introduction	103
6.2	Thermodynamics of the GRG	105
6.3	Contribution of heavier glueballs	108
6.4	Glueball-glueball interactions	111
6.5	Conclusion	118
7	Conclusions and discussions	119
	Bibliography	123

List of figures	145
------------------------	------------

List of tables	147
-----------------------	------------

Chapter 1

Introduction

1.1 QCD: a brief recall

The discovery of various short-living resonances in the 1960s motivated the postulation of quarks and gluons in order to understand that, at first sight, complicated "zoo" of particles [5,6]. However, another concept, the so-called color of quarks and gluons, is introduced to explain the resonance Δ^{++} (1232), which is made of three quarks of the type up (with aligned spin). Because of the Pauli principle, the wave function has to be anti-symmetric, which makes the color part of the wave function necessary. According to the hypothesis about color confinement, only color singlet objects (i.e. white) can be seen in particle detectors.

Quarks are fermions with half spin and carry $\pm \frac{1}{3}$ or $\pm \frac{2}{3}$ units of the electric charge. Mathematically, the quark fields take the form

$$q_i = \begin{pmatrix} q_{i,r} \\ q_{i,g} \\ q_{i,b} \end{pmatrix}, \quad (1.1)$$

where r, g, b stands for "red", "green" and "blue" and each $q_{i,c}$ is a Dirac spinor. Moreover, $i = u, d, s, c, b, t$ represents the so-called quark flavor.

As we shall see later on, the bound states of quark and antiquark states exist in nature because they appear as a color singlet:

$$3 \otimes \bar{3} = 1 \oplus 8. \quad (1.2)$$

Gluons are spin-1 massless gauge bosons, which mediate the color in the strong interaction where the color has to be conserved.

Quantum Chromodynamics (QCD) is a renormalizable quantum field theory of the strong interaction that describes the interaction of quarks and gluons. The QCD Lagrangian for N_f number of flavors involves the quark q_i and anti-quark \bar{q}_i fields

$$\mathcal{L}_{\text{QCD}} = \sum_{i=1}^{N_f} \text{tr} \left(\bar{q}_i(x) (i\gamma_\mu D^\mu - m_i) q_i(x) \right) + \mathcal{L}_{\text{YM}}, \quad (1.3)$$

where the covariant derivative with the QCD coupling g has the following form:

$$D_\mu := \partial_\mu - igA_\mu(x). \quad (1.4)$$

The gluonic fields

$$A_\mu(x) := \sum_{a=1}^8 A_\mu^a(x) \frac{\lambda^a}{2}, \quad (1.5)$$

are represented in terms of the eight Gell-Mann matrices λ_a . The pure Yang-Mills (YM) part of the QCD Lagrangian is defined as:

$$\mathcal{L}_{\text{YM}} = -\frac{1}{2} \text{Tr} \left[G_{\mu\nu}(x) G^{\mu\nu}(x) \right] \quad (1.6)$$

where

$$G_{\mu\nu}(x) := D_\mu A_\nu(x) - D_\nu A_\mu(x) - ig[A_\mu(x), A_\nu(x)]. \quad (1.7)$$

By considering $N_f = 3$ (thus, with quarks u, d, s), the QCD Lagrangian in Eq.(1.3) has the following classical symmetries:

- Chiral symmetry $U(3)_L \times U(3)_R$ and dilation symmetry in the massless quark limit¹ ($m_u = m_d = m_s = 0$);
- Flavor symmetry $SU(3)_F$ in the equal mass limit of the three light quarks ($m_u = m_d = m_s \neq 0$);

¹This is the so-called the chiral limit of QCD. Including quantum fluctuations leads to the anomalous breaking of the axial ($U_A(1)$) and dilation symmetry, the so-called chiral and trace anomalies.

- Color symmetry $SU(3)_c$, which is an exact local symmetry and is expected to lead to confinement.

As a result of confinement, we only measure hadrons in the detectors rather than separate quarks and gluons. Hadrons can be classified as mesons with integer spins and baryons with half-integer spins. Mesons themselves are classified as conventional (quark-antiquark objects) and non-conventional mesons, such as glueballs (only gluons), and hybrids (quark-antiquark and gluons). While conventional baryons are made up of three quarks, pentaquarks are examples of non-conventional baryons.

At low energies one works with hadronic degrees of freedom, rather than quarks and gluons, in effective model approaches. Effective models that use the chiral symmetry are, for example, chiral perturbation theory (ChPT) [7–17], in which chiral symmetry is nonlinearly realized and sigma models, in which it is linearly realized [18–23]. I make use of an extension of the latter, called the extended Linear Sigma Model (eLSM), throughout my thesis.

At large distances ($\gtrsim 1$ fm) quarks are confined, and only non-perturbative methods are applicable. Lattice QCD (LQCD) simulation is a well-known example of a non-perturbative approach, which starts from QCD Lagrangian and evaluates certain quantities (i.e. masses of hadrons) on a computer grid (lattice). The comparison of the models above with LQCD is a useful way to understand QCD at low energy.

Upon quantizing QCD and considering the renormalization procedure, the coupling constant g in Eq. (1.4) turns out to be a function of the energy scale μ

$$g^2(\mu) = \frac{48\pi^2}{(11N_c - 2N_f) \log\left(\frac{\mu}{\Lambda_{\text{YM}}}\right)}, \quad (1.8)$$

where the YM scale is around $\Lambda_{\text{YM}} \approx 200$ MeV. At short distances, quarks behave as free particles. This is also a non-trivial feature of QCD and is so-called “asymptotic freedom”. Perturbation theory is applicable in this regime.

1.2 Conventional mesons

Conventional mesons consist of quark and antiquark pairs. To explain them, let us first present the properties of the three light quarks of QCD. Light (anti-)quarks have

the following quantum numbers: the electric charge related to the isospin I_3 and hypercharge Y :

$$Q = I_3 + \frac{Y}{2}, \quad (1.9)$$

where the hypercharge Y is the sum of the baryon number B and the strangeness quantum number S

$$Y := B + S. \quad (1.10)$$

We list the quantum numbers for the quarks and anti-quarks in Table 1.1. In addition,

	Q	I	I_3	Y	S	B
u	$\frac{2}{3}$	$\frac{1}{2}$	$\frac{1}{2}$	$\frac{1}{3}$	0	$\frac{1}{3}$
d	$-\frac{1}{3}$	$\frac{1}{2}$	$-\frac{1}{2}$	$\frac{1}{3}$	0	$\frac{1}{3}$
s	$-\frac{1}{3}$	0	0	$-\frac{2}{3}$	1	$\frac{1}{3}$
$\bar{\mathbf{u}}$	$-\frac{2}{3}$	$\frac{1}{2}$	$-\frac{1}{2}$	$-\frac{1}{3}$	0	$-\frac{1}{3}$
$\bar{\mathbf{d}}$	$\frac{1}{3}$	$\frac{1}{2}$	$\frac{1}{2}$	$-\frac{1}{3}$	0	$-\frac{1}{3}$
$\bar{\mathbf{s}}$	$\frac{1}{3}$	0	0	$\frac{2}{3}$	-1	$-\frac{1}{3}$

Table 1.1: Quantum numbers for the light (anti-)quarks.

conventional mesons carry the total angular momentum \vec{J}

$$\vec{J} = \vec{L} + \vec{S}, \quad (1.11)$$

as a sum of the spin \vec{S} and the angular momentum \vec{L} , where $S = 0$ refers to anti-parallel quarks and $S = 1$ for parallel quarks, while the angular momentum can take the values $L = 0, 1, 2, \dots$.

The parity operator (that corresponds to the transformation $\vec{x} \rightarrow -\vec{x}$) acting on conventional mesons has eigenvalues as

$$P = (-1)^{L+1}, \quad (1.12)$$

while the charge conjugation operator (particles \leftrightarrow anti-particles) has the following eigenvalues:

$$C = (-1)^{L+S}. \quad (1.13)$$

Strong interaction processes are also G-symmetry invariant. G-symmetry is the combination of $SU(2)$ isospin symmetry and the charge conjugation symmetry [24].

Based on the eigenvalues of the spin-S, we can make the following considerations:

1. In the case of anti-parallel quark-antiquark states

$$|S = 0\rangle = \frac{1}{\sqrt{2}}|\uparrow_q\downarrow_{\bar{q}} - \downarrow_q\uparrow_{\bar{q}}\rangle, \quad (1.14)$$

conventional mesons have the quantum numbers

$$J^{PC} \in \{\mathbf{even}^{-+}, \mathbf{odd}^{+-}\}. \quad (1.15)$$

2. The parallel structure of the quark-antiquark pairs

$$|S = 1\rangle = |\uparrow_q\uparrow_{\bar{q}}\rangle, \frac{1}{\sqrt{2}}|\uparrow_q\downarrow_{\bar{q}} + \downarrow_q\uparrow_{\bar{q}}\rangle, |\downarrow_q\downarrow_{\bar{q}}\rangle, \quad (1.16)$$

leads to the following quantum numbers for the conventional mesons

$$J^{PC} \in \{\{0, 1, 2, \dots\}^{++}, \{1, 2, \dots\}^{--}\}. \quad (1.17)$$

3. The following quantum numbers correspond to so-called exotic states

$$J^{PC} \in \{\mathbf{even}^{+-}, \mathbf{odd}^{-+}, 0^{--}\}. \quad (1.18)$$

Namely, they are impossible for $\bar{q}q$ pairs. A notable example is the resonance $\pi_1(1600)$ with $J^{PC} = 1^{-+}$, see e.g., Refs. [25,26].

We list the conventional mesons up to $J = 3$ in Table 1.2, where the first row shows the spectroscopic notation of the quantum numbers with radial quantum number n , angular momentum $L = S, P, D, \dots$, as well as $2S + 1$ and J .

$n^{2S+1}L_J$	J^{PC}	$u\bar{d}, d\bar{u}, \frac{d\bar{d}-u\bar{u}}{\sqrt{2}}$	$u\bar{s}, d\bar{s}, s\bar{d}, s\bar{u}$	$\approx \frac{u\bar{u}+d\bar{d}}{\sqrt{2}}$	$\approx s\bar{s}$	Meson names
1^1S_0	0^{-+}	π	K	$\eta(547)$	$\eta'(958)$	Pseudoscalar
1^3P_0	0^{++}	$a_0(1450)$	$K_0^*(1430)$	$f_0(1370)$	$f_0(1500)/f_0(1710)$	Scalar
1^3S_1	1^{--}	$\rho(770)$	$K^*(892)$	$\omega(782)$	$\phi(1020)$	Vector
1^3P_1	1^{++}	$a_1(1260)$	K_{1A}	$f_1(1285)$	$f_1'(1420)$	Axial-vector
1^1P_1	1^{+-}	$b_1(1235)$	K_{1B}	$h_1(1170)$	$h_1(1415)$	Pseudovector
1^3D_1	1^{--}	$\rho(1700)$	$K^*(1680)$	$\omega(1650)$	$\phi(???)$	Excited-vector
1^3P_2	2^{++}	$a_2(1320)$	$K_2^*(1430)$	$f_2(1270)$	$f_2'(1525)$	Tensor
1^3D_2	2^{--}	$\rho_2(???)$	K_{2A}	$\omega_2(???)$	$\phi_2(???)$	Axial-tensor
1^1D_2	2^{-+}	$\pi_2(1670)$	K_{2P}	$\eta_2(1645)$	$\eta_2(1870)$	Pseudotensor
1^3D_3	3^{--}	$\rho_3(1690)$	$K_3^*(1780)$	$\omega_3(1670)$	$\phi_3(1850)$	Spin-3 Tensor

Table 1.2: List of conventional $q\bar{q}$ mesons following the quark model review of Ref. [27] up to $J = 3$ and for the lowest radial excitation ($n=1$). Bold entries with question marks have not been assigned to known resonances yet.

1.3 Open problems with $J = 2, 3$ mesons

The last four rows of Table 1.2 are phenomenologically interesting because of various reasons:

1. Many decay channels are known for tensor ($J^{PC} = 2^{++}$) and spin-3 tensor ($J^{PC} = 3^{--}$) mesons [27], which allow for further theoretical and experimental tests of the $\bar{q}q$ assignment.
2. Predictions for not-yet measured strong and radiative decay rates are possible.
3. Decays of spin-3 tensor ($J^{PC} = 3^{--}$) and axial-tensor ($J^{PC} = 2^{--}$) mesons have been recently estimated in LQCD calculations [28].
4. Three axial-tensor mesons are still missing in this list.
5. The mixing angle between the isoscalar members of the pseudotensor ($J^{PC} = 2^{-+}$) mesons is unknown.
6. There is an unknown mixing in the kaonic sector between $K_2^*(1820)$ and $K_2(1770)$.

The decay widths versus masses of the resonances under study are summarized in Figure 1.1.

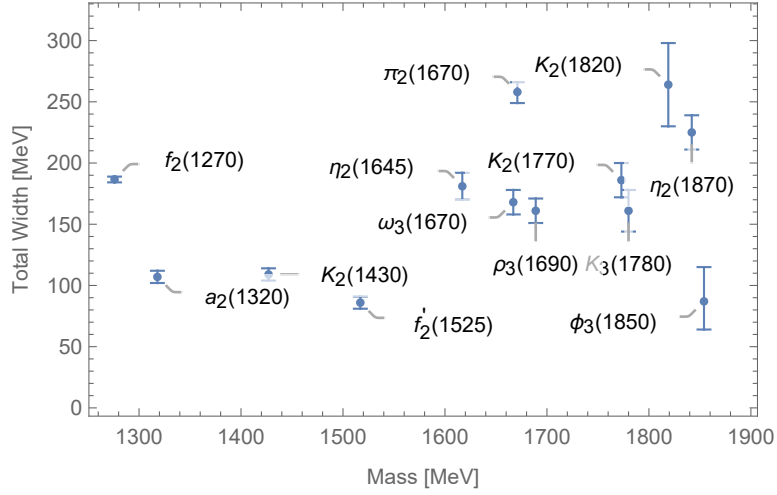


Figure 1.1: List of conventional mesons with $2 \leq J \leq 3$.

One type of non-conventional mesons is the so-called “glueball” which is defined as a pure gluonic state. Despite the lack of experimental data, various LQCD simulations observe glueball states in which the 2^{++} glueball is the second lightest state after the scalar glueball (see e.g., a recent analysis of the glueball spectrum in Ref. [29]). From a phenomenological perspective, there are several resonances in PDG [27] whose physical masses are close to the LQCD value of 2.2 GeV, such as $f_2(1910)$, $f_2(1950)$, $f_2(2010)$, $f_2(2150)$, $f_J(2200)$, $f_2(2300)$ and $f_2(2340)$, see Figure 1.2. Which of them,

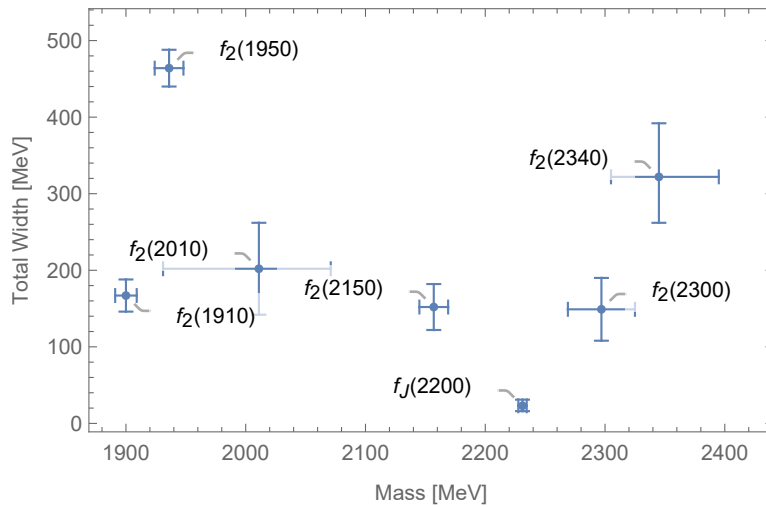


Figure 1.2: List of spin-2 resonances with a mass above 1.9 GeV.

if any, could be the best candidate for the tensor glueball? Exploring it is one of our goals.

Figure 1.3 shows the parts of the thesis where some of the aforementioned open questions will be investigated. I will construct effective models to investigate those resonances as follows:

1. Use chiral symmetry to construct an effective model which links tensor and axial-tensor mesons with spin-2.
2. Extend the chiral model to the spin-2 glueball sector.
3. Flavor symmetry-based model for spin-3 mesons and hypothetical spin-3 glueball.

Moreover, I will show that LQCD simulations for the thermodynamical properties of the pure YM sector [30] are explained well within the Glueball Resonance Gas (GRG) based on the spectrum obtained in [29] up to the critical temperature for deconfinement. In addition to the above-mentioned goals, I will also show the role of the spin-2 tensor glueball within the GRG.

There is, of course, a full plethora of theoretical methods devoted to the investigations of the aforementioned problems, such as the already mentioned LQCD [28,31], Holographic QCD [32,33], QCD sum rules [34], Functional Methods [35,36], the Bethe-Salpeter approach of Ref. [37], Chiral Perturbation theory [38], etc. Whenever it is possible, we will compare the results obtained within the employed chiral model (the eLSM) with those from the approaches listed above, especially with LQCD.

1.4 Publications

My thesis is based on the following publications² [1–4,39]:

- Chapter 3
1. Shahriyar Jafarzade, Arthur Vereijken, Milena Piotrowska, Francesco Giacosa
“From well-known tensor mesons to yet unknown axial-tensor mesons”
Phys. Rev. D 106(2022) 3, 036008
<https://doi.org/10.1103/PhysRevD.106.036008>
arXiv:2203.16585 [hep-ph]

²Here, we report the correct title of Refs. [1–4,39].

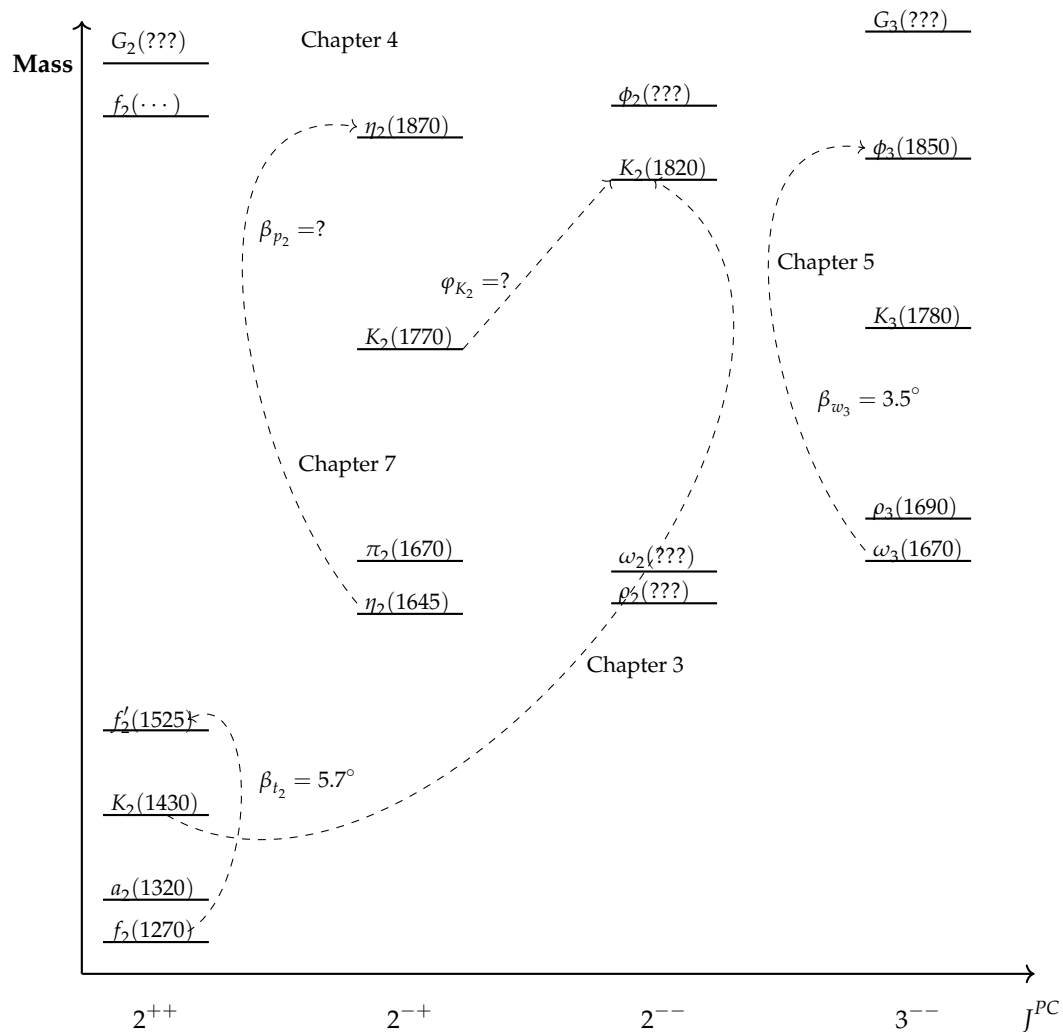


Figure 1.3: Ground-state light mesons with $2 \leq J \leq 3$.

2. Shahriyar Jafarzade

“A phenomenological note on the missing ρ_2 meson”

PoS ICHEP2022 (2022) 903

<https://doi.org/10.22323/1.414.0903>

arXiv:2210.12421 [hep-ph]

- Chapter 4

3. Arthur Vereijken, Shahriyar Jafarzade, Milena Piotrowska, Francesco Giacosa

“Is $f_2(1950)$ the tensor glueball?”

Phys. Rev. D 108 (2023) 1, 014023

<https://doi.org/10.1103/PhysRevD.108.014023>

arXiv:2304.05225 [hep-ph]

- Chapter 5
4. Shahriyar Jafarzade, Adrian Koenigstein, Francesco Giacosa
 “Phenomenology of $J^{PC} = 3^{--}$ tensor mesons”
 Phys. Rev. D 103 (2021) 9, 096027
<https://doi.org/10.1103/PhysRevD.103.096027>
 arXiv:2101.03195 [hep-ph]
- Chapter 6
5. Enrico Trotti, Shahriyar Jafarzade, Francesco Giacosa
 “Thermodynamics of the glueball resonance gas”
 Eur. Phys. J. C 83 (2023) 5, 390
<https://doi.org/10.1140/epjc/s10052-023-11557-0>
 arXiv:2212.03272 [hep-ph].

1.5 Main Results

1. We have studied the ground state spin-2 mesons ($J^{PC} = 2^{++}$)

$$\{a_2(1320), K_2^*(1430), f_2(1270), f_2'(1525)\}$$

within the extended Linear Sigma Model. Various predictions for hadronic and radiative decay rates are presented. Their quark-antiquark picture is confirmed. Some predicted radiative decay rates can be investigated at e.g., GlueX and CLAS12 experiments at the Jefferson Lab.

2. The chiral partners of the above-mentioned resonances (axial-tensor mesons with $J^{PC} = 2^{--}$) have not been yet discovered experimentally. Nevertheless, we have some information about the kaonic member of it, namely, that it is a mixture of $K_2(1820)$ and $K_2(1770)$. Under the assumption that $K_2(1820)$ belongs most dominantly to this nonet, we have obtained the masses of the other missing resonances with the same quantum numbers. While the lightest member of this meson family has a mass of around 1.7 GeV, its decay width is larger than that of its chiral partner. Decay rate results are compared to LQCD outcomes. Our results could be useful for an eventual future identification of these resonances, even though their large expected widths make them difficult to be observed.

3. Another missing resonance for the spin-2 sector is the tensor glueball ($J^{PC} = 2^{++}$). Its mass is expected to be around 2 GeV (LQCD). Indeed, various tensor resonances are listed in PDG with a mass close to that value. Therefore, we have studied the tensor glueball within the eLSM, showing that $f_2(1950)$ is at present, the best glueball candidate, despite being a quite broad resonance. We have also presented some decay ratios for the mass value of 2.21 GeV, which corresponds to an enhancement in the $\pi\pi$ invariant mass spectrum of the recent BESIII data analyses implying a pole at 2.21 GeV. The dominant decay channel for the tensor glueball turns out to be the decay into two vector mesons.
4. The ground-state spin-3 mesons ($J^{PC} = 3^{--}$) are

$$\{\rho_3(1690), K_3^*(1780), \phi_3(1850), \omega_3(1670)\}. \quad (1.19)$$

Their description within the chiral model is limited to the $SU(3)$ flavor symmetry because of their unknown chiral partners. We have constructed an effective model in order to study their decay properties. Interestingly, model results are in good agreement with the PDG data and LQCD results for hadronic decays. Analogously to the spin-2 case, we made some predictions for radiative decays, which can be interesting for photoproduction experiments such as GlueX and CLAS12. We have shown additional predictions for the decay ratios of the spin-3 tensor glueball by using the mass ~ 3 GeV estimates from LQCD simulations.

5. The last topic is the non-zero temperature description of the pure Yang-Mills $SU(3)$ theory. The role of the recent glueball spectrum and the interaction between the lightest glueballs are investigated within the Glueball Resonance Gas Model (GRG). Results are compared to the pure Yang-Mills thermodynamic simulations for the pressure in the region below the critical temperature. Further radially excited glueball states, assuming Regge trajectory, and scalar and tensor glueball interactions lead to negligible contributions.

1.6 Organization of the thesis

In chapter 1 I have described the main properties of QCD and a list of the conventional mesons, as well as the open problems in mesons with $2 \leq J \leq 3$. Chapter 2 presents the LSM and mesons within certain nonets. The phenomenology of spin-2 mesons and

the glueball within the eLSM is discussed in Chapter 3 and Chapter 4, respectively. Chapter 5 is devoted to the ground-state spin-3 mesons and a spin-3 glueball. The role of the glueball states at non-zero T within the GRG is described in Chapter 6. Conclusions and discussions are given in Chapter 7.

Chapter 2

Linear Sigma Model and its extension

2.1 Introduction

As we mentioned in the previous chapter, effective models are based on the symmetries of QCD and involve hadronic degrees of freedom. One example of an effective model is the so-called Linear Sigma Model (LSM). Historically, it was introduced in order to study the pion-nucleon interaction [18]. The Lagrangian contains the free terms of mesons as well as the nucleon in addition to the Yukawa type interaction between them:

$$\mathcal{L}_{\text{LSM}} = \mathcal{L}_{\text{mesons}} + \mathcal{L}_{\text{nucleons}} + \mathcal{L}_{\text{Yukawa}}. \quad (2.1)$$

The explicit forms of the above Lagrangian in terms of the mesons $(\sigma, \vec{\pi})$ and nucleon Ψ read

$$\mathcal{L}_{\text{mesons}} = \frac{1}{2}(\partial_\mu \sigma)^2 + \frac{1}{2}(\partial_\mu \vec{\pi})^2 + \frac{\mu^2}{2}(\sigma^2 + \vec{\pi}^2) - \frac{\lambda^2}{4}(\sigma^2 + \vec{\pi}^2)^2, \quad (2.2)$$

$$\mathcal{L}_{\text{nucleons}} = \bar{\Psi} \gamma^\mu \partial_\mu \Psi, \quad (2.3)$$

$$\mathcal{L}_{\text{Yukawa}} = ig_y \bar{\Psi} \gamma_5 \vec{\tau} \cdot \vec{\pi} \Psi + g_y \bar{\Psi} \sigma \Psi. \quad (2.4)$$

Chiral perturbation theory (ChPT), in which chiral symmetry is realized nonlinearly [7–17], and the LSM, in which it is realized linearly [18–23], are two examples of theories that use chiral symmetry as a guiding principle. We see that LSM keeps both the scalar σ and the pseudoscalar $\vec{\pi}$ fields, while in the case of the chiral perturbation theory, the scalar d.o.f. are integrated out. A mass difference between chiral partner mesons results from the spontaneous breaking of chiral symmetry. In the Functional

Renormalization Group studies of the chiral symmetry dynamics, consideration of the finite temperature and chemical potential was performed in Refs. [40–45]. The framework is used to characterize chiral symmetry breaking (and phase transitions), see Refs. [46–57].

Our main focus on the LSM regards mesons. The LSM was extended to mesons with $J = 1$ in [20,21,58,59] and it will be generalized to $J = 2, 3$ in the present thesis.

2.2 Chiral symmetry and its breakings

According to Noether's theorem, there is a conserved current for the following infinitesimal field transformation of the fields $\phi_i(x)$ which leaves the Lagrangian density invariant

$$\begin{aligned} \phi_i(x) &\longrightarrow \phi_i(x) + \delta\phi_i(x), \quad \text{with} \quad \delta\phi_i(x) = i\epsilon^a t_{ij}^a \phi_j(x) \\ \mathcal{L}(\phi_i(x)) &= \mathcal{L}(\phi_i(x) + \delta\phi_i(x)), \end{aligned} \quad (2.5)$$

where ϵ^a is the small space-time independent parameter and t^a 's are the generators of the Lie algebra satisfying

$$[t^a, t^b] = iC^{abc} t^c, \quad (2.6)$$

for some structure constants C^{abc} . The form of the conserved current reads

$$J_\mu^a = -i \frac{\delta \mathcal{L}}{\delta(\partial^\mu \phi_i)} t_{ij}^a \phi_j, \quad (2.7)$$

while the conserved charges have the form

$$Q^a = \int d^3x J_0^a(x), \quad \text{with} \quad \frac{dQ^a}{dt} = 0. \quad (2.8)$$

In the case of the three flavors, we have the following mass term for the fermionic sector of QCD Lagrangian:

$$\mathcal{L} = i\bar{q}^i \gamma^\mu \partial_\mu q_i + m_u \bar{u}u + m_d \bar{d}d + m_s \bar{s}s. \quad (2.9)$$

This is basically a free fermionic Lagrangian for 3 quarks. Indeed, including gluons does not change the following considerations. The above Lagrangian is flavor symmetry in the case of $m_u = m_d = m_s \equiv m_i$. Namely, it is invariant under the infinitesimal transformation of the quark fields

$$\delta q_i(x) = i\alpha^a \frac{\lambda_{ij}^a}{2} q_j(x) \longrightarrow \mathcal{L}(m_i, q_i(x)) = \mathcal{L}(m_i, q_i(x) + \delta q_i(x)), \quad (2.10)$$

for small parameters α^a . Here λ^a 's are the eight Gell-Mann matrices satisfying the following algebra

$$\left[\frac{\lambda_a}{2}, \frac{\lambda_b}{2} \right] = i f^{abc} \frac{\lambda_c}{2}, \quad (2.11)$$

with the structure constants f^{abc} . The conserved charges ($a = 1, \dots, 8$) for $SU(3)$ symmetry

$$Q^a(t) = \int d^3x V_0^a(x), \quad \text{for} \quad V_\mu^a(x) := \bar{q}(x) \gamma_\mu \frac{\lambda_a}{2} q(x), \quad (2.12)$$

satisfy also the algebra

$$\left[Q^a(t), Q^b(t) \right] = i f^{abc} Q^c(t). \quad (2.13)$$

In the case of the zero quark mass limit, there is another conserved current, called $Q_5^a(t)$ ¹

$$Q_5^a(t) = \int d^3x A_0^a(x), \quad \text{for} \quad A_\mu^a(x) := \bar{q}(x) \gamma_5 \gamma_\mu \frac{\lambda_a}{2} q(x), \quad (2.14)$$

with the following algebraic structure:

$$\left[Q_5^a(t), Q_5^b(t) \right] = i f^{abc} Q^c(t). \quad (2.15)$$

One can construct linear combinations of the conserved charges and end up with the following algebra:

$$\left[Q_L^a(t), Q_L^b(t) \right] = i f^{abc} Q_L^c(t), \quad (2.16)$$

$$\left[Q_R^a(t), Q_R^b(t) \right] = i f^{abc} Q_R^c(t), \quad (2.17)$$

¹Subscript "5" indicates a γ_5 matrix within the conserved charge.

$$\left[Q_L^a(t), Q_R^b(t) \right] = 0, \quad \text{where} \quad Q_{L,R}^a := \frac{1}{2} \left(Q^a \mp Q_5^a \right). \quad (2.18)$$

They are $SU(3)_L \times SU(3)_R$ chiral algebras.

Let us now consider a certain Hamiltonian H_0 , which is invariant under $SU(3)_L \times SU(3)_R$. Thus, U being the element of this transformation group leaves the H_0 invariant via

$$UH_0U^\dagger = H_0. \quad (2.19)$$

Upon considering a state $|A\rangle$, let us define $|B\rangle$ as

$$U|A\rangle = |B\rangle. \quad (2.20)$$

Based on the ones above, one can write

$$\langle B|H_0|B\rangle = \langle A|H_0|A\rangle. \quad (2.21)$$

Considering the action of the creation operators on the vacuum $|0\rangle$

$$\phi_A|0\rangle = |A\rangle, \quad \text{and} \quad \phi_B|0\rangle = |B\rangle \quad (2.22)$$

we get

$$U\phi_AU^\dagger = \phi_B. \quad (2.23)$$

If then

$$U|0\rangle = |0\rangle, \quad (2.24)$$

one gets

$$U|A\rangle = U\phi_A|0\rangle = U\phi_AU^\dagger U|0\rangle = \phi_B|0\rangle = |B\rangle, \quad (2.25)$$

and thus $|A\rangle$ and $|B\rangle$ are degenerate; namely,

$$H|B\rangle = m_B|B\rangle = HU|A\rangle = m_AU|A\rangle = m_A|B\rangle \longrightarrow m_A = m_B. \quad (2.26)$$

Otherwise, the Spontaneous Symmetry Breaking (SSB) $U|0\rangle = |0'\rangle \neq |0\rangle$ appears. When we write U in terms of the conserved current

$$U = e^{i\epsilon^a Q^a}, \quad (2.27)$$

for the parameter ϵ^a , we can represent the SSB in terms of the conserved charges such that, using

$$HQ^a|0\rangle = Q^aH|0\rangle = 0|0\rangle, \quad (2.28)$$

then

$$Q^a|0\rangle \neq 0, \quad (2.29)$$

implies a massless state.

According to Goldstone's theorem, SSB of a continuous symmetry leads to particles with no mass and no spin, which are defined as Nambu-Goldstone bosons.

As a concrete example, let us consider the potential with two real fields σ and π

$$V(\sigma, \pi) := -\frac{\mu^2}{2}(\sigma^2 + \pi^2) + \frac{\lambda}{4}(\sigma^2 + \pi^2)^2. \quad (2.30)$$

It has an $U(1) \simeq SO(2)$ continuous symmetry

$$\begin{pmatrix} \pi \\ \sigma \end{pmatrix} \rightarrow \begin{pmatrix} \pi' \\ \sigma' \end{pmatrix} = \begin{pmatrix} \cos \theta & \sin \theta \\ -\sin \theta & \cos \theta \end{pmatrix} \begin{pmatrix} \pi \\ \sigma \end{pmatrix}. \quad (2.31)$$

The potential term in Eq. (2.30) has the extremum as

$$\frac{\partial V}{\partial \sigma} = \sigma(-\mu^2 + \lambda v^2) = 0, \quad \frac{\partial V}{\partial \pi} = \pi(-\mu^2 + \lambda v^2) = 0, \quad v^2 := \sigma^2 + \pi^2. \quad (2.32)$$

In the case of $\mu^2 > 0$, the minima are the points of the circle with radius $v = \sqrt{\frac{\mu^2}{\lambda}}$ (left panel of Fig. 2.1). These points are equivalent, and the vacuum is infinitely degenerated. One can choose any point in this circle that is the true vacuum (e.g., $\langle 0|\sigma|0\rangle = v$ and $\langle 0|\pi|0\rangle = 0$) and spontaneously break the original symmetry of the Lagrangian.

The conserved current for the Lagrangian with $U(1)$ symmetry has the following form:

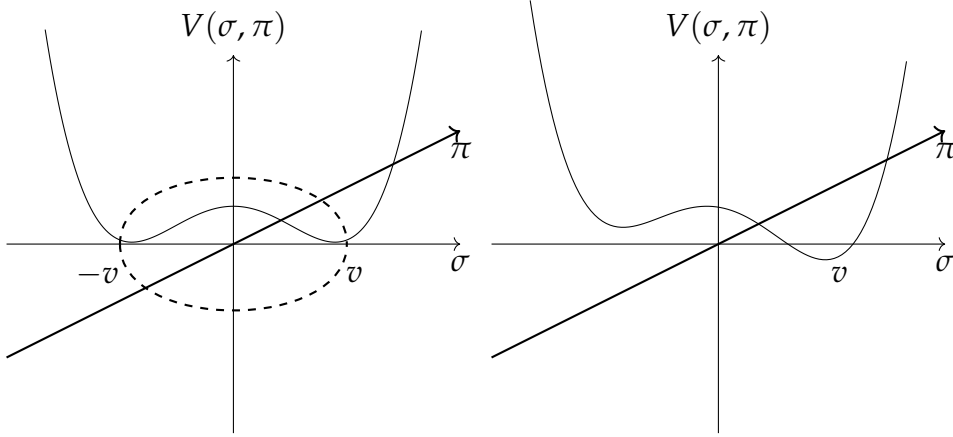


Figure 2.1: Mexican hat potential with minima along the chiral circle (left) and the explicit breaking of the chiral symmetry (right).

$$J_\mu = (\partial_\mu \pi)\sigma - (\partial_\mu \sigma)\pi, \quad (2.33)$$

which implies the following conserved charge:

$$Q = \int d^3x \left((\partial_0 \pi)\sigma - (\partial_0 \sigma)\pi \right). \quad (2.34)$$

Using the canonical commutation relation between the fields, we get the commutation between the charge and the fields

$$[Q, \pi(0)] = -i\sigma(0), \quad \text{and} \quad [Q, \sigma(0)] = i\pi(0). \quad (2.35)$$

One can show that, having a non-zero expectation value for the sigma field $\langle 0|\sigma(0)|0\rangle = v$ implies the existence of a massless pion (see e.g., Ref. [60]).

Let us consider the shift on the σ field, $\sigma = \bar{\sigma} + v$ and rewrite the Lagrangian in terms of the $\bar{\sigma}$

$$\mathcal{L}(\bar{\sigma}, \pi) = \frac{1}{2} \left((\partial_\mu \bar{\sigma})^2 + (\partial_\mu \pi)^2 \right) - \frac{\lambda}{4} \left(\bar{\sigma}^2 + \pi^2 \right)^2 - \mu^2 \bar{\sigma}^2 - \lambda v \bar{\sigma} (\bar{\sigma}^2 + \pi^2), \quad (2.36)$$

which leads to the massless π and the mass for the σ' as $m_{\bar{\sigma}} = \sqrt{2\mu^2}$. As the pion is not massless in reality, one needs to add an explicit symmetry breaking term \mathcal{L}_{ESB}

$$\mathcal{L}_{ESB} = -h\sigma. \quad (2.37)$$

The non-abelian version of LSM with $SU(2)_L \otimes SU(2)_R$ symmetry can be written as

$$\mathcal{L}_{\text{mesons}} = \frac{1}{2} \text{tr} \left(\partial_\mu \Sigma^\dagger \partial^\mu \Sigma \right) + \frac{\mu^2}{4} \text{tr} \left(\Sigma^\dagger \Sigma \right) - \frac{\lambda}{16} \left(\text{tr} \left(\Sigma^\dagger \Sigma \right) \right)^2, \quad (2.38)$$

where $\Sigma := \sigma + i\vec{\tau} \cdot \vec{\pi}$ for the three Pauli matrices $\vec{\tau}$. In this case, we will have the following commutation relation:

$$\left[Q^{5a}, \pi^b \right] = -i\sigma \delta^{ab}, \quad \text{where} \quad Q^{5a} = \int d^3x \left((\partial_0 \pi^a) \sigma - (\partial_0 \sigma) \pi^a \right). \quad (2.39)$$

However, the other conserved charge corresponding to the vector current annihilates the vacuum, $Q^a|0\rangle = 0$, where

$$Q^a(t) = \int d^3x \epsilon^{abc} \pi^b(x, t) (\partial_0 \pi^c(x, t)), \quad (2.40)$$

which implies the spontaneous breaking of the $SU(2)_L \otimes SU(2)_R$ to the $SU(2)$ symmetry. In the next chapter, spontaneous breaking of the chiral symmetry will be the main method to obtain the masses of spin-2 mesons.

2.3 Decay process of $\rho \rightarrow \pi\pi$ within effective model

In this section, I describe the decay process based on an illustrative effective Lagrangian. The decay processes in the next chapters will be extensions of this relatively simple example.

A free Proca style Lagrangian for massive vector meson reads

$$\mathcal{L} = -\frac{1}{4} \rho_{\mu\nu} \rho^{\mu\nu} + \frac{m_\rho^2}{2} \rho_\mu \rho^\mu, \quad \text{where} \quad \rho_{\mu\nu} := \partial_\mu \rho_\nu - \partial_\nu \rho_\mu. \quad (2.41)$$

Using the Euler-Lagrange equation

$$\partial_\mu \frac{\partial \mathcal{L}}{\partial (\partial_\mu \rho_\nu)} - \frac{\partial \mathcal{L}}{\partial \rho_\nu} = 0, \quad (2.42)$$

we obtain the following equation of motion:

$$\square \rho^\mu - \partial^\mu (\partial_\nu \rho^\nu) + m^2 \rho^\mu = 0. \quad (2.43)$$

Acting by ∂_μ on all terms leads to the constraint equation

$$\partial_\mu \rho^\mu = 0. \quad (2.44)$$

Thus, a massive vector field has three degrees of freedom instead of four. The replacement of Eq. (2.44) within the equation of motion leads to the Klein-Gordon equation for the vector field

$$(\square + m_\rho^2)\rho^\mu = 0. \quad (2.45)$$

By quantizing the solutions of the above equation we obtain the following expression for the massive vector field

$$\rho_\mu = \frac{1}{\sqrt{V}} \sum_{\vec{k}} \frac{1}{\sqrt{2\omega}} \sum_{r=1,2,3} \left[a_{\vec{k}}^{(r)} \varepsilon_\mu^{(r)}(\vec{k}) e^{-ikx} + a_{\vec{k}}^{\dagger(r)} \varepsilon_\mu^{(r)}(\vec{k}) e^{ikx} \right], \quad \omega = \sqrt{m_\rho^2 + \vec{k}^2}. \quad (2.46)$$

Taking into account the constraint of the massive vector field, we observe

$$k_\mu \varepsilon^{(r)\mu}(\vec{k}) = 0. \quad (2.47)$$

There is also a diagonality condition between the polarization vectors such that

$$\varepsilon_\mu^{(r)}(\vec{k}) \varepsilon^{(s)\mu}(\vec{k}) = -\delta^{rs}. \quad (2.48)$$

By using these two formulas, we get the form of the polarization vectors. The following formula describes the polarization sums for the massive vector field, which is useful for the computation of the decay rates

$$\sum_{r=1}^3 \varepsilon_\mu^{(r)}(\vec{k}) \varepsilon_\nu^{(r)}(\vec{k}) = -g_{\mu\nu} + \frac{k_\mu k_\nu}{m_\rho^2}. \quad (2.49)$$

Now, let us compute the decay process $\rho(770) \rightarrow \pi\pi$ within a Lagrangian based on the $U(2)$ -flavor symmetry. Considering pseudoscalar mesons within a multiplet in

the case of two flavors²

$$\mathbb{P} = \begin{pmatrix} \pi^0 & \sqrt{2}\pi^+ \\ \sqrt{2}\pi^- & -\pi^0 \end{pmatrix}, \quad (2.50)$$

and analogously for the vector mesons

$$\mathbb{V}_\mu = \begin{pmatrix} \rho_\mu^0 & \sqrt{2}\rho_\mu^+ \\ \sqrt{2}\rho_\mu^- & -\rho_\mu^0 \end{pmatrix}, \quad (2.51)$$

the following Lagrangian describes an isospin-invariant interaction between the vector and pseudoscalar mesons:

$$\begin{aligned} \mathcal{L}_{VPP} &= \frac{ig}{2} \text{Tr} \left(\mathbb{V}_\mu \partial^\mu \mathbb{P} \mathbb{P} - \mathbb{V}_\mu \mathbb{P} \partial^\mu \mathbb{P} \right) \\ &= ig\rho_\mu^0 \{ \pi^+ \partial^\mu \pi^- + \pi^- \partial^\mu \pi^+ \} + ig\rho_\mu^+ \{ \pi^- \partial^\mu \pi^0 + \pi^0 \partial^\mu \pi^- \} \\ &\quad + ig\rho_\mu^- \{ \pi^+ \partial^\mu \pi^0 + \pi^0 \partial^\mu \pi^+ \}. \end{aligned} \quad (2.52)$$

The first thing we read from this Lagrangian is the equality of the following decays

$$\Gamma_{\rho^0 \rightarrow \pi^+ \pi^-} = \Gamma_{\rho^+ \rightarrow \pi^+ \pi^0} = \Gamma_{\rho^- \rightarrow \pi^0 \pi^-}. \quad (2.53)$$

Application of the Feynmann rules to the interaction Lagrangian leads to the amplitude

$$-i\mathcal{M}^a = \varepsilon_\mu^a(\vec{p})(ik_2 - ik_1)i(ig) = -ig\varepsilon_\mu^a(\vec{p})(k_2 - k_1) \equiv ig\varepsilon_\mu^a(\vec{p})k^\mu, \quad (2.54)$$

where $k = k_1 - k_2$ and $k_{1,2} = (\omega_{1,2}, \vec{k}_{1,2})$. Thus, the average of the amplitude squared reads

$$\begin{aligned} \overline{|-i\mathcal{M}|^2} &= \frac{1}{3} \sum_a \overline{|-i\mathcal{M}^a|^2} = \frac{g^2}{3} \sum_a \varepsilon_\mu^a(\vec{p})k^\mu \varepsilon_\nu^a(\vec{p})k^\nu = \frac{g^2}{3} \left(-g_{\mu\nu} + \frac{p_\mu p_\nu}{m_\rho^2} \right) k^\mu k^\nu = \\ &= \frac{g^2}{3} \left(-k^2 + \frac{(p \cdot k)^2}{m_\rho^2} \right). \end{aligned} \quad (2.55)$$

²For simplicity, I ignore the singlet mesons. The next section is devoted to the proper description of mesons within certain nonets.

Considering the pions as identical particles and in the rest frame of the decaying particle $p = (m_\rho, \vec{0})$, one has:

$$p \cdot k = p \cdot (k_1 - k_2) = m_\rho(\omega_1 - \omega_2) = 0, \quad (2.56)$$

thus, we obtain the following kinematical relation:

$$-k^2 = -k_1^2 - k_2^2 + 2k_1 \cdot k_2 = -2m_\pi^2 + 2\left(\frac{m_\rho^2 - 2m_\pi^2}{2}\right) = m_\rho^2 - 4m_\pi^2. \quad (2.57)$$

The final expression for the decay of ρ meson into two pions has the following form:

$$\Gamma_{\rho \rightarrow \pi\pi} = \frac{\sqrt{\frac{m_\rho^2}{4} - m_\pi^2}}{8\pi m_\rho} \cdot \frac{g^2}{3} (m_\rho^2 - 4m_\pi^2) \cdot \Theta(m_\rho - 2m_\pi) = \frac{g^2 \left(\frac{m_\rho^2}{4} - m_\pi^2\right)^{\frac{3}{2}}}{6\pi m_\rho} \Theta(m_\rho - 2m_\pi). \quad (2.58)$$

From the comparison with experimental data $\Gamma_{\rho \rightarrow \pi\pi} \approx 150$ MeV [27], we get $g \approx 6$. In the next three chapters we will use analogous (but more general) Lagrangians to describe the decays of $J = 2, 3$ mesons within effective models.

2.4 Conventional mesons within nonets

The classification of observed mesonic resonances into nonets of quark-antiquark ($q\bar{q}$) states using flavor and/or chiral symmetry is one of the most significant achievements of modern high-energy physics.

Let us describe the mesons in Table 1.2 within certain nonets using 3×3 matrices. For convenience, I use the strange-non-strange basis for the isoscalar members of the nonet entries. The first entries of Table 1.2 are pseudoscalar mesons $\{\pi, K, \eta(547), \eta'(958)\}$ (with $J^{PC} = 0^{-+}$) that correspond to:

$$P = \frac{1}{\sqrt{2}} \begin{pmatrix} \frac{\eta_{N+\pi^0}}{\sqrt{2}} & \pi^+ & K^+ \\ \pi^- & \frac{\eta_{N-\pi^0}}{\sqrt{2}} & K^0 \\ K^- & \bar{K}^0 & \eta_S \end{pmatrix}, \quad (2.59)$$

where the mesons with purely non-strange quarks η_N and pure strange quarks η_S are defined below

$$\eta_N \equiv (\bar{u} i\gamma^5 u + \bar{d} i\gamma^5 d) / \sqrt{2}, \quad \eta_S \equiv \bar{s} i\gamma^5 s. \quad (2.60)$$

The mixing relation between the isospin $I = 0$ mesons is

$$\begin{pmatrix} \eta \\ \eta'(958) \end{pmatrix} = \begin{pmatrix} \cos \beta_p & \sin \beta_p \\ -\sin \beta_p & \cos \beta_p \end{pmatrix} \begin{pmatrix} \eta_N \\ \eta_S \end{pmatrix}. \quad (2.61)$$

We will use $\beta_p = -43.4^\circ$ obtained in Ref. [61]. Such a large mixing angle is related to the so-called chiral (or axial) $U_A(1)$ anomaly [62,63].

Scalar mesons (with $J^{PC} = 0^{++}$) form a chiral multiplet together with the pseudoscalar mesons. We shall not include any decay width regarding this nonet because of their unclear identification. However, it is worth mentioning that $\{a_0(1450), K_0^*(1430), f_0(1370), f_0(1500)/f_0(1710)\}$ has a fair chance of building the scalar nonet with the scalar currents

$$S_{ij} \equiv 2^{-1/2} \bar{q}_j q_i. \quad (2.62)$$

The corresponding matrix is

$$S = \frac{1}{\sqrt{2}} \begin{pmatrix} \frac{\sigma_N + a_0^0}{\sqrt{2}} & a_0^+ & K_0^{*+} \\ a_0^- & \frac{\sigma_N - a_0^0}{\sqrt{2}} & K_0^{*0} \\ K_0^{*-} & \bar{K}_0^{*0} & \sigma_S \end{pmatrix}. \quad (2.63)$$

Unlike the pseudoscalar case, consideration of the glueball in the scalar sector is needed, since $\bar{n}n$, $\bar{s}s$, and $\bar{g}g$ are believed to generate the resonances $f_0(1370)$, $f_0(1500)$, and $f_0(1710)$, see e.g. Refs. [22,64–76].

Vector mesons $\{\rho(770), K^*(892), \omega(782), \phi(1020)\}$ (with $J^{PC} = 1^{--}$) are given in the third column of Table 1.2 and appear in the matrix form as

$$V_1^\mu = \frac{1}{\sqrt{2}} \begin{pmatrix} \frac{\omega_{1,N}^\mu + \rho_1^{0\mu}}{\sqrt{2}} & \rho_1^{+\mu} & K_1^{*+\mu} \\ \rho_1^{-\mu} & \frac{\omega_{1,N}^\mu - \rho_1^{0\mu}}{\sqrt{2}} & K_1^{*0\mu} \\ K_1^{*-\mu} & \bar{K}_1^{*0\mu} & \omega_{1,S}^\mu \end{pmatrix}. \quad (2.64)$$

In this case, the vector currents have the following form:

$$V_{1,ij}^\mu = (\bar{q}_j \gamma^\mu q_i) / \sqrt{2}, \quad (2.65)$$

The isoscalar states in the strange and non-strange basis are given by

$$\begin{pmatrix} \omega(782) \\ \phi(1020) \end{pmatrix} = \begin{pmatrix} \cos \beta_{v_1} & \sin \beta_{v_1} \\ -\sin \beta_{v_1} & \cos \beta_{v_1} \end{pmatrix} \begin{pmatrix} \omega_{1,N} \\ \omega_{1,S} \end{pmatrix}, \quad (2.66)$$

and the small mixing angle $\beta_{v_1} = -3.9^\circ$ is taken from the PDG [27]. It implies that $\omega(782)$ is almost made up of non-strange quarks, while $\phi(1020)$ is nearly composed of strange ones.

The next two meson families of Table 1.2 are the axial-vector mesons $\{a_1(1260), K_1(1270)/K_1(1400), f_1(1420), f_1(1285)\}$ (with $J^{PC} = 1^{++}$)

$$A_1^\mu = \frac{1}{\sqrt{2}} \begin{pmatrix} \frac{f_{1,N}^\mu + a_1^{0\mu}}{\sqrt{2}} & a_1^{+\mu} & K_{1,A}^{+\mu} \\ a_1^{-\mu} & \frac{f_{1,N}^\mu - a_1^{0\mu}}{\sqrt{2}} & K_{1,A}^{0\mu} \\ K_{1,A}^{-\mu} & \bar{K}_{1,A}^{0\mu} & f_{1,S}^\mu \end{pmatrix}, \quad (2.67)$$

and the pseudovector mesons $\{b_1(1235), K_1(1270)/K_1(1400), h_1(1415), h_1(1170)\}$ (with $J^{PC} = 1^{+-}$)

$$B_1^\mu = \frac{1}{\sqrt{2}} \begin{pmatrix} \frac{h_{1,N}^\mu + b_1^{0\mu}}{\sqrt{2}} & b_1^{+\mu} & K_{1,B}^{+\mu} \\ b_1^{-\mu} & \frac{h_{1,N}^\mu - b_1^{0\mu}}{\sqrt{2}} & K_{1,B}^{0\mu} \\ K_{1,B}^{-\mu} & \bar{K}_{1,B}^{0\mu} & h_{1,S}^\mu \end{pmatrix}. \quad (2.68)$$

They are in good agreement with the quark model of Ref. [77] and the Bethe-Salpeter approach of Ref. [37]. The mixing angles in these nonets are still unknown. These two matrices contain the corresponding currents

$$A_{1,ij}^\mu = (\bar{q}_j \gamma^5 \gamma^\mu q_i) / \sqrt{2}, \quad (2.69)$$

$$B_{1,ij}^\mu = (\bar{q}_j \gamma^5 \overleftrightarrow{\partial}^\mu q_i) / \sqrt{2} \quad \text{where} \quad \overleftrightarrow{\partial}^\mu := \overrightarrow{\partial}^\mu - \overleftarrow{\partial}^\mu. \quad (2.70)$$

The kaonic sector of these nonets displaces an important and different mixing between $K_{1,A}$ and $K_{1,B}$. Throughout this thesis, I focus on the physical resonances $K_1(1270)$ and $K_1(1400)$ that emerge as:

$$\begin{pmatrix} K_1(1270) \\ K_1(1400) \end{pmatrix} = \begin{pmatrix} \cos \varphi_K & -i \sin \varphi_K \\ -i \sin \varphi_K & \cos \varphi_K \end{pmatrix} \begin{pmatrix} K_{1,A} \\ K_{1,B} \end{pmatrix}. \quad (2.71)$$

Note, this is a mixing between members of different nonets. Such mixing is sometimes also represented in another basis [78–80]

$$\begin{pmatrix} |K_1^+(1270)\rangle \\ |K_1^+(1400)\rangle \end{pmatrix} = \begin{pmatrix} \sin \theta_K & \cos \theta_K \\ \cos \theta_K & -\sin \theta_K \end{pmatrix} \begin{pmatrix} |K_{1,A}^+\rangle \\ |K_{1,B}^+\rangle \end{pmatrix}. \quad (2.72)$$

The two angles are related via the following relation

$$\theta_K = \varphi_K + 90^\circ. \quad (2.73)$$

Numerically, one obtains

$$\varphi_K = (56.4 \pm 4.3)^\circ, \quad (2.74)$$

which makes us to conclude that $K_1(1270)$ is predominantly $K_{1,B}$ while $K_1(1400)$ is predominantly $K_{1,A}$ (despite the large mixing angle).

The orbitally excited vector mesons $\{\rho(1700), K^*(1680), \omega(1650), \phi(?)\}$ (with $J^{PC} = 1^{--}$) form a nonet

$$V_E^\mu = \frac{1}{\sqrt{2}} \begin{pmatrix} \frac{\omega_{E,N}^\mu + \rho_E^{0\mu}}{\sqrt{2}} & \rho_E^{+\mu} & K_E^{*+\mu} \\ \rho_E^{-\mu} & \frac{\omega_{E,N}^\mu - \rho_E^{0\mu}}{\sqrt{2}} & K_E^{*0\mu} \\ K_E^{*- \mu} & \bar{K}_E^{*0\mu} & \omega_{E,S}^\mu \end{pmatrix}, \quad (2.75)$$

with the currents

$$V_{E,ij}^\mu = (\bar{q}_j \overleftrightarrow{\partial}^\mu q_i) / \sqrt{2}. \quad (2.76)$$

Recent detailed phenomenological analyses for these mesons were performed in Ref. [81].

Next, I start the discussion about mesons with $J = 2, 3$ which are the last four entries of Table 1.2 and the main objects of this thesis.

The tensor mesons $\{a_2(1320), K_2^*(1430), f_2(1270), f_2'(1525)\}$ (with $J^{PC} = 2^{++}$) correspond to the following tensor currents:

$$T_{ij}^{\mu\nu} = \bar{q}_j [(i\gamma^\mu \overleftrightarrow{\partial}^\nu + \dots)] q_i / \sqrt{2}, \quad (2.77)$$

and are grouped in the following nonet matrix

$$T^{\mu\nu} = \frac{1}{\sqrt{2}} \begin{pmatrix} \frac{f_{2,N}^{\mu\nu} + a_2^{0\mu\nu}}{\sqrt{2}} & a_2^{+\mu\nu} & K_2^{*+\mu\nu} \\ a_2^{-\mu\nu} & \frac{f_{2,N}^{\mu\nu} - a_2^{0\mu\nu}}{\sqrt{2}} & K_2^{*0\mu\nu} \\ K_2^{*-\mu\nu} & \bar{K}_2^{*0\mu\nu} & f_{2,S}^{\mu\nu} \end{pmatrix}. \quad (2.78)$$

The mixing relation for the tensor mesons reads

$$\begin{pmatrix} f_2(1270) \\ f_2'(1525) \end{pmatrix} = \begin{pmatrix} \cos \beta_T & \sin \beta_T \\ -\sin \beta_T & \cos \beta_T \end{pmatrix} \begin{pmatrix} f_{2,N} \\ f_{2,S} \end{pmatrix}, \quad (2.79)$$

where the small mixing angle $\beta_T = 5.7^\circ$ is given in the PDG [27]³. These mesons have been studied previously in various papers (see, e.g., Refs. [71, 82, 83]).

The pseudotensor mesons $\{\pi_2(1670), K_2(1770)/K_2(1820), \eta_2(1870), \eta_2(1645)\}$ (with $J^{PC} = 2^{-+}$) are described by

$$P_2^{\mu\nu} = \frac{1}{\sqrt{2}} \begin{pmatrix} \frac{\eta_{2,N}^{\mu\nu} + \pi_2^{0\mu\nu}}{\sqrt{2}} & \pi_2^{+\mu\nu} & K_{2P}^{+\mu\nu} \\ \pi_2^{-\mu\nu} & \frac{\eta_{2,N}^{\mu\nu} - \pi_2^{0\mu\nu}}{\sqrt{2}} & K_{2P}^{0\mu\nu} \\ K_{2P}^{-\mu\nu} & \bar{K}_{2P}^{0\mu\nu} & \eta_{2S}^{\mu\nu} \end{pmatrix}. \quad (2.80)$$

The form of the pseudotensor current reads Ref. [84]

$$P_{2,ij}^{\mu\nu} = \bar{q}_j [(i\gamma^5 \partial^\mu \partial^\nu + \dots)] q_i / \sqrt{2} \quad (2.81)$$

³Later on, we will present an independent determination of this mixing.

The unknown mixing angle β_{pt} within isoscalar sector is given below

$$\begin{pmatrix} \eta_2(1645) \\ \eta_2(1870) \end{pmatrix} = \begin{pmatrix} \cos \beta_{pt} & \sin \beta_{pt} \\ -\sin \beta_{pt} & \cos \beta_{pt} \end{pmatrix} \begin{pmatrix} \eta_{2N} \\ \eta_{2S} \end{pmatrix}. \quad (2.82)$$

A large mixing angle $\beta_{pt} \approx -40^\circ$ is possible (see e.g. Refs. [85–87]).

The next entries in Table 1.2 are axial-tensor mesons (with $J^{PC} = 2^{--}$) whose currents are

$$A_{2ij}^{\mu\nu} = 2^{-1/2} \bar{q}_j \left(\gamma^5 \gamma^\mu \partial^\nu + \dots \right) q_i. \quad (2.83)$$

Apart from the kaonic spin-2 resonances $K_2(1770)/K_2(1820)$ (the second one shall be assigned to $J^{PC} = 2^{--}$, even if the mixing is expected), we know very little about them. One can find recent theoretical works dedicated to the vacuum properties and thermal properties of these resonances in Refs. [88–90] as well as in Refs. [34, 91]. The axial-tensor nonet reads:

$$A_2^{\mu\nu} = \frac{1}{\sqrt{2}} \begin{pmatrix} \frac{\omega_{2,N}^{\mu\nu} + \rho_2^{0\mu\nu}}{\sqrt{2}} & \rho_2^{+\mu\nu} & K_{2A}^{+\mu\nu} \\ \rho_2^{-\mu\nu} & \frac{\omega_{2,N}^{\mu\nu} - \rho_2^{0\mu\nu}}{\sqrt{2}} & K_{2A}^{0\mu\nu} \\ K_{2A}^{-\mu\nu} & \bar{K}_{2A}^{0\mu\nu} & \omega_{2,S}^{\mu\nu} \end{pmatrix}, \quad (2.84)$$

where the mixing in the isoscalar mixing is assumed to be zero

$$\omega_{2,N} \simeq \omega_2, \quad \omega_{2,S} \simeq \phi_2. \quad (2.85)$$

This assumption is supported because of the so-called homochiral nature of this nonet according to Ref. [87] in which homochiral and heterochiral classification of the multiplets were introduced. Generally, a small mixing angle appears in homochiral multiplets, such as vector and axial-vector mesons.

The last entries of Table 1.2 are spin-3 mesons $\{\rho_3(1690), K_3^*(1780), \phi_3(1850), \omega_3(1670)\}$ (with $J^{PC} = 3^{--}$) which are combined in the following nonet matrix:

$$W_3^{\mu\nu\rho} = \frac{1}{\sqrt{2}} \begin{pmatrix} \frac{\omega_{3,N}^{\mu\nu\rho} + \rho_3^{0\mu\nu\rho}}{\sqrt{2}} & \rho_3^{+\mu\nu\rho} & K_3^{+\mu\nu\rho} \\ \rho_3^{-\mu\nu\rho} & \frac{\omega_{3,N}^{\mu\nu\rho} - \rho_3^{0\mu\nu\rho}}{\sqrt{2}} & K_3^{0\mu\nu\rho} \\ K_3^{-\mu\nu\rho} & \bar{K}_3^{0\mu\nu\rho} & \omega_{3,S}^{\mu\nu\rho} \end{pmatrix}. \quad (2.86)$$

The isoscalar members of this nonet are:

$$\begin{pmatrix} \omega_3(1670) \\ \phi_3(1850) \end{pmatrix} = \begin{pmatrix} \cos \beta_{w_3} & \sin \beta_{w_3} \\ -\sin \beta_{w_3} & \cos \beta_{w_3} \end{pmatrix} \begin{pmatrix} \omega_{3,N} \\ \omega_{3,S} \end{pmatrix}, \quad (2.87)$$

where the small mixing angle is $\beta_{w_3} = 3.5^\circ$ [27]. This small value is also in favor of their homochiral nature. The currents read

$$W_{ij}^{\mu\nu\rho} = \bar{q}_j [(\gamma^\mu \partial^\nu \partial^\rho + \dots)] q_i / \sqrt{2}.$$

Spin-3 mesons were previously studied in Refs. [28,92–98].

The transformation rules under parity, charge conjugation, and flavor transformations for all the relevant nonets of this thesis ($P, S, V, A_1, B_1, V_E, T, P_2, A_2, W_3$) are summarized in Table 2.1.

Nonet	Parity (P)	Charge conjugation (C)	Flavour ($U_V(3)$)
$0^{-+} = P$	$-P(t, -\vec{x})$	P^t	UPU^\dagger
$0^{++} = S$	$S(t, -\vec{x})$	S^t	USU^\dagger
$1^{--} = V_1^\mu$	$V_{1\mu}(t, -\vec{x})$	$-(V_1^\mu)^t$	$UV_1^\mu U^\dagger$
$1^{++} = A_1^\mu$	$-A_{1\mu}(t, -\vec{x})$	$(A_1^\mu)^t$	$UA_1^\mu U^\dagger$
$1^{+-} = B_1^\mu$	$-B_{1,\mu}(t, -\vec{x})$	$-(B_1^\mu)^t$	$UB_1^\mu U^\dagger$
$1^{--} = V_E^\mu$	$V_{E,\mu}(t, -\vec{x})$	$-(V_E^\mu)^t$	$UV_E^\mu U^\dagger$
$2^{++} = T^{\mu\nu}$	$T_{\mu\nu}(t, -\vec{x})$	$(T^{\mu\nu})^t$	$UT^{\mu\nu} U^\dagger$
$2^{-+} = P_2^{\mu\nu}$	$P_{2\mu\nu}(t, -\vec{x})$	$(P_2^{\mu\nu})^t$	$UP_2^{\mu\nu} U^\dagger$
$2^{--} = A_2^{\mu\nu}$	$-A_{2\mu\nu}(t, -\vec{x})$	$-(A_2^{\mu\nu})^t$	$UA_2^{\mu\nu} U^\dagger$
$3^{--} = W_3^{\mu\nu\rho}$	$W_{3,\mu\nu\rho}(t, -\vec{x})$	$-(W_3^{\mu\nu\rho})^t$	$UW_3^{\mu\nu\rho} U^\dagger$

Table 2.1: Mesonic nonets under P, C and $U_V(3)$ transformations.

I also present the chiral nonets that shall be used in the next chapter for spin-2 eLSM

$$\begin{aligned} \Phi &:= S + iP, & L^\mu &:= V_1^\mu + A_1^\mu, & R^\mu &:= V_1^\mu - A_1^\mu, \\ \mathbf{L}^{\mu\nu} &:= T^{\mu\nu} + A_2^{\mu\nu}, & \mathbf{R}^{\mu\nu} &:= T^{\mu\nu} - A_2^{\mu\nu}. \end{aligned} \quad (2.88)$$

These objects are useful because they transform in a simple way under chiral transformation and can be used as a starting point to build chiral interaction Lagrangians.

Chapter 3

Spin-2 mesons

In this section, we present a phenomenological investigation based on the extended Linear Sigma Model of the masses, strong, and radiative decays of spin-2 ground state mesons (with $J^{PC} = 2^{++}, 2^{--}$), focusing on the missing axial-tensor mesons.

3.1 Introduction

According to the Table 1.2, there are three ground state spin-2 meson families:

1. Tensor mesons: $\{a_2(1320), K_2^*(1430), f_2(1270), f_2'(1525)\}$ (with $S = L = 1$, and $J^{PC} = 2^{++}$);
2. Pseudotensor mesons: $\{\pi_2(1670), K_2(1770)/K_2(1820), \eta_2(1870), \eta_2(1645)\}$ (with $S = 0, L = 2$, and $J^{PC} = 2^{-+}$);
3. Axial-tensor mesons: $\{\rho_2(?), K_2(1820)/K_2(1770), \phi_2(?), \omega_2(?)\}$ (with $S = 1, L = 2$, and $J^{PC} = 2^{--}$).

For tensor mesons, we know their masses, hadronic and two-photon decay rates. A small mixing angle in the isoscalar sector, obtained from the mass relations, is also confirmed by decay rates (as we shall see in the next sections).

There are two main problems with the pseudotensor mesons:

- A non-trivial mixing in the kaonic sector: Because of the non-diagonal C-parity of the kaons, 2^{--} and 2^{-+} states may mix in order to form $K_2(1770)$ and $K_2(1820)$ [99].

- Unknown mixing angle between $\eta_2(1870)$ and $\eta_2(1645)$ (see the discussion in Chapter 7).

The resonance $K_2(1820)$, which is supposed to be predominantly an axial-tensor meson, has a larger total decay width compared to $K_2(1770)$

$$\Gamma_{K_2(1820)}^{\text{tot}} = 264 \pm 34 \text{ MeV}, \quad \Gamma_{K_2(1770)}^{\text{tot}} = 186 \pm 14 \text{ MeV}. \quad (3.1)$$

Other members belonging to axial-tensor meson nonet have not been identified yet. There are additionally, four axial-tensor mesons $\rho_2(1940)$, $\omega_2(1975)$, $\omega_2(2195)$, and $\rho_2(2225)$ indicated as “further states” in PDG [27], but they are too heavy to be identified as ground-state axial-tensor states.

The scalar and the axial-vector mesons, as well as their corresponding chiral partners, the pseudoscalar and vector mesons, introduced in the previous chapter, were successfully described using the eLSM in Ref. [19]. This model is useful in the case of a lack of information on one of the chiral nonet—the same J but opposite G-parity—because it permits the analysis of the chiral partners on an equal basis.

Using the eLSM to describe both tensor and axial-tensor mesons in a chiral framework then seems well-motivated. With sufficient experimental data, we postdict the known results (as well as previously not-yet measured radiative decays) for tensor mesons, fit the model parameter to the experiment, and then evaluate the masses and decay widths of the unknown axial-tensor mesons. The excited (pseudo)scalar mesons [22, 100], pseudovector and orbitally excited vector mesons [101] and hybrid mesons [102] were also studied within this chiral model.

We find that there is generally a good agreement between theory and experiment, which supports the predominant $q\bar{q}$ nature of the ground-state tensor mesons. Next, it turns out that the decay of the axial-tensor mesons into vector-pseudoscalar mesons is dominant and quite large. Our prediction for the mass of ρ_2 from the spontaneous breaking of the chiral symmetry agrees with the relativistic quark model [77]. Our findings can be useful for the current experiments at BESIII [103, 104], CLAS12 [105], COMPASS [106], GlueX [107–109], CMD-3 [110] and the future PANDA experiment [111], where axial-tensor mesons can be investigated.

3.2 Spin-2 eLSM

In the chiral limit of QCD ($m_{u,d,s} = 0$) the spontaneous breaking of the chiral symmetry

$$SU_L(3) \times SU_R(3) \times U_V(1), \quad (3.2)$$

into $SU_V(3)$ flavor symmetry and $U_V(1)$ symmetry (conservation of baryon number). In 1961, Nambu and Jona-Lasinio presented the first powerful model describing this process using four-fermion Fermi interactions in Refs. [112, 113]. As seen in the previous chapter, quark-antiquark mesons are grouped into nonets at the level of confined light hadrons [114–116].

Effective low-energy hadronic models, such as the previously described LSM, can be used to describe low-energy QCD. Confinement and color neutrality are automatically built in when hadrons are the relevant degrees of freedom. These models typically include chiral symmetry and its spontaneous and explicit breaking in such a way as to mimic properties of QCD.

In order to study spin-2 mesons, we use the chiral nonets introduced in the previous chapter. The transformation laws of these chiral nonets are shown in Table 3.1. As can be seen, these are quite simple transformations that enable the formulation of chirally invariant terms. Moreover, according to the classifications of Ref. [87], (pseudo)scalar mesons form a heterochiral multiplet with a possible large isoscalar mixing angle, while (axial-)vector and (axial-)tensor build homochiral multiplets with expected small isoscalar mixing angles. The (pseudo)scalar and (axial-)vector mesons as well as the

Nonet	Parity (P)	Charge conjugation (C)	$U_L(3) \times U_R(3)$
$\Phi(t, \vec{x})$	$\Phi^\dagger(t, -\vec{x})$	$\Phi^t(t, \vec{x})$	$U_L \Phi U_R^\dagger$
$R^\mu(t, \vec{x})$	$L_\mu(t, -\vec{x})$	$-(L^\mu(t, \vec{x}))^t$	$U_R R^\mu U_R^\dagger$
$L^\mu(t, \vec{x})$	$R_\mu(t, -\vec{x})$	$-(R^\mu(t, \vec{x}))^t$	$U_L L^\mu U_L^\dagger$
$\mathbf{R}^{\mu\nu}(t, \vec{x})$	$\mathbf{L}_{\mu\nu}(t, -\vec{x})$	$(\mathbf{L}^{\mu\nu}(t, \vec{x}))^t$	$U_R \mathbf{R}^{\mu\nu} U_R^\dagger$
$\mathbf{L}^{\mu\nu}(t, \vec{x})$	$\mathbf{R}_{\mu\nu}(t, -\vec{x})$	$(\mathbf{R}^{\mu\nu}(t, \vec{x}))^t$	$U_L \mathbf{L}^{\mu\nu} U_L^\dagger$

Table 3.1: Chiral nonets under P , C , and $U_L(3) \times U_R(3)$ transformations.

dilaton (or scalar glueball) field G are all ingredients of the standard form of the eLSM

Lagrangian, as shown in Refs. [19, 22, 102]:

$$\begin{aligned} \mathcal{L}_{\text{eLSM}} = & V_{\text{dil}} + \text{Tr} \left[(D_\mu \Phi)^\dagger (D_\mu \Phi) \right] - m_0^2 \left(\frac{G}{G_0} \right)^2 \text{Tr} [\Phi^\dagger \Phi] - \frac{1}{4} \text{Tr} \left[(L_{\mu\nu}^2 + R_{\mu\nu}^2) \right] \\ & + \text{Tr} \left[\left(\frac{m_{\text{vec}}^2 G^2}{2G_0^2} + \Delta \right) (L_\mu^2 + R_\mu^2) \right] + (\text{higher order terms}), \end{aligned} \quad (3.3)$$

where V_{dil} is the dilaton Lagrangian for the field G [117, 118], which has the following form

$$V_{\text{dil}}(G) = \frac{1}{4} \lambda \left(G^4 \ln \left| \frac{G}{G_0} \right| - \frac{G^4}{4} \right), \quad (3.4)$$

where $G_0 \sim 0.4 \text{ GeV}$ is the corresponding vacuum expectation value (v.e.v.) of a dilaton field G . Note, $V_{\text{dil}}(G)$ mimics the trace anomaly feature of the YM part of QCD. The dilaton field G is formally important for dilatation invariance and its breaking even if it will not show up as a decay product. The ‘‘covariant derivative’’ in Eq.(3.3) is defined as

$$D_\mu \Phi := \partial_\mu \Phi - ig_1 (L_\mu \Phi - \Phi R_\mu). \quad (3.5)$$

Information about the explicit breaking of the flavor symmetry, that is the inclusion of strange quark mass larger than of non-strange quarks, is considered in the following matrix Δ

$$\Delta = \begin{pmatrix} \delta_N & 0 & 0 \\ 0 & \delta_N & 0 \\ 0 & 0 & \delta_S \end{pmatrix}, \quad (3.6)$$

where $\delta_N \sim m_u^2$ and $\delta_S \sim m_s^2$. Dilatation and chiral invariances, as well as their explicit and spontaneous breaking patterns, are thus properly handled in eLSM.¹ Here I briefly review the results for fitted model parameters from Refs. [19, 22] relevant to my thesis. Firstly, as a result of SSB isoscalar members of Eq. (2.63) get a v.e.v. which can be understood as a consequence of $m_0^2 < 0$. This is the generalization of the simple Mexican hat form of effective potential previously studied in [18]. As a consequence,

¹Examples of additional chiral models that used dilatation invariance can be found, for instance, in Refs. [20, 21].

shifts of scalar fields are necessary:

$$S \rightarrow S + \Phi_0 \quad \text{with} \quad \Phi_0 := \frac{1}{\sqrt{2}} \begin{pmatrix} \frac{\phi_N}{\sqrt{2}} & 0 & 0 \\ 0 & \frac{\phi_N}{\sqrt{2}} & 0 \\ 0 & 0 & \phi_S \end{pmatrix}, \quad (3.7)$$

where the numerical values are given in Table 3.2. In the virtue of the breaking of dilatation symmetry, the dilaton field G condenses to G_0 too. The second consequence of SSB is that the mixing between axial-vector and pseudoscalar mesons [19, 100] is proportional to the parameter g_1 (see Table 3.2). It requires the following shift:

$$A_{1\mu} \rightarrow A_{1\mu} + \partial_\mu \mathcal{P} \quad \text{with} \quad \mathcal{P} := \frac{1}{\sqrt{2}} \begin{pmatrix} \frac{Z_\pi w_\pi (\eta_N + \pi^0)}{\sqrt{2}} & Z_\pi w_\pi \pi^+ & Z_K w_K K^+ \\ Z_\pi w_\pi \pi^- & \frac{Z_\pi w_\pi (\eta_N - \pi^0)}{\sqrt{2}} & Z_K w_K K^0 \\ Z_K w_K K^- & Z_K w_K \bar{K}^0 & Z_{\eta_S} w_{\eta_S} \eta_S \end{pmatrix}, \quad (3.8)$$

where the modified version of the pseudoscalar nonet Eq. (2.80) with renormalization factors given in Table 3.2 is introduced. The application of these two shifts related to SSB leads to novel interaction terms in the next sections.

Chiral invariant Lagrangians that consider the spin-2 chiral nonets as well are grouped into two types: mass and interaction terms. We first start with the mass terms

$$\begin{aligned} \mathcal{L}_{\text{mass}} = & \text{Tr} \left[\left(\frac{m_{\text{ten}}^2 G^2}{2 G_0^2} + \Delta^{\text{ten}} \right) (\mathbf{L}_{\mu\nu}^2 + \mathbf{R}_{\mu\nu}^2) \right] + \frac{h_1^{\text{ten}}}{2} \text{Tr} [\Phi^\dagger \Phi] \text{Tr} [\mathbf{L}^{\mu\nu} \mathbf{L}_{\mu\nu} + \mathbf{R}^{\mu\nu} \mathbf{R}_{\mu\nu}] \\ & + h_2^{\text{ten}} \text{Tr} [\Phi^\dagger \mathbf{L}^{\mu\nu} \mathbf{L}_{\mu\nu} \Phi + \Phi \mathbf{R}^{\mu\nu} \mathbf{R}_{\mu\nu} \Phi^\dagger] + 2h_3^{\text{ten}} \text{Tr} [\Phi \mathbf{R}^{\mu\nu} \Phi^\dagger \mathbf{L}_{\mu\nu}], \end{aligned} \quad (3.9)$$

where the only dimensionful constants are collected within the following matrix:

$$\Delta^{\text{ten}} = \begin{pmatrix} \delta_N^{\text{ten}} & 0 & 0 \\ 0 & \delta_N^{\text{ten}} & 0 \\ 0 & 0 & \delta_S^{\text{ten}} \end{pmatrix}. \quad (3.10)$$

This is analogous to Eq. (3.6) but refers to (axial-)tensor multiplet. Upon setting $\delta_N^{\text{ten}} = 0$ (this is possible because a term proportional to the identity matrix can be subtracted and absorbed in the m_{ten}^2 -term) and using the physical masses for the tensor

Parameters	Expressions	Numerical values [19]
$Z_\pi = Z_{\eta_N}$	$\frac{m_{a_1}}{\sqrt{m_{a_1}^2 - g_1^2 \phi_S^2}}$	1.709
$w_\pi = w_{\eta_N}$	$\frac{g_1 \phi_N}{m_{a_1}^2}$	0.683 GeV^{-1}
Z_K	$\frac{2m_{K_{1A}}}{\sqrt{4m_{K_{1A}}^2 - g_1^2 (\phi_N + \sqrt{2}\phi_S)^2}}$	1.604
w_K	$\frac{g_1 (\phi_N + \sqrt{2}\phi_S)}{2m_{K_{1A}}^2}$	0.611 GeV^{-1}
Z_{η_S}	$\frac{m_{f_{1,S}}}{\sqrt{m_{f_{1,S}}^2 - 2g_1^2 \phi_S^2}}$	1.539
w_{η_S}	$\frac{\sqrt{2}g_1 \phi_S}{m_{f_{1,S}}^2}$	0.554 GeV^{-1}
ϕ_N	$Z_\pi f_\pi$	0.158 GeV
ϕ_S	$\frac{2Z_K f_K - \phi_N}{\sqrt{2}}$	0.138 GeV
g_1	$\frac{m_{a_1}}{Z_\pi f_\pi} \sqrt{1 - \frac{1}{Z_\pi^2}}$	5.8

Table 3.2: Fit results for the parameters of the basic version of the eLSM. They will be used in this and the next chapter (see for details in Ref. [19]). Note, these values are one specific solution of the fit. For instance, in the case of Z_π , an uncertainty of about 20% was estimated.

mesons from PDG [27], we obtain the following relation

$$\delta_S^{\text{ten}} = m_{K_2}^2 - m_{a_2}^2 \simeq 0.3 \text{ GeV}^2. \quad (3.11)$$

In the large- N_c limit ² h_1^{ten} is suppressed because of the following N_c scalings of the parameters

- $m_{\text{ten}}^2 / G_0^2 \propto N_c^{-2}$;
- $h_1^{\text{ten}} \propto N_c^{-3}$;
- $h_2^{\text{ten}} \propto N_c^{-1}$ and $h_3^{\text{ten}} \propto N_c^{-1}$.

²Although $N_c = 3$ in nature, studying QCD for large values of N_c is useful since numerous simplifications take place in this limit. In particular, conventional mesons and glueballs become stable [119,120].

The decays of (axial-)tensor mesons are produced by additional interaction terms, which is what we will discuss next. The first and the simplest Lagrangian (that can also be rewritten in a dilation invariant form) reads:

$$\begin{aligned} \mathcal{L}_{g_2^{\text{ten}}} = & \frac{g_2^{\text{ten}}}{2} \left(\text{Tr} \left[\mathbf{L}_{\mu\nu} \{L^\mu, L^\nu\} \right] + \text{Tr} \left[\mathbf{R}_{\mu\nu} \{R^\mu, R^\nu\} \right] \right) \\ & + \frac{g_2'^{\text{ten}}}{6} \text{Tr} \left[\mathbf{L}_{\mu\nu} + \mathbf{R}_{\mu\nu} \right] \text{Tr} \left[\{L^\mu, L^\nu\} + \{R^\mu, R^\nu\} \right], \end{aligned} \quad (3.12)$$

where the first term is dominant in the large- N_c limit since the dimensionful coupling constants scale as $g_2^{\text{ten}} \propto N_c^{-1/2}$, while $g_2'^{\text{ten}}$ is suppressed since $g_2'^{\text{ten}} \propto N_c^{-3/2}$. Further suppressed terms are ignored. The Lagrangian in Eq. (3.12) leads to the following two important decay channels, which are the dominant ones, as we shall see in the next sections:

1. Tensor mesons with quantum numbers $J^{PC} = 2^{++}$ decaying into two pseudoscalar mesons (with $J^{PC} = 0^{-+}$);
2. Axial-tensor mesons with quantum numbers $J^{PC} = 2^{--}$ decaying into a pseudoscalar meson (with $J^{PC} = 0^{-+}$) and into a vector meson (with $J^{PC} = 1^{-}$).

Experimental results for the well-established 2^{++} nonet will be used to determine the couplings g_2^{ten} and $g_2'^{\text{ten}}$, that are later on implemented to derive chiral model estimations for the missing 2^{--} meson nonet decays. Just as two-pseudoscalar decays are the dominant decay channels for the tensor mesons, the vector and pseudoscalar meson decay channels are the dominant ones for the axial-tensor mesons. Both decay modes are present in the Lagrangian of Eq. (3.12).

The following chiral Lagrangian for the chiral fields

$$L^{\mu\nu} := \partial^\mu L^\nu - \partial^\nu L^\mu, \quad R^{\mu\nu} := \partial^\mu R^\nu - \partial^\nu R^\mu, \quad (3.13)$$

describes the coupling of (axial-)tensor mesons to two (axial-)vector ones:

$$\begin{aligned} \mathcal{L}_{a^{\text{ten}}} = & \frac{a^{\text{ten}}}{2} \text{Tr} \left[\mathbf{L}_{\mu\nu} \{L_{\beta'}^\mu, L^{\nu\beta'}\} + \mathbf{R}_{\mu\nu} \{R_{\beta'}^\mu, R^{\nu\beta'}\} \right] + \\ & + \frac{a'^{\text{ten}}}{6} \text{Tr} \left[\mathbf{L}_{\mu\nu} + \mathbf{R}_{\mu\nu} \right] \text{Tr} \left[\{L_{\beta'}^\mu, L^{\nu\beta'}\} + \{R_{\beta'}^\mu, R^{\nu\beta'}\} \right]. \end{aligned} \quad (3.14)$$

This Lagrangian generates radiative decays of the tensor mesons via the vector meson dominance (VDM) assumption [121–123], which features the photon-vector-meson

mixing generated by the shift on the massive vector field strength

$$V_{\mu\nu} \mapsto V_{\mu\nu} + \frac{eQ}{g_\rho} F_{\mu\nu}, \quad F_{\mu\nu} := \partial_\mu A_\nu - \partial_\nu A_\mu, \quad V_{\mu\nu} := \partial_\mu V_\nu - \partial_\nu V_\mu, \quad (3.15)$$

where the up, down, and strange quark charges are included in the matrix

$$Q = \text{diag}\left(\frac{2}{3}, -\frac{1}{3}, -\frac{1}{3}\right). \quad (3.16)$$

Moreover, the electric coupling constant e is expressed in terms of the fine structure constant as $e = \sqrt{4\pi\alpha}$ and the transition parameter $g_\rho \simeq 5.5 \pm 0.5$.

The coupling constants of the Lagrangian in Eq. (3.14) carry the dimension of [Energy⁻¹] and are distinguished according to their large- N_c behavior, with the dominant $a^{\text{ten}} \propto N_c^{-1/2}$ and the subdominant $a'^{\text{ten}} \propto N_c^{-3/2}$ ³.

Thus, the Lagrangian in Eq. (3.14) will be used to describe the following decays of the tensor mesons:

1. two-photon decay;
2. photon and vector mesons decay;
3. three and four body decays via intermediate two vector mesons.

Since there is experimental data [27] about the vector and pseudoscalar decay channels of the tensor mesons with $J^{PC} = 2^{++}$, we introduce the following (dilatation breaking) chiral Lagrangian that links axial-tensor fields to axial-vector and pseudoscalar ones:

$$\begin{aligned} \mathcal{L}_c^{\text{ten}} = & c_1^{\text{ten}} \text{Tr} \left[\partial^\mu \mathbf{L}^{\nu\alpha} \tilde{L}_{\mu\nu} \partial_\alpha \Phi \Phi^\dagger - \partial^\mu \mathbf{R}^{\nu\alpha} \Phi^\dagger \partial_\alpha \Phi \tilde{R}_{\mu\nu} \right. \\ & \left. - \partial^\mu \mathbf{R}^{\nu\alpha} \tilde{R}_{\mu\nu} \partial_\alpha \Phi^\dagger \Phi + \partial^\mu \mathbf{L}^{\nu\alpha} \Phi \partial_\alpha \Phi^\dagger \tilde{L}_{\mu\nu} \right] + \\ & + c_2^{\text{ten}} \text{Tr} \left[\partial^\mu \mathbf{L}^{\nu\alpha} \partial_\alpha \Phi \tilde{R}_{\mu\nu} \Phi^\dagger - \partial^\mu \mathbf{R}^{\nu\alpha} \Phi^\dagger \tilde{L}_{\mu\nu} \partial_\alpha \Phi - \right. \\ & \left. - \partial^\mu \mathbf{R}^{\nu\alpha} \partial_\alpha \Phi^\dagger \tilde{L}_{\mu\nu} \Phi + \partial^\mu \mathbf{L}^{\nu\alpha} \Phi \tilde{R}_{\mu\nu} \partial_\alpha \Phi^\dagger \right], \quad (3.17) \end{aligned}$$

³This term can be made dilation invariant upon multiplying $\left(\frac{G}{G_0}\right)^b$ with $b > 0$. Indeed, $b = -1$ would be recovered, but that leads to non-analytic parts. For more details, see [19].

where

$$\tilde{R}_{\mu\nu} := \frac{\varepsilon_{\mu\nu\rho\sigma}}{2} (\partial^\rho R^\sigma - \partial^\sigma R^\rho), \quad \tilde{L}_{\mu\nu} := \frac{\varepsilon_{\mu\nu\rho\sigma}}{2} (\partial^\rho L^\sigma - \partial^\sigma L^\rho). \quad (3.18)$$

The dimensionful constants c_1^{ten} and c_2^{ten} scale as $N_c^{-1/2}$ and cannot be constrained independently (but their sum can be fixed, see next section) within the current data for tensor mesons. Upon performing the shift of the axial-vector fields and the scalar fields, the following decay channels will be described using the Lagrangian in Eq. (3.17):

1. $2^{++} \rightarrow 0^{-+} + 1^{--}$;
2. $2^{--} \rightarrow 0^{-+} + 1^{++}$.

These decay channels are also connected by chiral symmetry.

Decay Mode	$\frac{1}{5} \mathcal{M} ^2$
$2^{++} \rightarrow 0^{-+} + 0^{-+}$	$g_2^{\text{ten}2} \times \frac{2 \vec{k}_{t,p}^{(1),p(2)} ^4}{15}$
$2^{--} \rightarrow 0^{-+} + 1^{--}$	$g_2^{\text{ten}2} \times \frac{ \vec{k}_{t,v,p} ^2}{15} \left(5 + \frac{2 \vec{k}_{t,v,p} ^2}{m_v^2} \right)$
$2^{--} \rightarrow 0^{-+} + 2^{++}$	$\frac{4h_3^{\text{ten}2}}{45} \left(45 + \frac{4 \vec{k}_{a_2,t,p} ^4}{m_t^4} + \frac{30 \vec{k}_{a_2,t,p} ^2}{m_t^2} \right)$
$2^{++} \rightarrow 0^{-+} + 1^{--}$	$\frac{(c_1^{\text{ten}} + c_2^{\text{ten}})^2 m_t^2 \vec{k}_{t,v,p} ^4}{5}$
$2^{--} \rightarrow 0^{-+} + 1^{++}$	$\frac{(c_1^{\text{ten}} - c_2^{\text{ten}})^2 m_a^2 \vec{k}_{a_2,a_1,p} ^4}{5}$

Table 3.3: Amplitude squares for the decay of spin-2 resonances.

The decay of a generic massive spin-2 state with mass m_t and decay products with masses m_a and m_b has the form [27, 124]:

$$\Gamma_{T \rightarrow A+B} = \frac{|\vec{k}_{t,a,b}|}{8\pi m_t^2} \times \frac{1}{5} |\mathcal{M}|^2 \times \kappa_i \times \Theta(m_t - m_a - m_b), \quad (3.19)$$

where $\Theta(x)$ stands for the Heaviside step-function, the κ_i are the numbers (possibly dimensionful) related to the Clebsh-Gordan coefficients, and the modulus of the

outgoing particle three-momentum reads

$$|\vec{k}_{t,a,b}| \equiv \frac{1}{2m_t} \sqrt{(m_t^2 - m_a^2 - m_b^2)^2 - 4m_a^2 m_b^2}. \quad (3.20)$$

The square of the amplitudes $|\mathcal{M}|^2$ in Table 3.3 are derived via Feynman rules (for textbook see e.g., [124]).

Results

We report the results for the (axial-)tensor mesons, including their masses, hadronic, and radiative decays. Chiral SSB is the basic method to predict the masses of the missing axial-tensor mesons. The model parameters listed in Table 3.4 are obtained via the fitting of the experimental data for the well-established tensor mesons. Sec. 3.3 is devoted to the masses of the spin-2 mesons, while the hadronic and radiative decays of the tensor mesons are presented in Sec. 3.4. Predictions for the missing axial-tensor meson decays are given in Sec. 3.5.

3.3 Masses of (axial-)tensor mesons

By extending Eq. (3.9) and considering the v.e.v. and shifts of Eq. (3.7) and Eq. (3.8), we derive the equations for the masses of the missing axial-tensor mesons:

$$m_{\rho_2}^2 = (m_{\text{ten}}^2 + 2\delta_N^{\text{ten}}) - \frac{h_3^{\text{ten}} \phi_N^2}{2} + \frac{h_2^{\text{ten}} \phi_N^2}{2} + \frac{h_1^{\text{ten}}}{2} (\phi_N^2 + \phi_S^2), \quad (3.21)$$

$$m_{K_{2A}}^2 = (m_{\text{ten}}^2 + \delta_N^{\text{ten}} + \delta_S^{\text{ten}}) + \frac{h_1^{\text{ten}}}{2} (\phi_N^2 + \phi_S^2) - \frac{1}{\sqrt{2}} h_3^{\text{ten}} \phi_N \phi_S + \frac{h_2^{\text{ten}}}{4} (\phi_N^2 + 2\phi_S^2), \quad (3.22)$$

$$m_{\omega_{2,N}}^2 = (m_{\text{ten}}^2 + 2\delta_N^{\text{ten}}) - \frac{h_3^{\text{ten}} \phi_N^2}{2} + \frac{h_2^{\text{ten}} \phi_N^2}{2} + \frac{h_1^{\text{ten}}}{2} (\phi_N^2 + \phi_S^2), \quad (3.23)$$

Parameters	Numerical Values	Fitting Data
h_3^{ten}	-41	Table 3.5
δ_S^{ten}	0.3 GeV^2	Table 3.5
g_2^{ten}	$(1.392 \pm 0.024) \cdot 10^4 (\text{MeV})$	Table 3.7
$g_2'^{\text{ten}}$	$(0.024 \pm 0.041) \cdot 10^4 (\text{MeV})$	Table 3.7
$g_{2\text{lat}}^{\text{ten}}$	$(0.7 \pm 0.4) \cdot 10^4 (\text{MeV})$	Table 3.13
c^{ten}	$(4.8 \pm 0.9) \cdot 10^{-7} (\text{MeV})^{-3}$	Table 3.8
a^{ten}	$(-2.09 \pm 0.06) \cdot 10^{-2} (\text{MeV})^{-1}$	Table 3.10
a'^{ten}	$(3.5 \pm 0.4) \cdot 10^{-3} (\text{MeV})^{-1}$	Table 3.10
β_T	$(3.16 \pm 0.81)^\circ$	Table 3.7

Table 3.4: Fit results to known experimental data of PDG fixes the parameters of the eLSM associated with the (axial-)tensor mesons (the details are given in the upcoming section). It should be noted that the suffix “lat” in $g_{2\text{lat}}^{\text{ten}}$ denotes that the data has been obtained through comparison to lattice reports in [31].

$$m_{\omega_{2,S}}^2 = (m_{\text{ten}}^2 + 2\delta_S^{\text{ten}}) - h_3^{\text{ten}} \phi_S^2 + h_2^{\text{ten}} \phi_S^2 + \frac{h_1^{\text{ten}}}{2} (\phi_N^2 + \phi_S^2). \quad (3.24)$$

The corresponding formulas for the experimentally well-known tensor mesons are as follows:

$$m_{a_2}^2 = (m_{\text{ten}}^2 + 2\delta_N^{\text{ten}}) + \frac{h_3^{\text{ten}} \phi_N^2}{2} + \frac{h_2^{\text{ten}} \phi_N^2}{2} + \frac{h_1^{\text{ten}}}{2} (\phi_N^2 + \phi_S^2) = m_{\rho_2}^2 + h_3^{\text{ten}} \phi_N^2, \quad (3.25)$$

$$m_{K_2}^2 = (m_{\text{ten}}^2 + \delta_N^{\text{ten}} + \delta_S^{\text{ten}}) + \frac{h_1^{\text{ten}}}{2} (\phi_N^2 + \phi_S^2) + \frac{1}{\sqrt{2}} h_3^{\text{ten}} \phi_N \phi_S + \frac{h_2^{\text{ten}}}{4} (\phi_N^2 + 2\phi_S^2), \quad (3.26)$$

$$m_{f_{2,N}}^2 = (m_{\text{ten}}^2 + 2\delta_N^{\text{ten}}) + \frac{h_3^{\text{ten}} \phi_N^2}{2} + \frac{h_1^{\text{ten}}}{2} (\phi_N^2 + \phi_S^2) + \frac{h_2^{\text{ten}} \phi_N^2}{2}, \quad (3.27)$$

$$m_{f_{2,S}}^2 = (m_{\text{ten}}^2 + 2\delta_S^{\text{ten}}) + \frac{h_1^{\text{ten}}}{2}(\phi_N^2 + \phi_S^2) + h_3^{\text{ten}}\phi_S^2 + h_2^{\text{ten}}\phi_S^2 = m_{\omega_{2,S}}^2 + 2h_3^{\text{ten}}\phi_S^2. \quad (3.28)$$

We note that for every nonet the masses of the isovector and the nonstrange isoscalar elements are the same:

$$m_{\rho_2}^2 = m_{\omega_{2,N}}^2, \text{ and } m_{\mathbf{a}_2}^2 = m_{f_{2,N}}^2. \quad (3.29)$$

However, the isoscalars $\omega_{2,N}$ and f_{2n} are not yet in the physical basis, but we know that the mixing angle for the tensor mesons is small from various experimental and theoretical constraints.

The masses of the kaonic members satisfy the following relation:

$$m_{K_{2A}}^2 = m_{K_2}^2 - \sqrt{2}h_3^{\text{ten}}\phi_N\phi_S. \quad (3.30)$$

Thus, the parameter h_3^{ten} is estimated using the PDG masses of $K_2(1820)$ and $K_2^*(1430)$:

$$h_3^{\text{ten}} = \frac{m_{K_{2A}}^2 - m_{K_2}^2}{\sqrt{2}\phi_N\phi_S} \simeq -41. \quad (3.31)$$

The second relevant parameter of the mass term Lagrangian is δ_S^{ten} . We obtain this parameter under the assumptions of $\delta_N^{\text{ten}} \simeq 0$ and $\phi_N^2 \simeq 2\phi_S^2$ by the following relation:

$$\delta_S^{\text{ten}} = m_{K_2}^2 - m_{\mathbf{a}_2}^2 \simeq 0.3 \text{ GeV}^2. \quad (3.32)$$

By using these two parameters, we are able to obtain the masses of the missing axial-tensor mesons:

1. The mass of the purely strange resonance $\omega_{2,S} \simeq \phi_2$ reads:

$$m_{\phi_2}^2 \simeq m_{\omega_{2,S}}^2 = m_{\mathbf{a}_2}^2 + 2\delta_S^{\text{ten}} - \frac{3}{2}h_3^{\text{ten}}\phi_N^2, \quad (3.33)$$

which means that the not-yet discovered $\bar{s}s$ resonance has the following numerical value:

$$m_{\phi_2} \approx 1971 \text{ MeV}. \quad (3.34)$$

2. The mass of the missing ρ_2 is obtained via the following relation

$$m_{\rho_2}^2 = m_{a_2}^2 - h_3^{\text{ten}} \phi_N^2,$$

which implies:

$$m_{\rho_2} = 1663 \text{ MeV}. \quad (3.35)$$

When the isoscalar mixing is disregarded, we also obtain

$$m_{\omega_{2n}} = 1663 \text{ MeV}. \quad (3.36)$$

So, it is expected that the new resonances $\rho_2(1663)$, $\omega_2(1663)$ and $\phi_2(1971)$ will show up in the mesonic spectrum between 1.5 and 2.0 GeV.

3. The eLSM estimates the mass of the purely strange isoscalar tensor meson as follows:

$$m_{f_{2,S}}^2 = m_{\omega_{2,S}}^2 + 2h_3^{\text{ten}} \phi_S^2 \simeq 1520 \text{ MeV}, \quad (3.37)$$

which is a bit less than the resonance actual value $m_{f_2'(1525)} = 1538 \text{ MeV}$. The degeneracy relation in this nonet $m_{a_2}^2 = m_{f_{2,N}}^2$, implies $m_{f_{2,N}} = 1317 \text{ MeV}$, which is slightly larger than the experimental mass $m_{f_2(1270)} = 1297 \text{ MeV}$.

By introducing a small isoscalar mixing angle it is possible to explain the minor deviations of the two isoscalar-tensor states. The new masses were found by including the mixing presented in Table 3.5, which is also the summary table of masses of tensor and axial-tensor mesons.

Resonances	Masses (in MeV)	Resonances	Masses (in MeV)
$a_2(1320)$	1317	$\rho_2(?)$	1663
$K_2^*(1430)$	1427	$K_2(1820)$	1819
$f_2(1270)$	1297	ω_2	1663
$f_2'(1525)$	1538	ϕ_2	1971

Table 3.5: Masses of the spin-2 mesons within eLSM where the small mixing angle in the tensor sector and no mixing in the axial-tensor are considered. The PDG values are shown as bold numbers.

3.4 Results for $J^{PC} = 2^{++}$ mesons

In this part, we present the strong and radiative decay predictions of tensor mesons and compare them to the PDG data that is currently available.

3.4.1 Decay channel $T \rightarrow P^{(1)} + P^{(2)}$

The chiral Lagrangian of Eq. (3.12) is followed by the interaction Lagrangian characterizing the decay of spin-2 tensor mesons to two pseudoscalar mesons by applying the shift of Eq. (3.8):

$$\mathcal{L}_{tpp} = g_2^{\text{ten}} \text{Tr} \left[T^{\mu\nu} \{ (\partial_\mu \mathcal{P}), (\partial_\nu \mathcal{P}) \} \right] + \frac{g_2'^{\text{ten}}}{3} \text{Tr} \left[T^{\mu\nu} \right] \text{Tr} \left[\{ (\partial_\mu \mathcal{P}), (\partial_\nu \mathcal{P}) \} \right]. \quad (3.38)$$

In order to achieve the same normalization for the singlet state, the factor $1/3$ in front of the second term was selected in this form⁴. For $\lambda^0 = \sqrt{\frac{2}{3}}\mathbf{1}$ and the eight Gell-Mann matrices λ^a 's, tensor meson can be decomposed as

$$\sqrt{2}T_{\mu\nu} = \sum_{a=0}^8 T_{\mu\nu}^a \frac{\lambda^a}{\sqrt{2}} \rightarrow T_{\mu\nu} = \frac{1}{\sqrt{6}} T_{\mu\nu}^0 \mathbf{1} + \dots, \quad (3.39)$$

which leads to the Lagrangian for the singlet state as:

$$\mathcal{L}_{tpp} = (g_2^{\text{ten}} + g_2'^{\text{ten}}) T^{0\mu\nu} \text{Tr} \left[\{ (\partial_\mu \mathcal{P}), (\partial_\nu \mathcal{P}) \} \right] + \dots. \quad (3.40)$$

Correspondingly, the tree-level decay rate reads

$$\Gamma_{T \rightarrow P^{(1)} + P^{(2)}}(m_t, m_{p^{(1)}}, m_{p^{(2)}}) = \kappa_{tpp,i} \frac{|\vec{k}_{t,p^{(1)},p^{(2)}}|^5}{60 \pi m_t^2} \Theta(m_t - m_{p^{(1)}} - m_{p^{(2)}}), \quad (3.41)$$

where Table 3.6 lists the coefficients $\kappa_{tpp,i}$ with dimension [Energy⁻²] because of the dimensionful quantities w 's.

⁴This is a useful convention, but of course it does not affect the results.

Decay process	$\kappa_{Tpp,i}$
$a_2(1320) \rightarrow \bar{K} K$	$2 \left(\frac{g_2^{\text{ten}} Z_K^2 w_K^2}{2} \right)^2$
$a_2(1320) \rightarrow \pi \eta$	$\left(g_2^{\text{ten}} Z_\pi Z_{\eta_N} w_\pi w_{\eta_N} \cos \beta_P \right)^2$
$a_2(1320) \rightarrow \pi \eta'$	$\left(-g_2^{\text{ten}} Z_\pi Z_{\eta_N} w_\pi w_{\eta_N} \sin \beta_P \right)^2$
$K_2^*(1430) \rightarrow \pi \bar{K}$	$3 \left(\frac{g_2^{\text{ten}} Z_K w_K Z_\pi w_\pi}{2} \right)^2$
$f_2(1270) \rightarrow \bar{K} K$	$2 \left(\frac{Z_K^2 w_K^2 \left((4g_2^{\prime\text{ten}} + 3g_2^{\text{ten}}) \cos \beta_T + \sqrt{2}(2g_2^{\prime\text{ten}} + 3g_2^{\text{ten}}) \sin \beta_T \right)}{6} \right)^2$
$f_2(1270) \rightarrow \pi \pi$	$6 \left(\frac{Z_\pi^2 w_\pi^2 \left((2g_2^{\text{ten}} + 3g_2^{\text{ten}}) \cos \beta_T + \sqrt{2}g_2^{\prime\text{ten}} \sin \beta_T \right)}{6} \right)^2$
$f_2(1270) \rightarrow \eta \eta$	$2 \left(\frac{Z_{\eta_N}^2 w_{\eta_N}^2 \cos \beta_P^2 \left((2g_2^{\prime\text{ten}} + 3g_2^{\text{ten}}) \cos \beta_T + \sqrt{2}g_2^{\prime\text{ten}} \sin \beta_T \right) + Z_{\eta_S}^2 w_{\eta_S}^2 \sin \beta_P^2 \left(\sqrt{2}(g_2^{\prime\text{ten}} + 3g_2^{\text{ten}}) \sin \beta_T + 2g_2^{\prime\text{ten}} \cos \beta_T \right)}{6} \right)^2$
$f_2'(1525) \rightarrow \bar{K} K$	$2 \left(\frac{Z_K^2 w_K^2 \left(-(4g_2^{\prime\text{ten}} + 3g_2^{\text{ten}}) \sin \beta_T + \sqrt{2}(2g_2^{\prime\text{ten}} + 3g_2^{\text{ten}}) \cos \beta_T \right)}{6} \right)^2$
$f_2'(1525) \rightarrow \pi \pi$	$6 \left(\frac{Z_\pi^2 w_\pi^2 \left(-(2g_2^{\prime\text{ten}} + 3g_2^{\text{ten}}) \sin \beta_T + \sqrt{2}g_2^{\prime\text{ten}} \cos \beta_T \right)}{6} \right)^2$
$f_2'(1525) \rightarrow \eta \eta$	$2 \left(\frac{Z_{\eta_N}^2 w_{\eta_N}^2 \cos \beta_P^2 \left(-(2g_2^{\prime\text{ten}} + 3g_2^{\text{ten}}) \sin \beta_T + \sqrt{2}g_2^{\prime\text{ten}} \cos \beta_T \right) + Z_{\eta_S}^2 w_{\eta_S}^2 \sin \beta_P^2 \left(\sqrt{2}(g_2^{\prime\text{ten}} + 3g_2^{\text{ten}}) \cos \beta_T - 2g_2^{\prime\text{ten}} \sin \beta_T \right)}{6} \right)^2$

Table 3.6: Clebsch-Gordan coefficients for $T \rightarrow P^{(1)} + P^{(2)}$.

During the fitting procedure, we have considered g_2^{ten} , $g_2^{\prime\text{ten}}$ and the isoscalar mixing angle β_T . The fit results are:

$$\begin{aligned}
 g_2^{\text{ten}} &= (1.392 \pm 0.024) \cdot 10^4 (\text{MeV}), \\
 g_2^{\prime\text{ten}} &= (0.024 \pm 0.041) \cdot 10^4 (\text{MeV}), \\
 \beta_T &= (3.16 \pm 0.81)^\circ.
 \end{aligned} \tag{3.42}$$

These results support the large- N_c predictions that the coupling constant $g_2^{\prime\text{ten}}$ is considerably smaller than g_2^{ten} . In this particular case, it is also compatible with zero because of the relatively large error. Yet, in general, the phenomenology of large- N_c suppressed decay (such as the decays of the J/ψ ; see [125]) reveals that such terms, even though small, do not disappear.

Decay process (in model)	eLSM (MeV)	PDG (MeV)
$a_2(1320) \rightarrow \bar{K} K$	4.06 ± 0.14	$7.0_{-1.5}^{+2.0} \leftrightarrow (4.9 \pm 0.8)\%$
$a_2(1320) \rightarrow \pi \eta$	25.37 ± 0.87	$18.5 \pm 3.0 \leftrightarrow (14.5 \pm 1.2)\%$
$a_2(1320) \rightarrow \pi \eta'(958)$	1.01 ± 0.03	$0.58 \pm 0.10 \leftrightarrow (0.55 \pm 0.09)\%$
$K_2^*(1430) \rightarrow \pi \bar{K}$	44.82 ± 1.54	$49.9 \pm 1.9 \leftrightarrow (49.9 \pm 0.6)\%$
$f_2(1270) \rightarrow \bar{K} K$	3.54 ± 0.29	$8.5 \pm 0.8 \leftrightarrow (4.6_{-0.4}^{+0.5})\%$
$f_2(1270) \rightarrow \pi \pi$	168.82 ± 3.89	$157.2_{-1.1}^{+4.0} \leftrightarrow (84.2_{-0.9}^{+2.9})\%$
$f_2(1270) \rightarrow \eta \eta$	0.67 ± 0.03	$0.75 \pm 0.14 \leftrightarrow (0.4 \pm 0.08)\%$
$f_2'(1525) \rightarrow \bar{K} K$	23.72 ± 0.60	$75 \pm 4 \leftrightarrow (87.6 \pm 2.2)\%$
$f_2'(1525) \rightarrow \pi \pi$	0.67 ± 0.14	$0.71 \pm 0.14 \leftrightarrow (0.83 \pm 0.16)\%$
$f_2'(1525) \rightarrow \eta \eta$	1.81 ± 0.05	$9.9 \pm 1.9 \leftrightarrow (11.6 \pm 2.2)\%$

Table 3.7: Decay rates for $T \rightarrow P^{(1)} + P^{(2)}$ compared to PDG [27].

The following prediction is also obtained, but it was not included in the fit because of the large experimental uncertainty.

$$\text{eLSM : } \Gamma [K_2^*(1430) \rightarrow \eta \bar{K}] = (1.13 \pm 0.03) \cdot 10^{-3} \text{ MeV, PDG : } 0.15_{-0.10}^{+0.34} \text{ MeV.} \quad (3.43)$$

We observe that our predicted value is in the same range as the PDG [27].

Interestingly, the isospin mixing angle $\beta_T = 3.16^\circ$ obtained from the fit of the decays is not far from the PDG value $\beta_T = 5.7^\circ$ obtained from the mass formula

$$\beta_T = 35.3^\circ - \arctan \left(\sqrt{\frac{4m_{K_2}^2 - m_{a_2}^2 - 3m_{f_2'}^2}{-4m_{K_2}^2 + m_{a_2}^2 + 3m_{f_2}^2}} \right). \quad (3.44)$$

Even if some of the experimental entries conflict with those in Table 3.7, the findings demonstrate a general good qualitative agreement ($\chi_{\text{red}}^2 = 37$). It is important to keep in mind that only three parameters were used, and the experimental data are fairly accurate. The main deviations from the experiment are related to the decay rates $f_2(1270) \rightarrow \bar{K} K$, $f_2'(1525) \rightarrow \bar{K} K$ and $f_2'(1525) \rightarrow \eta \eta$. For a more accurate description

of the tensor decays, additional large- N_c suppressed terms and flavor-symmetry-breaking contributions would be required.

It is worth mentioning that, considering the following form factor within the decay rate in Eq. (3.41) (see Ref. [67])

$$\exp\left(-\frac{|\vec{k}_{t,p^{(1)},p^{(2)}}|^2}{8\Lambda^2}\right), \quad (3.45)$$

does not improve the results. For simplicity, I choose $g_2'^{\text{ten}} = 0$ (it is anyhow subleading) and show the χ^2 - Λ dependence in Fig. 3.1. This fitting does not improve the

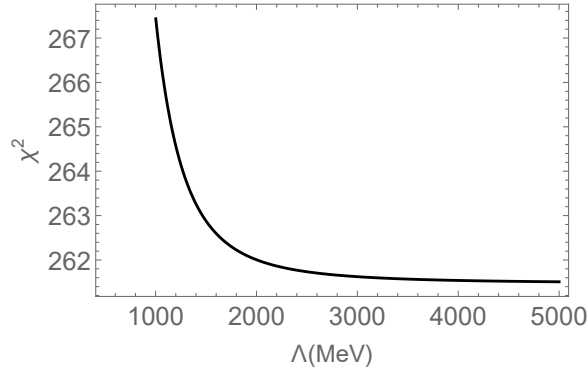


Figure 3.1: χ^2 dependence on Λ for $g_2'^{\text{ten}} = 0$.

overall results since at large values of Λ and the χ^2 becomes identical to the previous fit result in Table 3.7. On the other hand, the results get worse for smaller Λ .

3.4.2 Decay channel $T \rightarrow V_1 + P$

The decays of the tensor mesons into a vector-pseudoscalar pair are also experimentally measured. They can be described within the following Lagrangian, which is obtained from Eq. (3.17) by taking into account the shift of Eq. (3.7):

$$\mathcal{L}_{tvp} = (c_1^{\text{ten}} + c_2^{\text{ten}}) \varepsilon_{\mu\nu\rho\sigma} \text{Tr} \left[\partial^\mu T^{\nu\alpha} \left(\partial^\rho V_1^\sigma (\partial_\alpha P) \Phi_0 - \Phi_0 (\partial_\alpha P \partial^\rho V_1^\sigma) \right) \right]. \quad (3.46)$$

The tree-level decay rate formula reads

$$\Gamma_{T \rightarrow V+P}(m_t, m_v, m_p) = \frac{c^{\text{ten}2} |\vec{k}_{t,v,p}|^5}{40 \pi} \kappa_{tvp,i} \Theta(m_t - m_v - m_p), \quad (3.47)$$

where $c^{\text{ten}} := c_1^{\text{ten}} + c_2^{\text{ten}}$ and the dimensionful factors $\kappa_{tvp,i}$ are given in Table 3.8.

We use a χ^2 -fit to the data in Table 3.8 to determine the coupling's value, c^{ten} :

$$c^{\text{ten}} = (4.8 \pm 0.9) \cdot 10^{-7} (\text{MeV})^{-3}, \quad (3.48)$$

that leads to the model estimations of the decay widths in Table 3.8. They are in good agreement with PDG and provide an extra prediction ($f_2'(1525) \rightarrow \bar{K}^*(892) K + \text{c.c.}$).

Decay process (in model)	$\kappa_{tvp,i}$	eLSM (MeV)	PDG (MeV)
$a_2(1320) \rightarrow \rho(770) \pi$	$2\left(\frac{\phi_N}{4}\right)^2$	71.0 ± 2.6	$73.61 \pm 3.35 \leftrightarrow (70.1 \pm 2.7)\%$
$K_2^*(1430) \rightarrow \bar{K}^*(892) \pi$	$3\left(\frac{\phi_N}{8}\right)^2$	27.9 ± 1.0	$26.92 \pm 2.14 \leftrightarrow (24.7 \pm 1.6)\%$
$K_2^*(1430) \rightarrow \rho(770) K$	$3\left(\frac{\sqrt{2}\phi_S}{8}\right)^2$	10.3 ± 0.4	$9.48 \pm 0.97 \leftrightarrow (8.7 \pm 0.8)\%$
$K_2^*(1430) \rightarrow \omega(782) \bar{K}$	$\left(\frac{-\phi_S \cos \beta_V + \phi_N \sin \beta_V}{4\sqrt{2}}\right)^2$	3.5 ± 0.1	$3.16 \pm 0.88 \leftrightarrow (2.9 \pm 0.8)\%$
$f_2'(1525) \rightarrow \bar{K}^*(892) K + \text{c.c.}$	$4\left(\frac{2\phi_S \cos \beta_T + \phi_N \sin \beta_T}{8}\right)^2$	19.89 ± 0.73	

Table 3.8: Clebsch-Gordan coefficients and corresponding decay rates for $T \rightarrow P + V$ compared to PDG [27].

3.4.3 Decay channel $T \rightarrow \gamma + P$

The following Lagrangian is obtained from Eq. (3.17) and VMD shift of Eq. (3.15)

$$\mathcal{L}_{t\gamma p} = \frac{e}{g_\rho} c^{\text{ten}} \text{Tr} \left[\partial^\mu T^{\nu\alpha} \left(F_{\mu\nu} Q(\partial_\alpha P) \Phi_0 - \Phi_0 (\partial_\alpha P F_{\mu\nu} Q) \right) \right], \quad (3.49)$$

which leads to the decay rate

$$\Gamma_{T \rightarrow \gamma + P}(m_t, m_p) = \frac{c^{\text{ten}2} |\vec{k}_{t,\gamma,p}|^5}{40 \pi} \kappa_{t\gamma p,i} \Theta(m_t - m_p). \quad (3.50)$$

We use the couplings c^{ten} , g_ρ (and their errors) in order to evaluate the theoretical errors in the radiative decay rates presented in Table 3.9 via the following expression:

$$\delta \Gamma_{T \rightarrow \gamma P}(m_t, m_p) = \sqrt{\left(\frac{\partial \Gamma_{T \rightarrow \gamma P}(m_t, m_p)}{\partial c^{\text{ten}}} \delta c^{\text{ten}} \right)^2 + \left(\frac{\partial \Gamma_{T \rightarrow \gamma P}(m_t, m_p)}{\partial g_\rho} \delta g_\rho \right)^2}. \quad (3.51)$$

Decay process (in model)	$\kappa_{t\gamma p,i}$	eLSM	PDG
$K_2^\pm(1430) \rightarrow \gamma K^\pm$	$\frac{e^2}{g_\rho^2} \left(\frac{\phi_N + 2\sqrt{2}\phi_S}{12} \right)^2$	$1.12 \pm 0.47 \text{ MeV}$	$0.24 \pm 0.05 \text{ MeV}$
$K_2^0(1430) \rightarrow \gamma K^0$	$\frac{e^2}{g_\rho^2} \left(\frac{\phi_N - \sqrt{2}\phi_S}{12} \right)^2$	$5.1 \pm 2.2 \text{ keV}$	$< 5.4 \text{ keV}$
$a_2^\pm(1320) \rightarrow \gamma \pi^\pm$	$\frac{e^2}{g_\rho^2} \left(\frac{\phi_N}{4} \right)^2$	$1.01 \pm 0.43 \text{ MeV}$	$0.31 \pm 0.03 \text{ MeV}$

Table 3.9: Clebsch-Gordan coefficients and corresponding decay rates for $T \rightarrow \gamma + P$ compared to PDG [27].

In Table 3.9 our results for the photon-pseudoscalar decays are presented. Despite the large errors, they are somewhat larger but qualitatively consistent with the PDG results.

3.4.4 Decay channel $T \rightarrow \gamma + V_1$

We move to the next radiative decay of the tensor mesons through the two-photon decays. We first observe that the following vector-vector interaction term is part of the chiral Lagrangian of Eq. (3.14):

$$\mathcal{L}_{t\gamma\gamma} = a^{\text{ten}} \text{Tr} [T_{\mu\nu} \{V_{1\beta'}^\mu, V_1^{\nu\beta}\}] + \frac{a'^{\text{ten}}}{3} \text{Tr} [T_{\mu\nu}] \text{Tr} [\{V_{1\beta'}^\mu, V_1^{\nu\beta}\}]. \quad (3.52)$$

Applying the VMD shift (3.15) for both vector fields, we obtain the Lagrangian

$$\mathcal{L}_{t\gamma\gamma} = a^{\text{ten}} \frac{e^2}{g_\rho^2} \text{Tr} [T_{\mu\nu} \{QF_\beta^\mu, QF^{\nu\beta}\}] + \frac{a'^{\text{ten}}}{3} \frac{e^2}{g_\rho^2} \text{Tr} [T_{\mu\nu}] \text{Tr} [\{QF_\beta^\mu, QF^{\nu\beta}\}], \quad (3.53)$$

whose corresponding $\gamma\gamma$ decay rate reads

$$\Gamma_{T \rightarrow \gamma\gamma} = \frac{e^4}{g_\rho^4} \frac{2|\vec{k}|^5}{5\pi m_t^2} \kappa_{t\gamma\gamma,i} = \frac{e^4}{g_\rho^4} \frac{m_t^3}{80\pi} \kappa_{t\gamma\gamma,i}, \quad (3.54)$$

where we used $m_t = 2|\vec{k}|$ to get the r.h.s. of the above equation.

Using the typical χ^2 technique, employing the three experimental data points in Table 3.10 with two free parameters a^{ten} and a'^{ten} and keeping the mixing angle

$\beta_T = 3.16^\circ$ unchanged, results in:

$$a^{\text{ten}} = (-2.09 \pm 0.06) \cdot 10^{-2} (\text{MeV})^{-1}, \quad a'^{\text{ten}} = (3.5 \pm 0.4) \cdot 10^{-3} (\text{MeV})^{-1}. \quad (3.55)$$

We present our model results in Table 3.10. The results confirm that the mixing angle $\beta_T = 3.16^\circ$ is consistent with data in this channel as well. In line with the expectations of the large- N_c limit, the parameter a'^{ten} also turns out to be considerably smaller than a^{ten} .

Decay process (in model)	$\kappa_{t\gamma\gamma,i}$	eLSM (keV)	PDG (keV)
$a_2(1320) \rightarrow \gamma\gamma$	$\frac{a^{\text{ten}2}}{36}$	1.01 ± 0.06	1.00 ± 0.06
$f_2(1270) \rightarrow \gamma\gamma$	$\left(\frac{(5a^{\text{ten}} + 4a'^{\text{ten}}) \cos \beta_T + \sqrt{2}(a^{\text{ten}} + 2a'^{\text{ten}}) \sin \beta_T}{18} \right)^2$	1.95 ± 0.10	2.6 ± 0.5
$f_2'(1525) \rightarrow \gamma\gamma$	$\left(\frac{-(5a^{\text{ten}} + 4a'^{\text{ten}}) \sin \beta_T + \sqrt{2}(a^{\text{ten}} + 2a'^{\text{ten}}) \cos \beta_T}{18} \right)^2$	0.083 ± 0.009	0.082 ± 0.009

Table 3.10: Clebsch-Gordan coefficients and corresponding decay rates for $T \rightarrow \gamma\gamma$ compared to PDG [27].

The following Lagrangian, which describes the decay into a vector-photon pair, is obtained from Eq. (3.52) by VMD shifting only one vector field:

$$\mathcal{L}_{t\gamma V} = 2a^{\text{ten}} \frac{e}{g_\rho} \text{Tr} [T_{\mu\nu} \{QF_\beta^\mu, V_1^{\nu\beta}\}] + \frac{2a'^{\text{ten}}}{3} \frac{e}{g_\rho} \text{Tr} [T_{\mu\nu}] \text{Tr} [\{QF_\beta^\mu, V_1^{\nu\beta}\}]. \quad (3.56)$$

The decay rate into a vector-photon pair is expressed as

$$\Gamma_{T \rightarrow \gamma + V_1}(m_t, m_v) = \frac{\kappa_{t\gamma v,i} e^2}{15 \pi m_t^2 m_v^2 g_\rho^2} \left(3|\vec{k}_{t,v,\gamma}|^7 + 5|\vec{k}_{v,\gamma}|^3 m_v^2 + 5|\vec{k}_{t,v,\gamma}|^4 m_v^2 \sqrt{|\vec{k}_{t,v,\gamma}|^2 + m_v^2} + |\vec{k}_{t,v,\gamma}|^5 (10m_v^2 - 3(|\vec{k}_{t,v,\gamma}|^2 + m_v^2)) \right). \quad (3.57)$$

The related coefficients $\kappa_{t\gamma v,i}$ are included in Table 3.11 and Table 3.12, which display the numerical predictions for the decay rates. Note, while estimating the theoretical errors, we consider $g_\rho = 5.5 \pm 0.5$ together with the ones in Eq. (3.55).

Decay process (in model)	$\kappa_{T\gamma v, i}$
$a_2(1320) \rightarrow \rho(770) \gamma$	$\left(\frac{a^{\text{ten}}}{6}\right)^2$
$a_2^0(1320) \rightarrow \omega(782) \gamma$	$\left(\frac{a^{\text{ten}} \cos \beta_V}{2}\right)^2$
$a_2(1320) \rightarrow \phi(1020) \gamma$	$\left(\frac{a^{\text{ten}} \sin \beta_V}{2}\right)^2$
$K_2^{*\pm}(1430) \rightarrow \bar{K}^{*\pm}(892) \gamma$	$\left(\frac{a^{\text{ten}}}{6}\right)^2$
$K_2^{*0}(1430) \rightarrow \bar{K}^{*0}(892) \gamma$	$\left(\frac{a^{\text{ten}}}{3}\right)^2$
$f_2(1270) \rightarrow \rho(770) \gamma$	$\left(\frac{(a^{\text{ten}} + 2a'^{\text{ten}}) \cos \beta_T + \sqrt{2}a'^{\text{ten}} \sin \beta_T}{2}\right)^2$
$f_2(1270) \rightarrow \omega(782) \gamma$	$\left(\frac{\cos \beta_V ((a^{\text{ten}} + 2a'^{\text{ten}}) \cos \beta_T + \sqrt{2}a'^{\text{ten}} \sin \beta_T) - 2 \sin \beta_V ((a^{\text{ten}} + a'^{\text{ten}}) \sin \beta_T + \sqrt{2}a'^{\text{ten}} \cos \beta_T)}{6}\right)^2$
$f_2(1270) \rightarrow \phi(1020) \gamma$	$\left(\frac{\sin \beta_V ((a^{\text{ten}} + 2a'^{\text{ten}}) \cos \beta_T + \sqrt{2}a'^{\text{ten}} \sin \beta_T) + 2 \cos \beta_V ((a^{\text{ten}} + a'^{\text{ten}}) \sin \beta_T + \sqrt{2}a'^{\text{ten}} \cos \beta_T)}{6}\right)^2$
$f_2'(1525) \rightarrow \rho(770) \gamma$	$\left(\frac{-(a^{\text{ten}} + 2a'^{\text{ten}}) \sin \beta_T + \sqrt{2}a'^{\text{ten}} \cos \beta_T}{2}\right)^2$
$f_2'(1525) \rightarrow \omega(782) \gamma$	$\left(\frac{\sin \beta_T (-(a^{\text{ten}} + 2a'^{\text{ten}}) \cos \beta_V + 2\sqrt{2}a'^{\text{ten}} \sin \beta_V) + \cos \beta_T (\sqrt{2}a'^{\text{ten}} \cos \beta_V - 2(a^{\text{ten}} + a'^{\text{ten}}) \sin \beta_V)}{6}\right)^2$
$f_2'(1525) \rightarrow \phi(1020) \gamma$	$\left(\frac{\cos \beta_T (-2(a^{\text{ten}} + a'^{\text{ten}}) \cos \beta_V - \sqrt{2}a'^{\text{ten}} \sin \beta_V) + \sin \beta_T (2\sqrt{2}a'^{\text{ten}} \cos \beta_V + (a^{\text{ten}} + 2a'^{\text{ten}}) \sin \beta_V)}{6}\right)^2$

Table 3.11: Clebsch-Gordan coefficients for $T \rightarrow \gamma + V_1$.

For the sake of simplicity, additional sources of inaccuracy, such as mass uncertainty, were neglected. Because of this, the actual errors can be slightly larger but still in line with those listed in Table 3.12.

3.4.5 Decay channel $T \rightarrow V_1^{(1)} + V_1^{(2)}$

Our last results for the decay of tensor mesons are related to the Lagrangians in Eq. (3.12) and Eq. (3.14). We have the following data from the PDG:

$$\text{PDG} : \Gamma[f_2(1270) \rightarrow \pi^+ \pi^- 2\pi^0] \approx 19.5 \text{ MeV};$$

$$\text{PDG} : \Gamma[a_2(1320) \rightarrow \omega(782) \pi \pi] \approx 11.3 \text{ MeV};$$

$$\text{PDG} : \Gamma[K_2^*(1430) \rightarrow K^*(892) \pi \pi] = 13.5 \pm 2.3 \text{ MeV}.$$

The vector-vector decay modes $\rho(770)\rho(770)$, $\omega(782)\rho(770)$, and $K^*(892)\rho(770)$, in which the $\rho(770)$ meson further decays into two pions, provide a reasonable interpretation of these decays. In order to describe them, we introduce the properly normalized

Decay process (in model)	Decay Width (MeV)
$a_2(1320) \rightarrow \rho(770) \gamma$	0.22 ± 0.04
$a_2^0(1320) \rightarrow \omega(782) \gamma$	1.94 ± 0.04
$a_2(1320) \rightarrow \phi(1020) \gamma$	0.0024 ± 0.0005
$K_2^{*\pm}(1430) \rightarrow \bar{K}^{*\pm}(892) \gamma$	0.23 ± 0.04
$K_2^{*0}(1430) \rightarrow \bar{K}^{*0}(892) \gamma$	0.94 ± 0.18
$f_2(1270) \rightarrow \rho(770) \gamma$	0.70 ± 0.17
$f_2(1270) \rightarrow \omega(782) \gamma$	0.068 ± 0.017
$f_2(1270) \rightarrow \phi(1020) \gamma$	0.007 ± 0.002
$f_2'(1525) \rightarrow \rho(770) \gamma$	0.32 ± 0.08
$f_2'(1525) \rightarrow \omega(782) \gamma$	0.012 ± 0.005
$f_2'(1525) \rightarrow \phi(1020) \gamma$	0.61 ± 0.12

Table 3.12: Radiative decay rates for $T \rightarrow \gamma + V_1$.

“Sill” spectral function discussed in Ref. [126] for the ρ -meson as

$$d_\rho(y) = \frac{2y}{\pi} \frac{\sqrt{y^2 - 4m_\pi^2} \tilde{\Gamma}_\rho}{(y^2 - m_\rho^2)^2 + (\sqrt{y^2 - 4m_\pi^2} \tilde{\Gamma}_\rho)^2} \Theta(y - 2m_\pi), \quad \int_0^\infty dy d_\rho(y) = 1, \quad (3.58)$$

where the definition of $\tilde{\Gamma}_\rho$ is

$$\tilde{\Gamma}_\rho \equiv \frac{\Gamma_{\rho \rightarrow 2\pi} m_\rho}{\sqrt{m_\rho^2 - 4m_\pi^2}}, \quad (3.59)$$

with the PDG values $\Gamma_{\rho \rightarrow 2\pi} = 149.1$ MeV and $m_\rho = 775.11$ MeV.

The Sill spectral function is chosen because of the following advantages: it is normalized even for broad states, it has a vanishing real part contribution of virtual particles, and it takes into account the decay threshold. For further details, see Ref. [126].

We provide the following estimates by taking into account destructive interference between the relevant amplitudes (the constructive one leads to extremely large decay

rates):

$$\Gamma_{f_2 \rightarrow \rho \rho \rightarrow 4\pi} \simeq \int_0^\infty dy_1 d_\rho(y_1) \int_0^\infty dy_2 d_\rho(y_2) \Gamma_{f_2 \rightarrow \rho \rho}(m_{f_2}, y_1, y_2) \approx 29.9 \text{ MeV}; \quad (3.60)$$

$$\Gamma_{a_2 \rightarrow \omega \rho \rightarrow \omega 2\pi} \simeq \int_0^\infty dy_1 d_\rho(y_1) \Gamma_{a_2 \rightarrow \rho \omega}(m_{a_2}, m_{\omega_1}, y_1) \approx 11.1 \text{ MeV}; \quad (3.61)$$

$$\Gamma_{K_2 \rightarrow K^* \rho \rightarrow K 2\pi} \simeq \int_0^\infty dy_1 d_\rho(y_1) \Gamma_{K_2 \rightarrow \rho \omega}(m_{K_2}, m_{K_1}, y_1) \approx 6.6 \text{ MeV}. \quad (3.62)$$

Given that no new parameter is required, it is interesting that the results are qualitatively consistent with the experimental data. In fact, this is a complex process that includes the integral over the spectrum function of the ρ -meson and the destructive interference of two different interaction terms coming from different Lagrangians.

3.5 Results for $J^{PC} = 2^{--}$ mesons

In this subsection, we present the chiral model predictions for the decay rates of the ground-state mesons with $J^{PC} = 2^{--}$. Furthermore, comparisons with existing LQCD and other theoretical results are given.

3.5.1 Decay channel $A_2 \rightarrow V_1 + P$

The decay of axial-tensor mesons into a vector-pseudoscalar pair is contained in the chiral Lagrangian (3.12):

$$\mathcal{L}_{a_2 vp} = g_2^{\text{ten}} \text{Tr} \left[A_2^{\mu\nu} \{ (\partial_\mu \mathcal{P}), V_{1\nu} \} \right]. \quad (3.63)$$

The corresponding tree-level decay rate reads:

$$\Gamma_{A_2 \rightarrow V_1 + P}(m_{a_2}, m_v, m_p) = \frac{g_2^{\text{ten}2} |\vec{k}_{a_2, v, p}|^3}{120 \pi m_{a_2}^2} \left(5 + \frac{2 |\vec{k}_{a_2, v, p}|^2}{m_v^2} \right) \kappa_{a_2 vp, i} \Theta(m_{a_2} - m_v - m_p), \quad (3.64)$$

where the $\kappa_{a_2vp,i}$ are listed in Table 3.14. Table 3.14 shows rather large results for decay widths. For a number of reasons, we might consider our findings to be qualitative:

1. the data of the tensor mesons alone determines the intensity of the interaction of axial-tensors. Although, in line with chiral symmetry, no modifications have been implemented in the (axial-)tensor sector, chiral symmetry breaking effects can be noticeable between 1-2 GeV;
2. the decays of axial-tensor states depend on variables of the kind $(Zw)^2 \propto g_1^4$ (as seen from the Tables 3.14 and 3.2), therefore even a tiny variation in these parameters of the initial eLSM leads to a significant variation in the outcomes. Since a 20% uncertainty is estimated in Z 's that implies a factor 2 in decay rates;
3. it is assumed that the parameter g_1 , along with others like g_2^{ten} , is a constant over a wide range of energies; however, it is plausible to suppose that it has a (soft) energy dependence. Also, in this scenario, even a minor variation would have a significant impact on the results of Table 3.14.

In conclusion, it can be said that the chosen parameters, especially g_1 , represent a significant and challenging source of uncertainty in the decays of axial-tensor states. To be fair, we thus assume an error for the presented values in Table 3.14 of roughly 50%.

For the ρ_2 , $\omega_{2,N} \simeq \omega_2$, and $\omega_{2,S} \simeq \phi_2$, experimental data is not available, while for the kaonic member of the axial-tensors, it is believed to be a mixture of the resonances $K_2(1820)$ and $K_2(1770)$. This is an analogous mixing between the axial-vector and pseudovector kaonic mesons described in Eq. (2.71).

Assuming that K_{2A} is mostly located in $K_2(1820)$, the decay width for the K_{2A} state described in our model is almost twice as wide as the experimentally observed decay of $K_2(1820)$. This implies that the left sides of Table 3.14 range for the K_{2A} state are preferred.

By comparing our outcomes with the lattice QCD data shown in Table 3.13, this interpretation may be applied to the remaining decay rates. Namely, the outcomes are of the same order of magnitude as the LQCD results but are around 2-3 times greater. This comparison confirms that the lower part of the range of each decay mode of the eLSM should be favored, despite the significant uncertainty in both methods.

Decay process (in model)	eLSM (MeV)	LQCD (MeV) [28]
$\rho_2(?) \rightarrow \rho(770) \eta$	≈ 30	
$\rho_2(?) \rightarrow \bar{K}^*(892) K + \text{c.c.}$	≈ 27	36
$\rho_2(?) \rightarrow \omega(782) \pi$	≈ 122	125
$\rho_2(?) \rightarrow \phi(1020) \pi$	≈ 0.3	
$K_{2,A} \rightarrow \rho(770) K$	≈ 53	
$K_{2,A} \rightarrow \bar{K}^*(892) \pi$	≈ 87	
$K_{2,A} \rightarrow \bar{K}^*(892) \eta$	≈ 0.004	
$K_{2,A} \rightarrow \omega(782) \bar{K}$	≈ 13.8	
$K_{2,A} \rightarrow \phi(1020) \bar{K}$	≈ 13.7	
$\omega_{2,N} \rightarrow \rho(770) \pi$	≈ 363	365
$\omega_{2,N} \rightarrow \bar{K}^*(892) K + \text{c.c.}$	≈ 25	36
$\omega_{2,N} \rightarrow \omega(782) \eta$	≈ 27	17
$\omega_{2,N} \rightarrow \phi(1020) \eta$	≈ 0.02	
$\omega_{2,S} \rightarrow \bar{K}^*(892) K + \text{c.c.}$	≈ 100	148
$\omega_{2,S} \rightarrow \omega(782) \eta$	≈ 0.2	
$\omega_{2,S} \rightarrow \omega(782) \eta'(958)$	≈ 0.02	
$\omega_{2,S} \rightarrow \phi(1020) \eta$	≈ 17	44

Table 3.13: Decay rates for $A_2 \rightarrow V_1 + P$ compared to LQCD results [28].

In order to further check our results, we perform an additional fit to the decay rates obtained in LQCD simulations, which yields

$$g_{2\text{lat}}^{\text{ten}} \simeq (0.7 \pm 0.4) \cdot 10^4 (\text{MeV}), \quad (3.65)$$

where we assumed of 50 % error in [28]. The result is about two sigmas away from the former result in Eq. (3.42)⁵. The corresponding decays are given in Table 3.13. It's rather intriguing that the different results all match each other, indicating that any

⁵It should be noted that the lowest pseudoscalar meson in the $SU(3)$ flavor symmetry-based LQCD analysis has a mass of around 700 MeV.

ratio of decays generated using lattice data agrees with the appropriate eLSM ratio. Future lattice results could be useful to compare other decay channels too.

In conclusion, the result of our theoretical investigation is quite evident: even when assuming the lower limit of our estimations, the axial-tensor states are anticipated to be broad, despite the fact that there are still significant uncertainties. This information may eventually explain why the hypothesized states ρ_2 , ω_2 , and ϕ_2 have not yet been experimentally seen.

Decay process (in model)	$\kappa_{a_2vp,i}$	eLSM (MeV)
$\rho_2(?) \rightarrow \rho(770) \eta$	$\left(-w_{\eta_N} Z_{\eta_N} \cos \beta_P\right)^2$	$\approx 99 \pm 50$
$\rho_2(?) \rightarrow \bar{K}^*(892) K + \text{c.c.}$	$4\left(\frac{Z_K w_K}{2}\right)^2$	$\approx 85 \pm 43$
$\rho_2(?) \rightarrow \omega(782) \pi$	$\left(-w_\pi Z_\pi \cos \beta_V\right)^2$	$\approx 419 \pm 210$
$\rho_2(?) \rightarrow \phi(1020) \pi$	$\left(w_\pi Z_\pi \sin \beta_V\right)^2$	≈ 0.8
$K_{2,A} \rightarrow \rho(770) K$	$3\left(\frac{Z_K w_K}{2}\right)^2$	$\approx 195 \pm 98$
$K_{2,A} \rightarrow \bar{K}^*(892) \pi$	$3\left(\frac{Z_\pi w_\pi}{2}\right)^2$	$\approx 316 \pm 158$
$K_{2,A} \rightarrow \bar{K}^*(892) \eta$	$\left(-\frac{1}{2}(\sqrt{2}Z_{\eta_S} w_{\eta_S} \sin \beta_P + Z_{\eta_N} w_{\eta_N} \cos \beta_P)\right)^2$	≈ 0.01
$K_{2,A} \rightarrow \omega(782) \bar{K}$	$\left(-\frac{w_K Z_K}{2}(\sqrt{2} \sin \beta_V + \cos \beta_V)\right)^2$	$\approx 51 \pm 26$
$K_{2,A} \rightarrow \phi(1020) \bar{K}$	$\left(\frac{w_K Z_K}{2}(-\sqrt{2} \cos \beta_V + \sin \beta_V)\right)^2$	$\approx 50 \pm 25$
$\omega_{2,N} \rightarrow \rho(770) \pi$	$3\left(-Z_\pi w_\pi\right)^2$	$\approx 1314 \pm 657$
$\omega_{2,N} \rightarrow \bar{K}^*(892) K + \text{c.c.}$	$4\left(-\frac{Z_K w_K}{2}\right)^2$	$\approx 85 \pm 43$
$\omega_{2,N} \rightarrow \omega(782) \eta$	$\left(Z_{\eta_N} w_{\eta_N} \cos \beta_P \cos \beta_V\right)^2$	$\approx 93 \pm 47$
$\omega_{2,N} \rightarrow \phi(1020) \eta$	$\left(Z_{\eta_N} w_{\eta_N} \cos \beta_P \sin \beta_V\right)^2$	≈ 0.06
$\omega_{2,S} \rightarrow \bar{K}^*(892) K + \text{c.c.}$	$4\left(-\frac{Z_K w_K}{\sqrt{2}}\right)^2$	$\approx 510 \pm 255$
$\omega_{2,S} \rightarrow \omega(782) \eta$	$\left(-\sqrt{2}Z_{\eta_S} w_{\eta_S} \sin \beta_P \sin \beta_V\right)^2$	$\approx 1.0 \pm 0.5$
$\omega_{2,S} \rightarrow \omega(782) \eta'(958)$	$\left(-\sqrt{2}Z_{\eta_S} w_{\eta_S} \cos \beta_P \sin \beta_V\right)^2$	≈ 0.3
$\omega_{2,S} \rightarrow \phi(1020) \eta$	$\left(-\sqrt{2}Z_{\eta_S} w_{\eta_S} \cos \beta_V \sin \beta_P\right)^2$	$\approx 101 \pm 51$

Table 3.14: Clebsch-Gordan coefficients and corresponding decay rates for $A_2 \rightarrow V_1 + P$.

3.5.2 Decay channel $A_2 \rightarrow A_1 + P$

The decay of the axial-tensor mesons into an axial-vector and pseudoscalar pair is contained in the chiral Lagrangian of Eq. (3.17):

$$\mathcal{L}_{a_2 a_1 P} = c'^{\text{ten}} \varepsilon_{\mu\nu\rho\sigma} \text{Tr} \left[\partial^\mu A_2^{\nu\alpha} \left((\partial^\rho A_1^\sigma) (\partial_\alpha P) \Phi_0 - \Phi_0 (\partial_\alpha P) (\partial^\rho A_1^\sigma) \right) \right]. \quad (3.66)$$

The tree-level decay rate reads:

$$\Gamma_{A_2 \rightarrow A_1 + P}(m_{a_2}, m_{a_1}, m_P) = \frac{c'^{\text{ten}2} |\vec{k}_{a_2, a_1, P}|^5}{40 \pi} \kappa_{a_2 a P, i} \Theta(m_{a_2} - m_{a_1} - m_P), \quad (3.67)$$

where $c'^{\text{ten}} := c_1^{\text{ten}} - c_2^{\text{ten}}$ and $\kappa_{a_2 a P, i}$ as well as the theoretical predictions proportional to the factor $\frac{c'^{\text{ten}}}{c^{\text{ten}}}$ are given in Table 3.15 under the assumption that that $K_{1A} \approx K_1(1400)$.

Note, the presence of two components proportional to c_1^{ten} and c_2^{ten} in the main Lagrangian of Eq. (3.17), results in their sum ($c_1^{\text{ten}} + c_2^{\text{ten}}$) and difference ($c_1^{\text{ten}} - c_2^{\text{ten}}$) for tensors and axial-tensors, respectively. In this situation, the decay of the tensor mesons does not fix the coupling for the axial-tensors. In spite of this, it is fair to assume that c'^{ten} is of the same order as c^{ten} , which leads to relatively narrow partial decay widths. Interestingly, under the assumption of $c'^{\text{ten}} \simeq c^{\text{ten}}$, our result for the decay channel $\rho_2 \rightarrow a_1(1260)\pi$ is remarkably close to the prediction in Ref. [88].

Decay process (in model)	$\kappa_{a_2 a P, i}$	eLSM (MeV)
$\rho_2(?) \rightarrow a_1(1260) \pi$	$2 \left(\frac{\phi_N}{4} \right)^2$	$\simeq 13 \left(\frac{c'^{\text{ten}}}{c^{\text{ten}}} \right)^2$
$K_{2,A} \rightarrow a_1(1260) K$	$3 \left(\frac{\sqrt{2}\phi_S}{8} \right)^2$	$\simeq 0.1 \left(\frac{c'^{\text{ten}}}{c^{\text{ten}}} \right)^2$
$K_{2,A} \rightarrow \bar{K}_{1,A} \pi$	$3 \left(\frac{\phi_N}{8} \right)^2$	$\simeq 11 \left(\frac{c'^{\text{ten}}}{c^{\text{ten}}} \right)^2$
$K_{2,A} \rightarrow f_1(1285) \bar{K}$	$\left(\frac{\sqrt{2}}{8} (\phi_N \sin \beta_{A_1} - \phi_S \cos \beta_{A_1}) \right)^2$	$\simeq 0.2 \left(\frac{c'^{\text{ten}}}{c^{\text{ten}}} \right)^2$
$\omega_{2,S} \rightarrow \bar{K}_{1,A} K + \text{c.c.}$	$4 \left(\frac{\phi_S}{4} \right)^2$	$\simeq 6 \left(\frac{c'^{\text{ten}}}{c^{\text{ten}}} \right)^2$

Table 3.15: Clebsch-Gordan coefficients and corresponding decay rates for $A_2 \rightarrow A_1 + P$. We recall that $c^{\text{ten}} := c_1^{\text{ten}} + c_2^{\text{ten}}$ and $c'^{\text{ten}} := c_1^{\text{ten}} - c_2^{\text{ten}}$.

Decay process (in model)	$\kappa_{a_2tp,i}$	eLSM (MeV)
$\rho_2(?) \rightarrow a_2(1320) \pi$	$2\left(\frac{\phi_N}{4}\right)^2$	≈ 88
$K_{2,A} \rightarrow K_2^*(1430) \pi$	$3\left(\frac{\sqrt{2}\phi_S}{8}\right)^2$	≈ 49
$K_{2,A} \rightarrow a_2(1320) K$	$3\left(\frac{\sqrt{2}\phi_N}{8}\right)^2$	≈ 84
$K_{2,A} \rightarrow f_2(1270) K$	$\left(\frac{\phi_N \cos \beta_T - 2\phi_S \sin \beta_T}{8}\right)^2$	≈ 4
$\omega_{2,S} \rightarrow K_2^*(1430) K + \text{c.c.}$	$4\left(\frac{\phi_S}{8}\right)^2$	≈ 15

Table 3.16: Clebsch-Gordan coefficients and corresponding decay rates for $A_2 \rightarrow T + P$.

3.5.3 Decay channel $A_2 \rightarrow T + P$

We estimate how the axial-tensor mesons decay into a tensor-pseudoscalar pair using the last term of the Lagrangian Eq. (3.9), which contains the following interaction Lagrangian:

$$\mathcal{L}_{a_2tp} = 2ih_3^{\text{ten}} \text{Tr} \left[A_2^{\mu\nu} (PT_{\mu\nu} \Phi_0 - \Phi_0 T_{\mu\nu} P) \right]. \quad (3.68)$$

The tree-level decay rate reads

$$\Gamma_{A_2 \rightarrow T+P}(m_{a_2}, m_t, m_p) = \frac{(h_3^{\text{ten}})^2 |\vec{k}_{a_2,t,p}|}{2m_{a_2}^2 \pi} \left(1 + \frac{4|\vec{k}_{a_2,t,p}|^4}{45m_t^4} + \frac{2|\vec{k}_{a_2,t,p}|^2}{3m_t^2} \right) \kappa_{a_2tp,i} \Theta(m_{a_2} - m_t - m_p), \quad (3.69)$$

where $\kappa_{a_2tp,i}$ as well as the theoretical results are presented in Table 3.16. It is visible that rather large decays are produced in certain channels. It should be noted that the decay rate of $\rho_2(?) \rightarrow a_2(1320) \pi$ is computed in [88] to be roughly 200 MeV. This makes the expected overall decay widths of axial-tensor mesons even larger.

In conclusion, it should be emphasized that even assuming the lower part of the presented ranges, the total decay widths of the axial-tensor mesons are large. Nevertheless, it appears that the missing axial-tensor states could be found in ongoing and future experiments, particularly by examining the decay channels discussed in this subsection, even though it will be challenging to identify such broad states.

3.6 Conclusion

In the context of a chiral model for low-energy QCD called the eLSM, we have examined the well-known lightest tensor mesons and their chiral companions, the axial-tensor mesons. Results for the tensor mesons, e.g., masses and decay widths, qualitatively support the idea of a quark-anti-quark picture of this nonet, as indicated in Fig. 3.2.

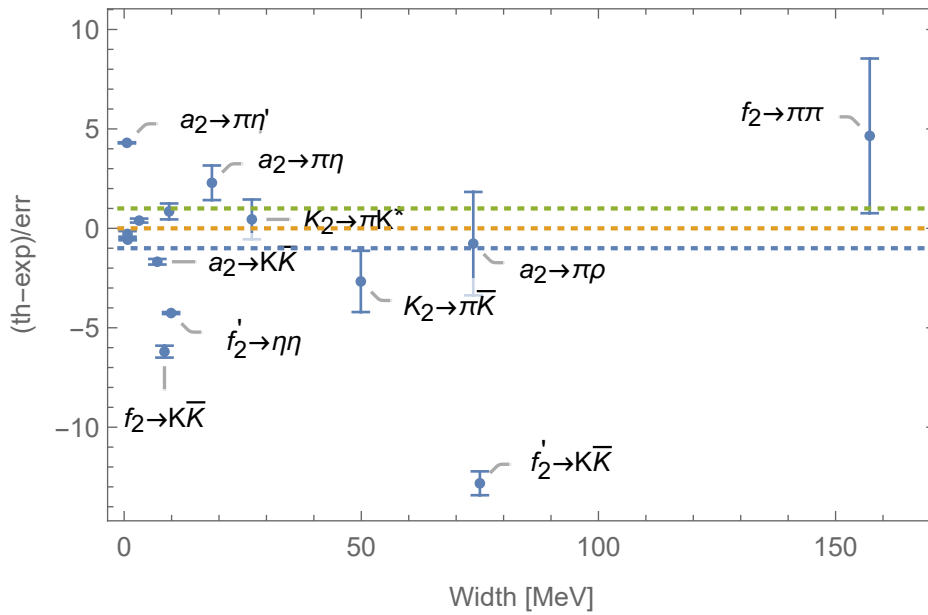


Figure 3.2: Comparison of the eLSM results to PDG [27].

Because of chiral symmetry, it is possible to predict masses and decay rates for the missing axial-tensor mesons using the parameters found in the tensor sector. We obtain large and dominant decay widths for the vector-pseudoscalar channel of axial-tensor mesons, yet with large uncertainties. Sizable decay widths for this decay channel are also achieved via LQCD, and the corresponding decay ratios match well with the ones calculated within our model.

Chapter 4

Spin-2 Glueball

In this chapter, we include the tensor glueball (with $J^{PC} = 2^{++}$) into the eLSM introduced in the previous chapter. This state is the second-lightest one in the LQCD glueball spectrum after the scalar glueball. The experimental observation of several resonances with $J^{PC} = 2^{++}$, such as $f_2(1430)$, $f_2(1565)$, $f_2(1640)$, $f_2(1810)$, $f_2(1910)$, $f_2(1950)$, $f_2(2010)$, $f_2(2150)$, $f_1(2220)$, poses the question if one of them can be interpreted as a tensor glueball.

4.1 Introduction

Mesons known as "glueballs" contain only gluons. Despite the existence of glueballs being one of the earliest predictions of QCD, these objects are still experimentally disputed (some candidates do exist but a final consensus is missing) [64, 127–129]. There are many lattice investigations that confirm the existence of glueballs [29, 130–135]. Yet, it is still difficult to distinguish glueballs in experiments because of their mixing with conventional quark-antiquark mesons. Nevertheless, new data analysis on J/ψ decays appears to be helpful toward identifying the scalar and tensor glueballs [71, 73, 136, 137].

Several masses for the tensor glueball are estimated by LQCD simulations, including:

- 2150(30)(100) MeV [132];
- 2324(42)(32) MeV [133];

- 2376(32) MeV [29];
- 2390(30)(120) MeV [130];
- 2400(25)(120) MeV [131].

The tensor glueball mass is predicted by other theoretical models as well. According to the QCD sum rules, it is predicted to be in the range 2000 MeV-2300 MeV [138, 139], functional methods prediction is around 2610 MeV [36], while the holographic techniques estimate lies in the interval 1900 MeV – 4300 MeV [33, 140–146].

Resonances	Masses (MeV)	Decay Widths (MeV)	Decay Channels
$f_2(1910)$	1900 ± 9	167 ± 21	$\pi\pi, KK, \eta\eta, \omega\omega, \eta\eta', \eta'\eta', \rho\rho, a_2(1320)\pi, f_2(1270)\eta$
$f_2(1950)$	1936 ± 12	464 ± 24	$\pi\pi, K^*K^*, KK, \eta\eta$
$f_2(2010)$	2011^{+60}_{-80}	202 ± 60	$\phi\phi, KK$
$f_2(2150)$	2157 ± 12	152 ± 30	$\pi\pi, \eta\eta, KK, a_2(1320)\pi, f_2(1270)\eta$
$f_J(2220)$	2231.1 ± 3.5	23^{+8}_{-7}	$\eta\eta'$
$f_2(2300)$	2297 ± 28	149 ± 41	$\phi\phi, KK$
$f_2(2340)$	2345^{+50}_{-40}	322^{+70}_{-60}	$\phi\phi, \eta\eta$

Table 4.1: Spin 2 resonances with masses around 2 GeV in PDG [27].

An effective model describing the tensor glueball can be found in Refs. [83, 147]. Recently, the role of the tensor glueball via the glueball scattering within the Glueball Resonance Gas model was studied in [4] (see also chapter 6). Various glueballs were studied within the eLSM, including the scalar glueball [148], the vector glueball [101], the pseudotensor glueball (with $J^{PC} = 2^{-+}$) [85], the spin-3 glueball (with $J^{PC} = 3^{--}$) [1], and glueball molecules [149].

4.2 Chiral Lagrangians for G_2

Starting from the chiral Lagrangians in Eq. (3.12) and in Eq. (3.14), we perform the following substitution in order to describe the tensor glueball decays:

$$T_{\mu\nu} \longrightarrow \frac{1}{\sqrt{6}} G_{2,\mu\nu} \cdot \mathbb{1}_{3 \times 3}, \quad (4.1)$$

which implies the flavor blindness of the glueball state. Thus, the Lagrangian for the tensor glueball interaction with (axial-)vector mesons reads

$$\mathcal{L}_{\lambda_2} = \frac{\lambda_2}{\sqrt{6}} G_{2,\mu\nu} \left(\text{Tr} \left[\{L^\mu, L^\nu\} \right] + \text{Tr} \left[\{R^\mu, R^\nu\} \right] \right), \quad (4.2)$$

which leads to three kinematically allowed decay channels:

- The vector-vector ($G_2 \rightarrow V_1 V_1$) decay rate of the tensor glueball has the following form:

$$\begin{aligned} \Gamma_{G_2 \rightarrow V_1^{(1)} + V_1^{(2)}}(m_{g_2}, m_{v^{(1)}}, m_{v^{(2)}}) &= \frac{\kappa_{g v v, i} \lambda_2^2 |\vec{k}_{g_2, v^{(1)}, v^{(2)}}|^2}{120 \pi m_{g_2}^2} \left(15 + \frac{5 |\vec{k}_{g_2, v^{(1)}, v^{(2)}}|^2}{m_{v^{(1)}}^2} + \right. \\ &\quad \left. + \frac{5 |\vec{k}_{g_2, v^{(1)}, v^{(2)}}|^2}{m_{v^{(2)}}^2} + \frac{2 |\vec{k}_{g_2, v^{(1)}, v^{(2)}}|^4}{m_{v^{(1)}}^2 m_{v^{(2)}}^2} \right) \Theta(m_{g_2} - m_{v^{(1)}} - m_{v^{(2)}}); \end{aligned} \quad (4.3)$$

- The decay of G_2 into axial-vector and pseudoscalar ($G_2 \rightarrow A_1 P$) mesons is obtained via the application of the shift Eq. (3.8) once in Eq. (4.2), leading to:

$$\Gamma_{G_2 \rightarrow A_1 + P}(m_{g_2}, m_{a_1}, m_p) = \frac{\kappa_{g a p, i} \lambda_2^2 |\vec{k}_{g_2, a_1, p}|^3}{120 \pi m_{g_2}^2} \left(5 + \frac{2 |\vec{k}_{g_2, a_1, p}|^2}{m_{a_1}^2} \right) \Theta(m_{g_2} - m_{a_1} - m_p); \quad (4.4)$$

- The decay into two pseudoscalars ($G_2 \rightarrow PP$) is obtained considering the SSB-related shift of Eq. (3.8) twice within Eq. (4.2)

$$\Gamma_{G_2 \rightarrow P^{(1)} + P^{(2)}}(m_{g_2}, m_{p^{(1)}}, m_{p^{(2)}}) = \frac{\kappa_{g p p, i} \lambda_2^2 |\vec{k}_{g_2, p^{(1)}, p^{(2)}}|^5}{60 \pi m_{g_2}^2} \Theta(m_{g_2} - m_{p^{(1)}} - m_{p^{(2)}}). \quad (4.5)$$

Since the coupling constant λ_2 is not known, we are at first limited to computing decay ratios rather than decay rates. Later on, a guess based on the large- N_c estimate for two pseudoscalar decays will be discussed in Sec. 4.4.

An analogous Lagrangian to the last term of Eq. (3.9) for the tensor glueball decay into a tensor meson and a pseudoscalar meson reads

$$\mathcal{L}_{\alpha_2} = \frac{\alpha_2}{\sqrt{6}} G_{2,\mu\nu} \left(\text{Tr} \left[\Phi \mathbf{R}^{\mu\nu} \Phi^\dagger \right] + \text{Tr} \left[\Phi^\dagger \mathbf{L}^{\mu\nu} \Phi \right] \right). \quad (4.6)$$

The decay rate for this process is given by

$$\Gamma_{G_2 \rightarrow T+P}(m_{g_2}, m_t, m_p) = \frac{\alpha_2^2 |\vec{k}_{g_2,t,p}|}{2 m_{g_2}^2 \pi} \left(1 + \frac{4 |\vec{k}_{g_2,t,p}|^4}{45 m_t^4} + \frac{2 |\vec{k}_{g_2,t,p}|^2}{3 m_t^2} \right) \times \kappa_{g_2 t p, i} \Theta(m_{g_2} - m_t - m_p), \quad (4.7)$$

where α_2 is a dimensionless unknown parameter.

The last chiral term for G_2 is derived from the Lagrangian in Eq. (3.14) and describes the decay of a tensor glueball into a vector and a pseudoscalar meson:

$$\begin{aligned} \mathcal{L}_{c^{\text{glu}}} = & \frac{c_1^{\text{glu}}}{\sqrt{6}} \partial^\mu G_2^{\nu\alpha} \text{Tr} \left[\tilde{L}_{\mu\nu} \partial_\alpha \Phi \Phi^\dagger - \Phi^\dagger \partial_\alpha \Phi \tilde{R}_{\mu\nu} - \tilde{R}_{\mu\nu} \partial_\alpha \Phi^\dagger \Phi + \Phi \partial_\alpha \Phi^\dagger \tilde{L}_{\mu\nu} \right] \\ & + \frac{c_2^{\text{glu}}}{\sqrt{6}} \partial^\mu G_2^{\nu\alpha} \text{Tr} \left[\partial_\alpha \Phi \tilde{R}_{\mu\nu} \Phi^\dagger - \Phi^\dagger \tilde{L}_{\mu\nu} \partial_\alpha \Phi - \partial_\alpha \Phi^\dagger \tilde{L}_{\mu\nu} \Phi + \Phi \tilde{R}_{\mu\nu} \partial_\alpha \Phi^\dagger \right]. \end{aligned} \quad (4.8)$$

The tree-level decay rate formula reads:

$$\Gamma_{G \rightarrow VP}(m_{g_2}, m_v, m_p) = \frac{c^{\text{glu}2} |\vec{k}_{g_2,v,p}|^5}{40 \pi} \kappa_{g v p, i} \Theta(m_{g_2} - m_v - m_p), \quad (4.9)$$

where $c^{\text{glu}} := c_1^{\text{glu}} + c_2^{\text{glu}}$. The only non-zero term in this channel is KK^* proportional to $(\phi_N - \sqrt{2}\phi_S)$, which vanishes in the chiral limit. It is then expected to be very small.

4.3 Results for the decay ratios

An enhancement in the mass distribution around 2210 MeV was observed in the analyses of BESIII data in Ref. [73]. We chose this value for the mass of the tensor glueball in order to estimate the decay ratios via $\kappa_{g_{\text{oo}}, i}$ in Table 4.2 and Eqs. (4.3), (4.5), (4.4). The corresponding results in Table 4.3 show that the dominant decays are $\rho\rho$ and K^*K^* decay channels.

Decay process	$\kappa_{g^{00},i}$
$G_2 \longrightarrow \rho(770) \rho(770)$	1
$G_2 \longrightarrow \bar{K}^*(892) K^*(892)$	$\frac{4}{3}$
$G_2 \longrightarrow \omega(782) \omega(782)$	$\frac{1}{3}$
$G_2 \longrightarrow \omega(782) \phi(1020)$	0
$G_2 \longrightarrow \phi(1020) \phi(1020)$	$\frac{1}{3}$
$G_2 \longrightarrow \pi \pi$	$(Z_\pi^2 w_\pi^2)^2$
$G_2 \longrightarrow \bar{K} K$	$\frac{4}{3} \times (Z_k^2 w_k^2)^2$
$G_2 \longrightarrow \eta \eta$	$\frac{1}{3} \times (Z_{\eta_N}^2 w_{\eta_N}^2 \cos \beta_P^2 + Z_{\eta_S}^2 w_{\eta_S}^2 \sin \beta_P^2)^2$
$G_2 \longrightarrow \eta \eta'(958)$	$\frac{1}{3} \times ((Z_{\eta_N}^2 w_{\eta_N}^2 - Z_{\eta_S}^2 w_{\eta_S}^2) \cos \beta_P \sin \beta_P)^2$
$G_2 \longrightarrow \eta'(958) \eta'(958)$	$\frac{1}{18} \times (Z_{\eta_S}^2 w_{\eta_S}^2 \cos \beta_P^2 + Z_{\eta_N}^2 w_{\eta_N}^2 \sin \beta_P^2)^2$
$G_2 \longrightarrow a_1(1260) \pi$	$\frac{1}{2} \times (Z_\pi w_\pi)^2$
$G_2 \longrightarrow f_1(1285) \eta$	$\frac{1}{6} (Z_{\eta_S} w_{\eta_S} \sin \beta_{A_1} \sin \beta_P + Z_{\eta_N} w_{\eta_N} \cos \beta_{A_1} \cos \beta_P)^2$
$G_2 \longrightarrow K_{1,A} K$	$\frac{2}{3} \times (Z_k w_k)^2$
$G_2 \longrightarrow f_1(1420) \eta'(958)$	$\frac{1}{6} (Z_{\eta_N} w_{\eta_N} \sin \beta_{A_1} \sin \beta_P + Z_{\eta_S} w_{\eta_S} \cos \beta_{A_1} \cos \beta_P)^2$
$G_2 \longrightarrow f_1(1285) \eta'(958)$	$\frac{1}{6} (Z_{\eta_S} w_{\eta_S} \sin \beta_{A_1} \cos \beta_P - Z_{\eta_N} w_{\eta_N} \cos \beta_{A_1} \sin \beta_P)^2$
$G_2 \longrightarrow f_2(1270) \eta$	$\frac{1}{24} (\phi_N \cos \beta_p \cos \beta_T + \phi_S \sin \beta_p \sin \beta_T)^2$
$G_2 \longrightarrow a_2(1320) \pi$	$\frac{\phi_N^2}{8}$
$G_2 \longrightarrow K^*(892) K + \text{c.c.}$	$\frac{1}{48} (\sqrt{2}\phi_N - 2\phi_S)^2$

Table 4.2: Clebsh-Gordan coefficients for the decays of G_2 .

Quite large errors are expected in the results of Table 4.3 because of SSB-related parameters Z_i 's. As we have discussed in the previous chapter, 50% indeterminacy for the decay ratio $\rho\rho\text{-}\pi\pi$ can be assumed. Nevertheless, this ratio is still expected to be large. Interestingly, dominant decay channels of G_2 into $\rho\rho$ and K^*K^* are also obtained in [33] despite being smaller than our estimation. The change in the decay ratios depending on the tensor glueball mass is illustrated in Fig. 4.1. Next, we check the tensor glueball assignment for the resonances listed in Table 4.1.

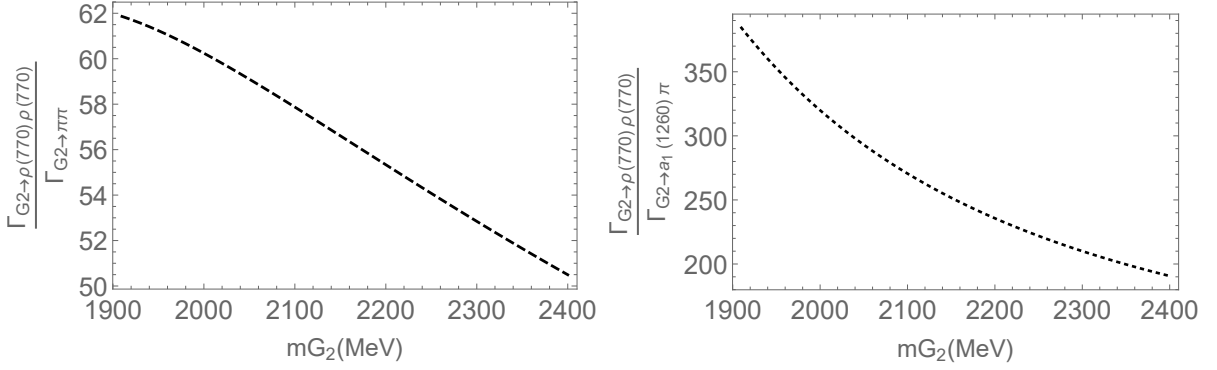


Figure 4.1: Decay ratios for different values of tensor glueball mass.

Decay Ratio	eLSM	Decay Ratio	eLSM	Decay Ratio	eLSM
$\frac{G_2(2210) \rightarrow \bar{K}K}{G_2(2210) \rightarrow \pi\pi}$	0.4	$\frac{G_2(2210) \rightarrow \rho(770)\rho(770)}{G_2(2210) \rightarrow \pi\pi}$	55	$\frac{G_2(2210) \rightarrow a_1(1260)\pi}{G_2(2210) \rightarrow \pi\pi}$	0.24
$\frac{G_2(2210) \rightarrow \eta\eta}{G_2(2210) \rightarrow \pi\pi}$	0.1	$\frac{G_2(2210) \rightarrow \bar{K}^*(892)\bar{K}^*(892)}{G_2(2210) \rightarrow \pi\pi}$	46	$\frac{G_2(2210) \rightarrow K_{1,A}K}{G_2(2210) \rightarrow \pi\pi}$	0.08
$\frac{G_2(2210) \rightarrow \eta\eta'}{G_2(2210) \rightarrow \pi\pi}$	0.004	$\frac{G_2(2210) \rightarrow \omega(782)\omega(782)}{G_2(2210) \rightarrow \pi\pi}$	18	$\frac{G_2(2210) \rightarrow f_1(1285)\eta}{G_2(2210) \rightarrow \pi\pi}$	0.02
$\frac{G_2(2210) \rightarrow \eta'\eta'}{G_2(2210) \rightarrow \pi\pi}$	0.006	$\frac{G_2(2210) \rightarrow \phi(1020)\phi(1020)}{G_2(2210) \rightarrow \pi\pi}$	6	$\frac{G_2(2210) \rightarrow f_1(1285)\eta}{G_2(2210) \rightarrow \pi\pi}$	0.02
				$\frac{G_2(2210) \rightarrow f_1(1420)\eta}{G_2(2210) \rightarrow \pi\pi}$	0.01

Table 4.3: Decay ratios of G_2 w.r.t. $\pi\pi$.

- We start with the resonance $f_2(1910)$ which has a total decay width of 167 ± 21 MeV. The following two decay ratios taken from Tables 4.5 and 4.4 agree well with PDG data:

$$\begin{aligned}
 \frac{\Gamma_{f_2(1910) \rightarrow \rho(770)\rho(770)}^{\text{PDG}}}{\Gamma_{f_2(1910) \rightarrow \omega(782)\omega(782)}^{\text{PDG}}} &= 2.6 \pm 0.4, & \frac{\Gamma_{f_2(1910) \rightarrow \rho(770)\rho(770)}^{\text{eLSM}}}{\Gamma_{f_2(1910) \rightarrow \omega(782)\omega(782)}^{\text{eLSM}}} &= 3.1, & (4.10) \\
 \frac{\Gamma_{f_2(1910) \rightarrow f_2(1270)\eta}^{\text{PDG}}}{\Gamma_{f_2(1910) \rightarrow a_2(1320)\pi}^{\text{PDG}}} &= 0.09 \pm 0.05, & \frac{\Gamma_{f_2(1910) \rightarrow f_2(1270)\eta}^{\text{eLSM}}}{\Gamma_{f_2(1910) \rightarrow a_2(1320)\pi}^{\text{eLSM}}} &= 0.07.
 \end{aligned}$$

Resonances	Decay Ratios	PDG	eLSM
$f_2(1910)$	$f_2(1270)\eta / a_2(1320)\pi$	0.09 ± 0.05	0.07
$f_2(2150)$	$f_2(1270)\eta / a_2(1320)\pi$	0.79 ± 0.11	0.1

Table 4.4: Decay ratios for the tensor-pseudoscalar pair compared to PDG [27].

Decay Ratios	eLSM
$\frac{G_2(1910) \rightarrow \rho(770)\rho(770)}{G_2(1910) \rightarrow \pi\pi}$	62
$\frac{G_2(1910) \rightarrow \omega(782)\omega(782)}{G_2(1910) \rightarrow \pi\pi}$	20
$\frac{G_2(1910) \rightarrow \eta\eta}{G_2(1910) \rightarrow \pi\pi}$	0.077
$\frac{G_2(1910) \rightarrow \eta\eta'(958)}{G_2(1910) \rightarrow \pi\pi}$	0.01
$\frac{G_2(1910) \rightarrow \bar{K}K}{G_2(1910) \rightarrow \pi\pi}$	0.31

Table 4.5: Results for the $f_2(1910)$ mass.

Decay Ratios	eLSM
$\frac{G_2(1950) \rightarrow \bar{K}^*(892)K^*(892)}{G_2(1950) \rightarrow \pi\pi}$	42
$\frac{G_2(1950) \rightarrow \eta\eta}{G_2(1950) \rightarrow \pi\pi}$	0.081
$\frac{G_2(1950) \rightarrow \bar{K}K}{G_2(1950) \rightarrow \pi\pi}$	0.32

Table 4.6: Results for the $f_2(1950)$ mass.

However, the interpretation of this resonance as mostly gluonic is problematic because of the following two large disagreements with PDG data:

$$\frac{\Gamma_{f_2(1910) \rightarrow \eta\eta}^{\text{PDG}}}{\Gamma_{f_2(1910) \rightarrow \eta\eta'(958)}^{\text{PDG}}} < 0.05, \quad \frac{\Gamma_{f_2(1910) \rightarrow \eta\eta}^{\text{eLSM}}}{\Gamma_{f_2(1910) \rightarrow \eta\eta'(958)}^{\text{eLSM}}} \approx 8, \quad (4.11)$$

$$\frac{\Gamma_{f_2(1910) \rightarrow \omega(782)\omega(782)}^{\text{PDG}}}{\Gamma_{f_2(1910) \rightarrow \eta\eta'(958)}^{\text{PDG}}} = 2.6 \pm 0.6, \quad \frac{\Gamma_{f_2(1910) \rightarrow \omega(782)\omega(782)}^{\text{eLSM}}}{\Gamma_{f_2(1910) \rightarrow \eta\eta'(958)}^{\text{eLSM}}} \approx 2000.$$

- The decay ratios of the resonance $f_2(1950)$ as a glueball are listed in Table 4.6. Both the theoretical and experimental ratios, $K\bar{K}/\pi\pi$ and $\eta\eta/\pi\pi$ agree with each other. When we assume that $\rho\rho$ decays into 4 pions, it is possible to estimate the lower bound of the ratio $4\pi/\eta\eta$, which leads to the order of about 100. The

Decay Ratios	eLSM
$\frac{G_2(2150) \rightarrow \eta\eta}{G_2(2150) \rightarrow \pi\pi}$	0.1
$\frac{G_2(2150) \rightarrow \bar{K}K}{G_2(2150) \rightarrow \pi\pi}$	0.38

Table 4.7: Results for the $f_2(2150)$ mass.

Decay Ratios	eLSM
$\frac{G_2(2300) \rightarrow \bar{K}K}{G_2(2300) \rightarrow \phi(1020)\phi(1020)}$	0.06
$\frac{G_2(2340) \rightarrow \eta\eta}{G_2(2340) \rightarrow \phi(1020)\phi(1020)}$	0.02

Table 4.8: Results for the $f_2(2300)$ and $f_2(2340)$ masses.

experimental total decay width of $f_2(1950)$ is broad, around 460 MeV. At present, $f_2(1950)$ is, according to our results, the best tensor glueball candidate; see the remainder of the chapter. Interestingly, the Witten-Sakai-Sugimoto model [33] also estimates a large total decay width for the tensor glueball. It is noteworthy that the decay $J/\psi \rightarrow \gamma K^*(892)\bar{K}^*(892)$ exhibits a branching ratio of $(7.0 \pm 2.2) 10^{-4}$, which is relatively high. Namely, a tensor glueball is predicted to have a strong coupling to J/ψ meson.

- The next resonance in Table 4.1 is $f_2(2010)$ with a total decay width of 202 ± 60 MeV. This state is listed as a well-established meson list of PDG [27]. The main reason for its interpretation as a strange-antistrange state and not as a glueball is because the only observed channels are $K\bar{K}$ and $\phi(1020)\phi(1020)$. The same argument for $f_2(2300)$ does not favor it being a tensor glueball state.
- Although the resonance $f_2(2150)$ does not belong to the list of well-established resonances of PDG, it is still interesting to present the comparison between the model and the experiment. The following three PDG data contradict the chiral model outcomes in Table 4.7 and Table 4.4

$$\frac{\Gamma_{f_2(2150) \rightarrow K\bar{K}}}{\Gamma_{f_2(2150) \rightarrow \eta\eta}} = 1.28 \pm 0.23, \quad (4.12)$$

$$\frac{\Gamma_{f_2(2150) \rightarrow \pi\pi}}{\Gamma_{f_2(2150) \rightarrow \eta\eta}} < 0.33, \quad (4.13)$$

$$\frac{\Gamma_{f_2(2150) \rightarrow f_2(1270)\eta}}{\Gamma_{f_2(2150) \rightarrow a_2(1320)\pi}} = 0.79 \pm 0.11. \quad (4.14)$$

Thus $f_2(2150)$ does not seem to be a good glueball candidate.

- In the literature, it has been thought that the meson $f_J(2220)$ (with $J = 2$ or $J = 4$) could be a good candidate for the tensor glueball. Our results disagree with this view since neither the model-predicted decay widths have been seen nor the ones seen in the experiment, such as $\eta\eta'$ agree with the model result.
- The last entry of the Table 4.1 is $f_2(2340)$, which decays into $\eta\eta$ and $\phi(1020)\phi(1020)$, what also suggests a strong strange-antistrange component. Still, further study of additional decays of this state is needed in the future.

4.4 Discussion

Large- N_c estimate of decays

Besides decay ratios, it is interesting to present an (albeit rough) estimate of the tensor glueball decays based on the large- N_c arguments.

Conventional tensor mesons, which were studied in the previous chapter, have the following quark structure (the small mixing angle between them is ignored)

$$\begin{aligned} f_2 &\equiv f_2(1270) \simeq \sqrt{1/2}(\bar{u}u + \bar{d}d), \\ f'_2 &\equiv f'_2(1525) \simeq \bar{s}s. \end{aligned} \quad (4.15)$$

Let us consider their two pions decay from the PDG [27]

$$\Gamma_{f_2 \rightarrow \pi\pi} = 157.2 \text{ MeV}, \quad \Gamma_{f'_2 \rightarrow \pi\pi} = 0.71 \text{ MeV}, \quad (4.16)$$

where we do not take into account small errors due to the qualitative nature of analysis. Because of the quark contents, the decay amplitudes have different N_c scalings:

$$A_{f_2 \rightarrow \pi\pi} \propto 1/\sqrt{N_c}, \quad A_{f'_2 \rightarrow \pi\pi} \propto 1/N_c^{3/2}. \quad (4.17)$$

The latter process is OZI suppressed [6, 150, 151] compared to the previous one. It can be considered as a result of the chain:

$$\bar{s}s \rightarrow gg \rightarrow \sqrt{1/2}(\bar{u}u + \bar{d}d) \rightarrow \pi\pi. \quad (4.18)$$

In order to be more definite, let us introduce a transition Hamiltonian as

$$H_{int} = \lambda_2 \left(|\bar{u}u\rangle \langle gg| + |\bar{d}d\rangle \langle gg| + |\bar{s}s\rangle \langle gg| + \text{h.c.} \right), \quad (4.19)$$

where $\lambda_2 \propto 1/\sqrt{N_c}$ is controlling $\bar{q}q$ - gg the mixing. The value $\lambda_2 \simeq 0.22$ is a consequence of the following ratios between two decays:

$$\frac{A_{f'_2 \rightarrow \pi\pi}}{A_{f_2 \rightarrow \pi\pi}} \simeq \sqrt{2}\lambda_2^2 \longrightarrow \frac{\Gamma_{f'_2 \rightarrow \pi\pi}}{\Gamma_{f_2 \rightarrow \pi\pi}} \simeq 2\lambda_2^4. \quad (4.20)$$

The numerical value of λ_2 enables us to estimate the two-pion decay of the tensor glueball as well as other decays within eLSM. In fact, the glueball decay is somehow an "intermediate stage" since a glueball is assumed to be a gg bound state. We obtain ¹

$$A_{G_2 \rightarrow \pi\pi} \simeq \sqrt{2}\lambda_2 A_{f_2 \rightarrow \pi\pi} \longrightarrow \Gamma_{G_2 \rightarrow \pi\pi} \simeq 2\lambda_2^2 \Gamma_{f_2 \rightarrow \pi\pi} \simeq 15 \text{ MeV}. \quad (4.21)$$

The other two pseudoscalar decay rates are presented in Table 4.9. As we did not consider other contributions such as phase space, form factors etc., this value is obviously just a very rough approximation. Still, it may be useful as a first guess.

Decay process	$\Gamma_i(\text{MeV})$
$G_2 \rightarrow \pi\pi$	~ 15
$G_2 \rightarrow \bar{K}K$	~ 6
$G_2 \rightarrow \eta\eta$	~ 1.6
$G_2 \rightarrow \eta\eta'(958)$	~ 0.06
$G_2 \rightarrow \eta'(958)\eta'(958)$	~ 0.08

Table 4.9: Two pseudoscalar decay estimations of the tensor glueball.

Interestingly, our estimation for $\pi\pi$ decay is comparable to the Witten-Sakai-Sugimoto (WSS) model result [33]

$$\frac{\Gamma_{G_2 \rightarrow \pi\pi}^{\text{WSS}}}{m_{G(2000)}} \simeq 0.014 \longrightarrow \Gamma_{G_2 \rightarrow \pi\pi}^{\text{WSS}} \simeq 28 \text{ MeV}. \quad (4.22)$$

Considering the decay ratio

$$\frac{\Gamma_{G_2 \rightarrow \rho\rho}^{\text{eLSM}}}{\Gamma_{G_2 \rightarrow \pi\pi}^{\text{eLSM}}} = 55, \quad (4.23)$$

and assuming the decay of each ρ into two pions, a large decay width for the four-pion decay of the tensor glueball is expected based on the large- N_c arguments.

¹The estimate of the coupling of glueballs to mesons follows a similar method in Refs. [152, 153].

Conventional excited tensor mesons

It is expected that some (not all) of the isoscalar tensor resonances of Fig. 1.2 fit radially and orbitally excited conventional tensor mesons rather than the tensor glueball (see, e.g., Refs. [154–156] for further details). Namely, we need to distinguish the tensor glueball from the radial excitation (with 2^3P_2) and orbital excitation (with 1^3F_2). The quark model predicts that [77], orbital excited tensor states are heavier than radial excitations, similar to the vector meson case [81].

Let us look at the radial excitations. The isotriplet $a_2(1700)$ and the isodoublet $K_2^*(1980)$ and the isoscalar (mostly nonstrange) $f_2(1640)$ are believed to belong to this nonet. According to the quark model review of the PDG [27], $f_2(1950)$ is also a radially excited tensor meson (the mostly $\bar{s}s$). Nevertheless, its experimental decay ratio does not favor this interpretation. The following decay ratio:

$$\frac{\Gamma_{f_2(1950) \rightarrow \bar{K}K}^{\text{PDG}}}{\Gamma_{f_2(1950) \rightarrow \pi\pi}^{\text{PDG}}} \sim 0.8, \quad (4.24)$$

should be larger for a $\bar{s}s$ state. The second argument for it not being a radially excited tensor is that its mass is too close to the isodoublet $K_2^*(1980)$.

Another possible candidate for the missing radially excited tensor meson would be the state $f_2(1910)$, which is not reported in the summary table of PDG [27]. Its mass difference with $K_2^*(1980)$ is not in favor of this resonance being a $\bar{s}s$ state. From a decay width point of view, the following decay ratio

$$\frac{\Gamma_{f_2(1910) \rightarrow f_2(1270)\eta}^{\text{PDG}}}{\Gamma_{f_2(1910) \rightarrow a_2(1320)\pi}^{\text{PDG}}} = 0.09 \pm 0.05, \quad (4.25)$$

does not support the strange-antistrange interpretation of $f_2(1910)$ as well.

In contrast, there is the well-established $f_2(2010)$ resonance that fits the strange quark structure mesons since it decays into $\phi\phi$ and $\bar{K}K$. Thus, among the three resonances $\{f_2(1910), f_2(1950), f_2(2010)\}$, the last one fits as a radially excited tensor meson. As a consequence, since $f_2(1910)$ is not established yet, the sole $f_2(1950)$ may be regarded as supernumerary. Thus its interpretation as a tensor glueball is feasible.

We have less information about the orbitally excited tensor mesons. There are three resonances $\{f_2(2150), f_2(2300), f_2(2340)\}$ that could possibly be candidates for

isoscalar 1^3F_2 states. While $f_2(2150)$ is omitted from the mesonic summary table of PDG [27], one may regard $f_2(2300)$ and $f_2(2340)$ as single state because of their similar mass. Their dominant $\phi\phi$ decay channel would support $\bar{s}s$ structure.

Finally, we present a summary of eLSM-based analyses of spin-2 mesons in Table 4.10.

Resonances	Interpretation status
$f_2(1910)$	Agreement with some data, but excluded by $\eta\eta/\eta\eta'$ and $\omega\omega/\eta\eta'$ ratios
$f_2(1950)$	$\eta\eta/\pi\pi$ ok, no contradictions with data, but implies broad tensor glueball Best fit as predominantly glueball among considered resonances
$f_2(2010)$	Likely strange-antistrange content
$f_2(2150)$	Most available data in disagreement with theoretical prediction
$f_1(2220)$	Data on $\pi\pi/K\bar{K}$ disagrees with theory, the largest predicted decay channels are not seen
$f_2(2300)$	Likely strange-antistrange content
$f_2(2340)$	Likely strange-antistrange content

Table 4.10: Status of spin-2 resonances within eLSM-based analyses.

4.5 Conclusions

In this chapter we studied the tensor glueball within the eLSM by using a chirally invariant Lagrangian approach. Results for the tree-level decay ratios imply the dominant channel into two vector mesons as decay products. Besides the decay ratios, we present the estimate for the decay rates, e.g., the $\pi\pi$ decay mode, to be of the order of 10 MeV. A small decay width of the tensor glueball into $K^*(892)K$ is another prediction of our model, which would make this mode potentially interesting to rule out future tensor glueball candidates.

Comparison of the eLSM results for various spin-2 resonances of PDG shows, at present, that the best match as a tensor glueball is the resonance $f_2(1950)$. Indeed, the inclusion of the additional meson-meson loop corrections in LQCD computation could potentially diminish the LQCD prediction for the tensor glueball mass from 2.2-2.4 GeV to the nearby value of the mass of $f_2(1950)$. The large decay width of $f_2(1950)$ supports its exotic structure rather than the conventional meson one. In future, mixing

between conventional $\bar{q}q$ states should be taken into account, as it is done in the scalar sector.

Our results might be useful for the tensor glueball search in ongoing experiments such as BESIII and LHCb.

Chapter 5

Spin-3 mesons

In this chapter, I present the results for spin-3 mesons (with $J^{PC} = 3^{--}$) within an effective model. In this case, the effective model is based on flavor symmetry $SU(3)_V$. This is due to the fact that chiral symmetry can not be used because no information about the ground-state spin-3 axial-tensor mesons (with $J^{PC} = 3^{++}$) is available. Yet, formally, also this model can be seen as a part of the eLSM generalized to include mesons with $J = 3$.

5.1 Introduction

In a series of articles, hadronic models have been built for various nonets where only the residual flavor symmetry $SU_V(3)$ is considered [66, 81, 83, 85, 157, 158]. The expansion in $1/N_c$ dominant and subdominant terms is performed when the interaction terms are written down. In addition, terms that explicitly violate flavor symmetry may be included, either as a result of the chiral anomaly or as a result of the underlying breaking caused by the presence of nonzero and unequal quark masses

$$m_u \approx 2 \text{ MeV}, \quad m_d \approx 5 \text{ MeV}, \quad m_s \approx 93 \text{ MeV}. \quad (5.1)$$

Within such a model approach, we analyze the decays of the ground-state $J^{PC} = 3^{--}$ nonet that contains the resonances $\rho_3(1690)$, $K_3^*(1780)$, $\phi_3(1850)$, $\omega_3(1670)$ existing in the PDG [27]. Because of the current degree of data accuracy, we will only take into account the dominant terms in the large- N_c expansion (see [119, 120, 159]) and ignore flavor symmetry breaking corrections.

5.2 Effective model

Based on $SU(3)_V$ flavor symmetry, we construct effective Lagrangians. In order to construct the interaction Lagrangians in Table 5.1, we use the symmetry transformations of the mesonic nonets listed in Table 2.1. We have derived the decay amplitudes

$J_c^{PC} \rightarrow J_a^{PC} + J_b^{PC}$	Interaction Lagrangians
$3^{--} \rightarrow 0^{-+} + 0^{-+}$	$\mathcal{L}_{w_3pp} = g_{w_3pp} \text{tr} [W_3^{\mu\nu\rho} [P, (\partial_\mu \partial_\nu \partial_\rho P)]_-]$
$3^{--} \rightarrow 0^{-+} + 1^{--}$	$\mathcal{L}_{w_3v_1p} = g_{w_3v_1p} \varepsilon^{\mu\nu\rho\sigma} \text{tr} [W_{3,\mu\alpha\beta} \{(\partial_\nu V_{1,\rho}), (\partial^\alpha \partial^\beta \partial_\sigma P)\}_+]$
$3^{--} \rightarrow 0^{-+} + 1^{--}$	$\mathcal{L}_{w_3\gamma p} = g_{w_3v_1p} \frac{e}{g_\rho} \varepsilon^{\mu\nu\rho\sigma} (\partial_\nu a_\rho) \text{tr} [W_{3,\mu\alpha\beta} \{Q, (\partial^\alpha \partial^\beta \partial_\sigma P)\}_+]$
$3^{--} \rightarrow 0^{-+} + 2^{++}$	$\mathcal{L}_{w_3tp} = g_{w_3tp} \varepsilon_{\mu\nu\rho\sigma} \text{tr} [W_{3\alpha\beta}^\mu [(\partial^\nu T^{\rho\alpha}), (\partial^\sigma \partial^\beta P)]_-]$
$3^{--} \rightarrow 0^{-+} + 1^{+-}$	$\mathcal{L}_{w_3b_1p} = g_{w_3b_1p} \text{tr} [W_3^{\mu\nu\rho} \{B_{1,\mu}, (\partial_\nu \partial_\rho P)\}_+]$
$3^{--} \rightarrow 0^{-+} + 1^{++}$	$\mathcal{L}_{w_3a_1p} = g_{w_3a_1p} \text{tr} [W_3^{\mu\nu\rho} [A_{1,\mu}, (\partial_\nu \partial_\rho P)]_-]$
$3^{--} \rightarrow 1^{--} + 1^{--}$	$\mathcal{L}_{w_3v_1v_1} = g_{w_3v_1v_1} \text{tr} [W_3^{\mu\nu\rho} [(\partial_\mu V_{1,\nu}), V_{1,\rho}]_-]$

Table 5.1: Interaction Lagrangians describing the decay of spin-3 mesons .

$|\mathcal{M}|^2$ via Feynman rules by using the polarization vectors and tensors as well as their corresponding completeness relations reported in Ref. [1]. The summary Table 5.2 shows the results for $\frac{1}{7}|\mathcal{M}|^2$.

Before presenting the results for decays, let us make the following comments for the interaction Lagrangians. The first comment is about the exclusion of the coupling between the spin-3 nonet of Eq. (2.86) to scalar mesons of Eq. (2.63). One kinematically allowed decay product would be a scalar and pseudoscalar meson. Yet, the corresponding CPT- and flavor-invariant interaction term:

$$\varepsilon_{\mu\nu\rho\sigma} \text{tr} (\partial^\mu W_{3\alpha\beta}^\nu [(\partial^\rho S), (\partial^\sigma \partial^\alpha \partial^\beta P)]_-) = 0, \quad (5.2)$$

that vanishes because of the contraction of antisymmetric and symmetric tensors. This is why we do not include the scalar mesons in our study in agreement with the absence

$J_c^{PC} \rightarrow J_a^{PC} + J_b^{PC}$	$\frac{1}{7} \mathcal{M} ^2$
$3^{--} \rightarrow 0^{-+} + 0^{-+}$	$g_{w_3 p p}^2 \frac{2}{35} \vec{k}_{w_3, p^{(1)}, p^{(2)}} ^6$
$3^{--} \rightarrow 0^{-+} + 1^{--}$	$g_{w_3 v_1 p}^2 \frac{8}{105} \vec{k}_{w_3, v, p} ^6 m_{w_3}^2$
$3^{--} \rightarrow 0^{-+} + 1^{--}$	$g_{w_3 v_1 p}^2 \left(\frac{e}{g_\rho}\right)^2 \frac{8}{105} \vec{k}_{w_3, \gamma, p} ^6 m_{w_3}^2$
$3^{--} \rightarrow 0^{-+} + 2^{++}$	$g_{w_3 t p}^2 \frac{2}{105} \vec{k}_{w_3, t, p} ^4 \frac{m_{w_3}^2}{m_t^2} (2 \vec{k}_{w_3, t, p} ^2 + 7 m_t^2)$
$3^{--} \rightarrow 0^{-+} + 1^{+-}$	$g_{w_3 b_1 p}^2 \frac{2}{105} \vec{k}_{w_3, b_1, p} ^4 \left(7 + 3 \frac{ \vec{k}_{w_3, b_1, p} ^2}{m_{b_1}^2}\right)$
$3^{--} \rightarrow 0^{-+} + 1^{++}$	$g_{w_3 a_1 p}^2 \frac{2}{105} \vec{k}_{w_3, a_1, p} ^4 \left(7 + 3 \frac{ \vec{k}_{w_3, a_1, p} ^2}{m_{a_1}^2}\right)$
$3^{--} \rightarrow 1^{--} + 1^{--}$	$\frac{g_{w_3 v_1 v_1}^2 \vec{k}_{w_3, v^{(1)}, v^{(2)}} ^2}{105 m_{v^{(1)}}^2 m_{v^{(2)}}^2} \left[6 \vec{k}_{w_3, v^{(1)}, v^{(2)}} ^4 + 35 m_{v^{(1)}}^2 m_{v^{(2)}}^2 + 14 \vec{k}_{w_3, v^{(1)}, v^{(2)}} ^2 (m_{v^{(1)}}^2 + m_{v^{(2)}}^2) \right]$

Table 5.2: Amplitude squares for the decay of spin-3 resonances.

of such experimental decay channels in the PDG [27]. Besides that, the assignment of the scalar mesons is still an open question in low-energy QCD [65, 67, 68, 160–162].

Furthermore, the Lagrangian terms that are taken into account in Table 5.1 are symmetric under $U_V(3)$ and dominant in large- N_c . As we will see later on, such an approximation is adequate at the current precision of the experiment data. For instance, in the case of the $W_3 B_1 P$ interaction, one can think of the Lagrangian $\mathcal{L}_{w_3 b_1 p}$ as the first term in the large- N_c expansion and/or symmetry-breaking terms, where further terms look as follows:

$$\begin{aligned}
\mathcal{L}_{w_3 b_1 p}^{\text{full}} &= g_{w_3 b_1 p} \text{tr} [W^{\mu\nu\rho} \{B_{1\mu}, (\partial_\nu \partial_\rho P)\}_+] + g_{w_3 b_1 p}^{(2)} \text{tr} [W^{\mu\nu\rho}] \text{tr} [B_{1\mu} (\partial_\nu \partial_\rho P)] + \\
&+ g_{w_3 b_1 p}^{(3)} \text{tr} [W^{\mu\nu\rho}] \text{tr} [B_{1\mu}] \text{tr} [\partial_\nu \partial_\rho P] + g_{w_3 b_1 p}^{(4)} \text{tr} [\hat{\delta} W^{\mu\nu\rho} \{B_{1\mu}, (\partial_\nu \partial_\rho P)\}_+] + \\
&+ g_{w_3 b_1 p}^{(5)} \text{tr} [\hat{\delta} W^{\mu\nu\rho}] \text{tr} [B_{1\mu} (\partial_\nu \partial_\rho P)] + g_{w_3 b_1 p}^{(6)} \text{tr} [W^{\mu\nu\rho}] \text{tr} [\hat{\delta} B_{1\mu} (\partial_\nu \partial_\rho P)] + \dots,
\end{aligned}$$

where the first term is reported in Table 5.1. It is a flavor symmetric term and scales as $g_{w_3 b_1 p} \propto N_c^{-1/2}$, thus it is the dominant term in the large- N_c expansion. The second and third terms are flavor symmetric but are suppressed, since they scale as $g_{w_3 b_1 p}^{(2)} \propto N_c^{-3/2}$ and $g_{w_3 b_1 p}^{(3)} \propto N_c^{-5/2}$ (typically they involve the exchange of gluon, see Eq. (4.19)). Starting from the fourth term, flavor symmetry is broken via the matrix

$$\hat{\delta} = \text{diag}\{\delta_u, \delta_d, \delta_s\}. \quad (5.3)$$

Flavor violation can be non-negligible (because the $\delta_s \propto m_s - m_u$ Ref. [67,68]), while it is expected to be very small for non-strange quarks. Upon setting $\delta_u = \delta_d = 0$, the coupling is expected to be of the order of

$$g_{w_3 b_1 p}^{(4)} \simeq g_{w_3 b_1 p} \text{diag}\{0, 0, 0.1 - 0.2\}, \quad (5.4)$$

and the actual value should be determined by performing an independent fit to the data.

Even if all of the interaction terms in Table 5.1 can be subject to the same analysis, it is interesting to note that the second and third terms would disappear anytime the commutator is present. It is expected that the largest next-to-leading-order contribution for those interaction terms will come from flavor-symmetry violation.

The following Lagrangian, in addition to the interaction terms discussed in this section, also includes the typical kinetic and mass terms of the used nonets.

$$\begin{aligned} \mathcal{L}_{W,\text{total}} = & \mathcal{L}_{\text{mass}} + \mathcal{L}_{\text{kin}} + \mathcal{L}_{w_3 pp} + \mathcal{L}_{w_3 v_1 p} + \\ & + \mathcal{L}_{w_3 tp} + \mathcal{L}_{w_3 a_1 p} + \mathcal{L}_{w_3 b_1 p} + \mathcal{L}_{w_3 v_1 v_1}. \end{aligned} \quad (5.5)$$

Only the lowest derivatives for each interaction term were retained in its construction. Two alternative lines of reasoning are used to support this choice. First, if the Lagrangian $\mathcal{L}_{W,\text{total}}$ is understood to be a component of a more complete and general chiral hadronic model in the vacuum, such as the eLSM, our effective model automatically arises. Second, such terms with the lowest derivatives are kept as the main contributions to our effective hadronic model, in accordance with the Functional Renormalization Group approach [46–57].

It is interesting to describe the former point in more detail. To this end, recall that the construction of the eLSM follows the assumption of chiral symmetry:

$$U_L(3) \times U_R(3) = SU_L(3) \times SU_R(3) \times U_L(1) \times U_R(1),$$

and the consideration of the scale invariance of the model. The symmetries are broken dynamically in addition to their small explicit breaking. Spontaneous breaking happens when $SU_L(3) \times SU_R(3) \rightarrow SU_V(3)$. Additionally, the *conformal/trace anomaly*, which is also known as the scale invariance breaking, occurs as a result of gluonic

quantum fluctuations and the creation of a gluon condensate [124, 163, 164]. The heavy mass of η' (958) as well as the large pseudoscalar mixing angle are both explained by a second anomaly, [63], the chiral anomaly, which also breaks $U_A(1)$. Besides anomaly terms, the eLSM interaction terms are scale/dilatation transformation invariant in the chiral limit and when the chiral anomaly is ignored.

All coupling constants of $\mathcal{L}_{w_3, \text{total}}$ in Eq. (5.5) are dimensionful, in contrast to the eLSM [19, 22], which uses dimensionless coupling constants for parametrization, with the exception of the last entries of Table 5.1. However, a closer look also reveals the benefits of keeping the lowest number of derivatives. Let us start by remembering that the axial-vector nonet shift A_1 of Eq. (3.8) originates from scalar-axial-vector mixing generated by SSB. For our illustrative purposes, it is sufficient to assume that $U_V(3)$ is exact in the simplified scenario [19, 102]:

$$A_1^\mu \rightarrow A_1^\mu + Z w \partial^\mu P, \quad (5.6)$$

where the pion decay constant $f_\pi = 92.4$ MeV appears in $w \approx \frac{g_1 Z f_\pi}{m_{a_1}^2}$ with $m_{a_1} \simeq 1.4$ GeV, $Z \approx 1.6$ and $g_1 \approx g_\rho \approx 5.5$.

Within this framework, the $W_3 PP$ -Lagrangian,

$$\mathcal{L}_{w_3 pp} = g_{w_3 pp} \text{tr} [W^{\mu\nu\rho} [P, (\partial_\mu \partial_\nu \partial_\rho P)]_-], \quad (5.7)$$

with the dimensionful coupling $g_{w_3 pp} = [\text{Energy}^{-2}]$ and the $W_3 A_1 P$ -Lagrangian,

$$\mathcal{L}_{w_3 a_1 p} = g_{w_3 a_1 p} \text{tr} [W^{\mu\nu\rho} [A_{1,\mu}, (\partial_\nu \partial_\rho P)]_-], \quad (5.8)$$

where $g_{w_3 pp} = [\text{Energy}^{-1}]$ can be seen as the outcome of the interaction Lagrangian

$$\mathcal{L}_{w_3 a_1 a_1} = g_{w_3 a_1 a_1} \text{tr} (W^{\mu\nu\rho} [A_{1,\mu}, \partial_\nu A_{1,\rho}]_-), \quad (5.9)$$

using only the dimensionless coupling $g_{w_3 a_1 a_1}$ obtained by shifting Eq. (5.6), applied once for $W_3 A_1 P$ and twice for $W_3 PP$. In other words, only the Lagrangian $\mathcal{L}_{w_3 a_1 a_1}$ is included in an eLSM chiral Lagrangian generalized to include $J = 3$ mesons:

$$\mathcal{L}_{g_3} = g_3 \text{tr} (L_3^{\mu\nu\rho} L_{1,\mu} \partial_\nu L_{1,\rho} + R_3^{\mu\nu\rho} R_{1,\mu} \partial_\nu R_{1,\rho}). \quad (5.10)$$

The Lagrangians $\mathcal{L}_{w_3 a_1 p}$ and $\mathcal{L}_{w_3 p p}$ are then a consequence of $\mathcal{L}_{w_3 a_1 a_1}$ via SSB, explaining how dimensional couplings occur in the model even if one starts just with dimensionless ones, although the decay channel $W_3 \rightarrow A_1 A_1$ is not kinematically allowed. The following two relations between the coupling constants

$$g_{w_3 p p} \approx Z^2 w^2 g_{w_3 a_1 a_1}, \quad \text{and} \quad g_{w_3 a_1 p} \approx Z w g_{w_3 a_1 a_1}, \quad (5.11)$$

leads to

$$g_{w_3 a_1 p} / g_{w_3 p p} \approx (Z w)^{-1}. \quad (5.12)$$

Based on this analysis, we shall estimate the decay rates of spin-3 mesons into an axial vector and a pseudoscalar meson pair in Sec. 5.3.6. However, it must be emphasized that the current heuristic discussion cannot give exact ratios of couplings; rather, it just serves as a guide to understanding the model's origin.

Similar arguments about understanding the chiral origin of the model can be applied to the following Lagrangian,

$$\mathcal{L}_{w_3 b_1 p} = g_{w_3 b_1 p} \text{tr}(W^{\mu\nu\rho} \{B_{1,\mu'} (\partial_\nu \partial_\rho P)\}_+), \quad (5.13)$$

where the dimensionful constant $g_{w_3 b_1 p} = [\text{Energy}^{-1}]$, which can be seen as emerging from the following Lagrangian with a dimensionless coupling $g_{w_3 b_1 a_1}$

$$\mathcal{L}_{w_3 b_1 a_1} = g_{w_3 b_1 a_1} \text{tr}[W^{\mu\nu\rho} \{B_{1,\mu'} (\partial_\nu A_{1,\rho})\}_+]. \quad (5.14)$$

The following ratio

$$\frac{g_{w_3 b_1 p}}{g_{w_3 b_1 a_1}} \approx Z w, \quad (5.15)$$

shows the magnitude of the coupling constant $g_{w_3 b_1 a_1}$, which cannot be used since this decay channel is kinematically forbidden.

Unlike the previous Lagrangians, the two other Lagrangians $\mathcal{L}_{w_3 v_1 p}$ and $\mathcal{L}_{w_3 t p}$ in Table 5.1 are not dilatation invariant, and one cannot obtain the dimensionful couplings $g_{w_3 v_1 p} = [\text{Energy}^{-3}]$ and $g_{w_3 t p} = [\text{Energy}^{-2}]$ via SSB of $\mathcal{L}_{w_3 v_1 a_1}$ and $\mathcal{L}_{w_3 t a_1}$ since their coupling constants $g_{w_3 v_1 a_1}$ and $g_{w_3 t a_1}$ still have dimension $[\text{Energy}^{-2}]$ and

[Energy⁻¹]. Nevertheless, this makes sense because these terms involve the Levi-Civita pseudotensor $\varepsilon_{\mu\nu\rho\sigma}$ and can be seen as a manifestation of the chiral anomaly.

Summarizing the discussion, terms that are components of the model are either (i) dilatation invariant, (ii) may be generated from dilatation invariant terms of a more fundamental underlying chiral model by shifting the axial-vector nonet, or (iii) they are connected to the chiral anomaly.

5.3 Results for $J^{PC} = 3^{--}$ mesons

This section is about our results for decay rates and branching ratios of the $J^{PC} = 3^{--}$ mesons and their comparison to available experimental data. Moreover, we confirm that our theoretical outcomes for the sum of all single decay channels never exceed the total decay widths of the $J^{PC} = 3^{--}$ listed in Table 5.3.

Resonances	Masses (MeV)	Total Decay Widths (MeV)
$\rho_3(1690)$	1690	161 ± 10
$K_3^*(1780)$	1780	159 ± 21
$\omega_3(1670)$	1670	168 ± 10
$\phi_3(1850)$	1850	87^{+28}_{-23}

Table 5.3: Total decay widths and masses of $J^{PC} = 3^{--}$ mesons [27].

Wherever possible, we calculate the coupling constants and their error using a fit to experimental decay widths and ratios. Because the experimental errors of the masses are typically small and have little effect on the overall errors, we disregard the experimental uncertainties. This approximation is reasonable because the systematic errors in the model, as well as the experimental errors for branching ratios and decay widths, are substantially larger. The quoted errors, however, only represent a lower bound of the actual errors, as other indeterminacies are present. Moreover, for $J = 3$ mesons, the contributions from loops are believed to be negligible due to the relatively small width/mass ratio for the decaying resonances [165,166]. In any case, calculations

at tree-level are required if the interaction terms are taken to be effective couplings in a full quantum-effective IR action [44].

5.3.1 Decay channel $W_3 \rightarrow P^{(1)} + P^{(2)}$

The decay of spin-3 tensor mesons into two pseudoscalar mesons is described by the following effective interaction term:

$$\mathcal{L}_{w_3pp} = g_{w_3pp} \text{tr} [W_3^{\mu\nu\rho} [P, (\partial_\mu \partial_\nu \partial_\rho P)]_-]. \quad (5.16)$$

The tree-level decay rate is

$$\Gamma_{W_3 \rightarrow P^{(1)} + P^{(2)}}(m_{w_3}, m_{p^{(1)}}, m_{p^{(2)}}) = g_{w_3pp}^2 \frac{|\vec{k}_{w_3, p^{(1)}, p^{(2)}}|^7}{140 m_{w_3}^2} \times \kappa_i \Theta(m_{w_3} - m_{p^{(1)}} - m_{p^{(2)}}), \quad (5.17)$$

where the amplitude square is given in Table 5.2 and κ_i are reported in Table 5.4. Using the above formula as well as the experimental results, which are listed in the fourth row of Table 5.4, we can calculate the coupling constant g_{w_3pp} by using a standard χ^2 -approach. We consider χ^2 as a function of the theoretical coupling square \tilde{g}

$$\chi^2 \equiv \sum_{i=1}^N \frac{(\tilde{g} - \tilde{g}_i)^2}{\Delta \tilde{g}_i}, \quad (5.18)$$

where \tilde{g}_i are the squared coupling square and $\Delta \tilde{g}_i$ the experimental errors on them defined from the experiment. Minimizing the χ^2 with respect to coupling $\frac{d\chi^2}{d\tilde{g}} = 0$ leads to the following relation for $N = 4$:

$$\tilde{g} \equiv g_{w_3pp}^2 = \frac{\sum_{i=1}^4 \frac{\tilde{g}_i}{\Delta \tilde{g}_i}}{\sum_{j=1}^4 \frac{1}{\Delta \tilde{g}_j}}, \quad \text{and} \quad \Delta \tilde{g} \equiv \Delta g_{w_3pp}^2 = \frac{1}{\sum_{j=1}^4 \frac{1}{\Delta \tilde{g}_j}}. \quad (5.19)$$

Thus, we obtain

$$g_{w_3pp}^2 = (1.5 \pm 0.1) \cdot 10^{-10} \text{ MeV}^{-4}. \quad (5.20)$$

Table 5.4 shows the comparison of theoretical and experimental results obtained by using this value for the coupling constant. Although there is a good overall agreement,

there is also a significant mismatch, as the experimental value for $K_3^*(1780) \rightarrow \bar{K} \eta$ is much larger than our theoretical prediction. However, the experimental error is substantial, and more accurate experimental results would be needed to clarify this point. Furthermore, a notable prediction for $\phi_3(1850) \rightarrow \bar{K} K$ is made for this channel: an experimental determination ought to be possible in the future.

decay process	κ_i	theory Γ/MeV	experiment Γ/MeV
$\rho_3(1690) \rightarrow \pi \pi$	1	32.7 ± 2.3	38.0 ± 3.2
$\rho_3(1690) \rightarrow \bar{K} K$	$2 \left(\frac{1}{2}\right)^2$	4.0 ± 0.3	2.54 ± 0.45
$K_3^*(1780) \rightarrow \pi \bar{K}$	$\left(\frac{1}{2}\right)^2 + \left(\frac{\sqrt{2}}{2}\right)^2$	18.5 ± 1.3	29.9 ± 4.3
$K_3^*(1780) \rightarrow \bar{K} \eta$	$\left[\frac{1}{2}(-\cos \beta_p + \sqrt{2} \sin \beta_p)\right]^2$	7.4 ± 0.5	48 ± 22
$K_3^*(1780) \rightarrow \bar{K} \eta'(958)$	$\left[\frac{1}{2}(\sqrt{2} \cos \beta_p + \sin \beta_p)\right]^2$	0.021 ± 0.001	
$\omega_3(1670) \rightarrow \bar{K} K$	$2 \left[\frac{1}{2}(-\cos \beta_{w_3} + \sqrt{2} \sin \beta_{w_3})\right]^2$	3.0 ± 0.2	
$\phi_3(1850) \rightarrow \bar{K} K$	$2 \left[\frac{1}{2}(\sqrt{2} \cos \beta_{w_3} + \sin \beta_{w_3})\right]^2$	18.8 ± 1.3	seen

Table 5.4: Clebsch-Gordan coefficients and corresponding decay rates for $W_3 \rightarrow P^{(1)} + P^{(1)}$ compared to PDG [27].

5.3.2 Decay channel $W_3 \rightarrow V_1 + P$

For the vector and pseudoscalar decay modes, the interaction Lagrangian is as follows:

$$\mathcal{L}_{w_3 v_1 p} = g_{w_3 v_1 p} \epsilon^{\mu\nu\rho\sigma} \text{tr}[W_{3,\mu\alpha\beta} \{(\partial_\nu V_{1,\rho}), (\partial^\alpha \partial^\beta \partial_\sigma P)\}_+]. \quad (5.21)$$

The tree-level decay rate formula in this scenario takes the form

$$\Gamma_{W_3 \rightarrow V_1 + P}(m_{w_3}, m_v, m_p) = g_{w_3 v_1 p}^2 \frac{|\vec{k}_{w_3, v, p}|^7}{105} \kappa_i \Theta(m_{w_3} - m_v - m_p), \quad (5.22)$$

where the factors κ_i are reported in Table 5.5. We follow the same steps as in the pseudoscalar-pseudoscalar case to define the coupling constant. We use the three experimental data points listed in Table 5.5, leading to:

$$g_{w_3 v_1 p}^2 = (9.2 \pm 1.9) \cdot 10^{-16} \text{ MeV}^{-6}, \quad (5.23)$$

out of which we get the theoretical estimates listed in Table 5.5. Although the $\Gamma_{K_3^*(1780) \rightarrow \rho(770) K}$ mode is theoretically underestimated (the experimental error is nevertheless large), we notice that a satisfactory agreement is achieved.

Interestingly, although they could not be quantified, the two theoretically large decays $\omega_3(1670) \rightarrow \rho(770) K$ and $\phi_3(1850) \rightarrow K^*(892) K$ have both been observed in experiments. Their determination in the future would serve as a test of our method.

decay process	κ_i	theory Γ/MeV	experiment Γ/MeV
$\rho_3(1690) \rightarrow \rho(770) \eta$	$(\frac{1}{2} \cos \beta_p)^2$	3.8 ± 0.8	seen
$\rho_3(1690) \rightarrow \bar{K}^*(892) K$	$4 (\frac{1}{4})^2$	3.4 ± 0.7	
$\rho_3(1690) \rightarrow \omega(782) \pi$	$(\frac{1}{2} \cos \beta_{v_1})^2$	35.8 ± 7.4	25.8 ± 9.8
$\rho_3(1690) \rightarrow \phi(1020) \pi$	$(\frac{1}{2} \sin \beta_{v_1})^2$	0.036 ± 0.007	
$K_3^*(1780) \rightarrow \rho(770) K$	$(\frac{1}{4})^2 + (\frac{\sqrt{2}}{4})^2$	16.8 ± 3.5	49.3 ± 15.7
$K_3^*(1780) \rightarrow \bar{K}^*(892) \pi$	$(\frac{1}{4})^2 + (\frac{\sqrt{2}}{4})^2$	27.2 ± 5.6	31.8 ± 9.0
$K_3^*(1780) \rightarrow \bar{K}^*(892) \eta$	$[\frac{1}{4} (\cos \beta_p + \sqrt{2} \sin \beta_p)]^2$	0.09 ± 0.02	
$K_3^*(1780) \rightarrow \omega(782) \bar{K}$	$[\frac{1}{4} (\cos \beta_{v_1} + \sqrt{2} \sin \beta_{v_1})]^2$	4.3 ± 0.9	
$K_3^*(1780) \rightarrow \phi(1020) \bar{K}$	$[\frac{1}{4} (\sqrt{2} \cos \beta_{v_1} - \sin \beta_{v_1})]^2$	1.2 ± 0.3	
$\omega_3(1670) \rightarrow \rho(770) \pi$	$3 (\frac{1}{2} \cos \beta_{w_3})^2$	97 ± 20	seen
$\omega_3(1670) \rightarrow \bar{K}^*(892) K$	$4 [\frac{1}{4} (\cos \beta_{w_3} + \sqrt{2} \sin \beta_{w_3})]^2$	2.9 ± 0.6	
$\omega_3(1670) \rightarrow \omega(782) \eta$	$[\frac{1}{2} (\cos \beta_{w_3} \cos \beta_{v_1} \cos \beta_p + \sqrt{2} \sin \beta_{w_3} \sin \beta_{v_1} \sin \beta_p)]^2$	2.8 ± 0.6	
$\omega_3(1670) \rightarrow \phi(1020) \eta$	$[\frac{1}{2} (-\cos \beta_{w_3} \sin \beta_{v_1} \cos \beta_p + \sqrt{2} \sin \beta_{w_3} \cos \beta_{v_1} \sin \beta_p)]^2$	$(7.6 \pm 1.6) \cdot 10^{-6}$	
$\phi_3(1850) \rightarrow \rho(770) \pi$	$3 (\frac{1}{2} \sin \beta_{w_3})^2$	1.1 ± 0.2	
$\phi_3(1850) \rightarrow \bar{K}^*(892) K$	$4 [\frac{1}{4} (\sqrt{2} \cos \beta_{w_3} - \sin \beta_{w_3})]^2$	35.5 ± 7.3	seen
$\phi_3(1850) \rightarrow \omega(782) \eta$	$[\frac{1}{2} (-\sin \beta_{w_3} \cos \beta_{v_1} \cos \beta_p + \sqrt{2} \cos \beta_{w_3} \sin \beta_{v_1} \sin \beta_p)]^2$	0.015 ± 0.003	
$\phi_3(1850) \rightarrow \omega(782) \eta'(958)$	$[\frac{1}{2} (\sin \beta_{w_3} \cos \beta_{v_1} \sin \beta_p + \sqrt{2} \cos \beta_{w_3} \sin \beta_{v_1} \cos \beta_p)]^2$	0.003 ± 0.001	
$\phi_3(1850) \rightarrow \phi(1020) \eta$	$[\frac{1}{2} (\sin \beta_{w_3} \sin \beta_{v_1} \cos \beta_p + \sqrt{2} \cos \beta_{w_3} \cos \beta_{v_1} \sin \beta_p)]^2$	3.8 ± 0.8	

Table 5.5: Clebsch-Gordan coefficients and corresponding decay rates for $W_3 \rightarrow V + P$ compared to PDG [27].

We also provide the following ratio

$$\frac{\Gamma_{\phi_3(1850) \rightarrow \bar{K}^*(892) K}}{\Gamma_{\phi_3(1850) \rightarrow \bar{K} K}} = 1.9 \pm 0.4, \quad (5.24)$$

which is roughly consistent with the PDG quote [27] average obtained from Ref. [167]

$$\frac{\Gamma_{\phi_3(1850) \rightarrow \bar{K}^*(892) K}^{\text{exp}}}{\Gamma_{\phi_3(1850) \rightarrow \bar{K} K}^{\text{exp}}} = 0.55_{-0.45}^{+0.85}. \quad (5.25)$$

Interestingly, Ref. [168] reports a slightly higher ratio of

$$\frac{\Gamma_{\phi_3(1850) \rightarrow \bar{K}^*(892) K}^{\text{exp}}}{\Gamma_{\phi_3(1850) \rightarrow \bar{K} K}^{\text{exp}}} = 0.8 \pm 0.4. \quad (5.26)$$

Additionally, we would like to draw attention to a current LQCD analysis [28], which supports both results that we have predicted. Table 5.6 shows up the comparison to LQCD results [28] (whose errors are not provided due to large uncertainties). It is rather remarkable how well our (quite simple) model outcomes agree with the LQCD study that makes contact with the underlying QCD. This leads us to the conclusion that even for conventional mesons with $J^{PC} = 3^{--}$ and with masses exceeding 1 GeV, symmetry-based predictions are useful.

decay process (in model)	Theory (MeV)	LQCD (MeV)
$\rho_3(1690) \rightarrow \bar{K}^*(892) K + \text{c.c.}$	3	2
$\rho_3(1690) \rightarrow \omega(782) \pi$	36	22
$\omega_3(1670) \rightarrow \rho(770) \pi$	97	62
$\omega_3(1670) \rightarrow \bar{K}^*(892) K + \text{c.c.}$	2.9	2
$\omega_3(1670) \rightarrow \omega(782) \eta$	2.8	1
$\phi_3(1850) \rightarrow \bar{K}^*(892) K + \text{c.c.}$	36	20
$\phi_3(1850) \rightarrow \phi(1020) \eta$	4	3

Table 5.6: Decay rates for $W_3 \rightarrow V_1 + P$ compared to LQCD [28].

Next, we study three body decays using the Sill distribution described in Chapter 3.

The decay process $\Gamma_{\rho_3(1690) \rightarrow K\bar{K}\pi} = 6.12 \pm 2.00$ MeV in [27] can be estimated as follows:

$$\begin{aligned} \Gamma_{\rho_3(1690) \rightarrow \bar{K}^*(892) K \rightarrow K\bar{K}\pi} &\simeq \int_0^\infty dx d_{K^*}(x) \Gamma_{\rho_3(1690) \rightarrow \bar{K}^*(892) K}(m_{K_3}, x, m_K) \\ &\simeq (3.4 \pm 0.7) \text{ MeV}, \end{aligned} \quad (5.27)$$

where

$$\begin{aligned} d_{K^*}(y) &= \frac{2y}{\pi} \frac{\sqrt{y^2 - m_K^2 - m_\pi^2} \tilde{\Gamma}_{K^*}}{(y^2 - m_{K^*}^2)^2 + (\sqrt{y^2 - m_K^2 - m_\pi^2} \tilde{\Gamma}_{K^*})^2} \Theta(y - m_K - m_\pi), \\ \text{with } \int_0^\infty dy d_{K^*}(y) &= 1, \end{aligned} \quad (5.28)$$

in which $\tilde{\Gamma}_{K^*}$ is linked to the PDG values $\Gamma_{K^* \rightarrow K\pi} = 51.4$ MeV and $m_{K^*} = 890$ MeV according to:

$$\tilde{\Gamma}_{K^*} \equiv \frac{\Gamma_{K^* \rightarrow K\pi} m_{K^*}}{\sqrt{m_{K^*}^2 - m_K^2 - m_\pi^2}}. \quad (5.29)$$

The other decay channel $\Gamma_{\rho_3 \rightarrow \eta\pi\pi}$ that has been seen experimentally is estimated as:

$$\Gamma_{\rho_3 \rightarrow \rho\eta \rightarrow \eta\pi\pi} \simeq \int_0^\infty dx d_\rho(x) \Gamma_{\rho_3 \rightarrow \rho\eta}(m_{\rho_3}, x, m_\eta) \simeq (3.95 \pm 0.81) \text{ MeV}. \quad (5.30)$$

5.3.3 Decay channel $W_3 \rightarrow \gamma + P$

In this subsection, we present the results of the radiative decay into a photon and a pseudoscalar meson. As a consequence of the VMD shift in Eq. (3.15), we obtain the following Lagrangian

$$\mathcal{L}_{w_3\gamma p} = g_{w_3v_1p} \frac{e}{g_\rho} \varepsilon^{\mu\nu\rho\sigma} (\partial_\nu a_\rho) \text{tr}[W_{3,\mu\alpha\beta} \{Q, (\partial^\alpha \partial^\beta \partial_\sigma P)\}_+]. \quad (5.31)$$

Using the amplitude squared in Table 5.2, we get the tree-level decay rate formula:

$$\Gamma_{W_3 \rightarrow \gamma + P}(m_{w_3}, m_p) = g_{w_3v_1p}^2 \left(\frac{e}{g_\rho}\right)^2 \frac{|\vec{k}_{w_3,\gamma,p}|^7}{105\pi} \kappa_i^\gamma. \quad (5.32)$$

All κ_i^γ are presented in Table 5.7¹.

decay process	κ_i	theory Γ/keV
$\rho_3^{\pm/0}(1690) \rightarrow \gamma \pi^{\pm/0}$	$(\frac{1}{6})^2$	69 ± 14
$\rho_3^0(1690) \rightarrow \gamma \eta$	$(\frac{1}{2} \cos \beta_p)^2$	157 ± 32
$\rho_3^0(1690) \rightarrow \gamma \eta'(958)$	$(\frac{1}{2} \sin \beta_p)^2$	20 ± 4
$K_3^\pm(1780) \rightarrow \gamma K^\pm$	$(\frac{1}{6})^2$	58 ± 12
$K_3^0(1780) \rightarrow \gamma K^0$	$(\frac{1}{3})^2$	231 ± 48
$\omega_3(1670) \rightarrow \gamma \pi^0$	$(\frac{1}{2} \cos \beta_{w_3})^2$	560 ± 120
$\omega_3(1670) \rightarrow \gamma \eta$	$[\frac{1}{6}(\cos \beta_{w_3} \cos \beta_p - 2 \sin \beta_{w_3} \sin \beta_p)]^2$	19 ± 4
$\omega_3(1670) \rightarrow \gamma \eta'(958)$	$[\frac{1}{6}(\cos \beta_{w_3} \sin \beta_p + 2 \sin \beta_{w_3} \cos \beta_p)]^2$	1.4 ± 0.3
$\phi_3(1850) \rightarrow \gamma \pi^0$	$(\frac{1}{2} \sin \beta_{w_3})^2$	4 ± 1
$\phi_3(1850) \rightarrow \gamma \eta$	$[\frac{1}{6}(\sin \beta_{w_3} \cos \beta_p + 2 \cos \beta_{w_3} \sin \beta_p)]^2$	129 ± 26
$\phi_3(1850) \rightarrow \gamma \eta'(958)$	$[\frac{1}{6}(\sin \beta_{w_3} \sin \beta_p - 2 \cos \beta_{w_3} \cos \beta_p)]^2$	35 ± 7

Table 5.7: Clebsch-Gordan coefficients and corresponding decay rates for $W_3 \rightarrow \gamma + P$.

In Table 5.7, predictions for the radiative decays $W_3 \rightarrow \gamma P$ are provided. The decay channels $\omega_3(1670) \rightarrow \gamma \pi^0$ and $K_3^0(1780) \rightarrow \gamma K^0$ are quite large. In fact, these processes imply that the photoproduction of mesons with spin $J^{PC} = 3^{--}$ is possible at the ongoing *GlueX* [107–109] and *CLAS12* [105] experiments at *Jefferson Lab*.

¹Due to the fact that all pseudoscalars are lighter than spin-3 mesons and that photons are massless, the Heaviside function is not required in the decay rate formula.

5.3.4 Decay channel $W_3 \rightarrow T + P$

The decay of spin-3 tensor mesons into spin-2 tensor and pseudoscalar mesons is described by the interaction Lagrangian

$$\mathcal{L}_{w_3tp} = g_{w_3tp} \varepsilon_{\mu\nu\rho\sigma} \text{tr} [W_3^{\mu}{}_{\alpha\beta} [(\partial^\nu T^{\rho\alpha}), (\partial^\sigma \partial^\beta P)]_-]. \quad (5.33)$$

Using the amplitude square in Table 5.2 yields the relevant decay equation as follows:

$$\Gamma_{W_3 \rightarrow T+P}(m_{w_3}, m_t, m_p) = g_{w_3tp}^2 \frac{|\vec{k}_{w_3,t,p}|^5}{420 m_t^2} (2 |\vec{k}_{w_3,t,p}|^2 + 7 m_t^2) \times \kappa_i \Theta(m_{w_3} - m_t - m_p), \quad (5.34)$$

where Table 5.8 contains a list of the κ_i . At present, there are no experimentally known branching ratios for this channel that make it possible to calculate the coupling constant.

Yet, the experimental ratio given by the PDG [27] and extracted from Ref. [169] can be used

$$\frac{\Gamma_{\rho_3(1690) \rightarrow a_2(1320) \pi}^{\text{exp}}}{\Gamma_{\rho_3(1690) \rightarrow \rho(770) \eta}^{\text{exp}}} = 5.5 \pm 2.0. \quad (5.35)$$

Using the theoretical prediction $\Gamma_{\rho_3(1690) \rightarrow \rho(770) \eta} = (3.8 \pm 0.8) \text{ MeV}$ in Table 5.5 leads to the coupling constant

$$g_{w_3tp}^2 = (2.8 \pm 1.2) \cdot 10^{-9} \text{ MeV}^{-4}. \quad (5.36)$$

After fixing the coupling constant in this way, we obtain the results for the decay rates shown in Table 5.8. Our model prediction for the decay channel $\Gamma_{K_3^*(1780) \rightarrow \bar{K}_2^*(1430) \pi}$ is safely smaller than the experimental upper limit [27, 170]. In addition, the rather large mode $\rho_3(1690) \rightarrow a_2(1320) \pi$ is quoted as “seen” in Ref. [27].

decay process	κ_i	theory Γ/MeV	experiment Γ/MeV
$\rho_3(1690) \rightarrow a_2(1320) \pi$	$2 \left(\frac{1}{2}\right)^2$	20.9 ± 8.7	seen
$K_3^*(1780) \rightarrow \bar{K}_2^*(1430) \pi$	$\left(\frac{1}{4}\right)^2 + \left(\frac{\sqrt{2}}{4}\right)^2$	5.8 ± 2.4	$< 25.4 \pm 3.4$
$K_3^*(1780) \rightarrow f_2(1270) \bar{K}$	$\left[\frac{1}{4} (\cos \beta_t - \sqrt{2} \sin \beta_t)\right]^2$	$(5.4 \pm 2.2) \cdot 10^{-5}$	

Table 5.8: Clebsch-Gordan coefficients and corresponding decay rates for $W_3 \rightarrow T + P$ compared to PDG [27].

5.3.5 Decay channel $W_3 \rightarrow B_1 + P$

The interaction Lagrangian given below describes the decay of the spin-3 mesons into a pseudovector and a pseudoscalar meson

$$\mathcal{L}_{w_3 b_1 p} = g_{w_3 b_1 p} \text{tr} [W_3^{\mu\nu\rho} \{B_{1,\mu'} (\partial_\nu \partial_\rho P)\}_+]. \quad (5.37)$$

Using the results in Table 5.2, the tree-level decay rate reads:

$$\Gamma_{W_3 \rightarrow B_1 + P}(m_{w_3}, m_{b_1}, m_p) = g_{w_3 b_1 p}^2 \frac{|\vec{k}_{w_3, b_1, p}|^5}{420 m_{w_3}^2} \left(7 + 3 \frac{|\vec{k}_{w_3, b_1, p}|^2}{m_{b_1}^2} \right) \kappa_i \Theta(m_{w_3} - m_{b_1} - m_p), \quad (5.38)$$

where the κ_i are listed in Table 5.9. Also, in this case, the lack of experimental data makes it impossible to directly determine the coupling constant $g_{w_3 b_1 p}$. Nevertheless, we proceed as shown below in order to estimate it in an indirect way:

1. The following lower bound in PDG [27] is taken from Ref. [171] (where it is not included as a PDG fit of average)

$$\frac{\Gamma_{\omega_3(1670) \rightarrow b_1(1235) \pi}}{\Gamma_{\omega_3(1670) \rightarrow \omega(782) \pi \pi}} > 0.75 [27], \quad \frac{\Gamma_{\omega_3(1670) \rightarrow b_1(1235) \pi}}{\Gamma_{\omega_3(1670) \rightarrow \omega(782) \pi \pi}} = 1.0_{-0.25}^{+0.0} [171]. \quad (5.39)$$

According to Ref. [171] the decay mode $\omega_3(1670) \rightarrow b_1(1235) \pi$ is the dominant contribution to the $\omega(782) \pi \pi$ final state via the subsequent decay $b_1(1235) \rightarrow$

$\omega(782) \pi$. Thus one can assume the following relation

$$\Gamma_{\omega_3(1670) \rightarrow b_1(1235) \pi} \approx \Gamma_{\omega_3(1670) \rightarrow \omega(782) \pi \pi} \cdot \quad (5.40)$$

2. On the basis of this assumption, we estimate the following:

$$\frac{\Gamma_{\omega_3(1670) \rightarrow b_1(1235) \pi}}{\Gamma_{\omega_3(1670) \rightarrow \rho(770) \pi}} \stackrel{\text{Eq. (5.40)}}{\approx} \frac{\Gamma_{\omega_3(1670) \rightarrow \omega \pi \pi}}{\Gamma_{\omega_3(1670) \rightarrow \rho(770) \pi}} \stackrel{\text{PDG}}{=} 0.71 \pm 0.27. \quad (5.41)$$

It should be noted that the PDG refers to Ref. [172] for the following ratios but still does not include them in their fitting analyses

$$\frac{\Gamma_{\omega_3(1670) \rightarrow \omega \pi \pi}}{\Gamma_{\omega_3(1670) \rightarrow \rho(770) \pi}} = 0.47 \pm 0.18, \quad \frac{\Gamma_{\omega_3(1670) \rightarrow b_1(1235) \pi}}{\Gamma_{\omega_3(1670) \rightarrow \rho(770) \pi}} = 0.32 \pm 0.16. \quad (5.42)$$

It may be important to point out that all experimental data on the $\omega_3(1670)$ are quite old and, at the time Refs. [171, 172] were published, its mass and total decay width could not be determined with high accuracy. A novel experimental determination would be welcome.

decay process	κ_i	theory for	theory for
		$\beta_{b_1} = 0$ Γ/MeV	$\beta_{b_1} = -40^\circ$ Γ/MeV
$\rho_3(1690) \rightarrow h_1(1170) \pi$	$(\frac{1}{2} \cos \beta_{b_1})^2$	53 ± 23	31 ± 13
$\rho_3(1690) \rightarrow h_1(1415) \pi$	$(\frac{1}{2} \sin \beta_{b_1})^2$	0	0.73 ± 0.31
$K_3^*(1780) \rightarrow b_1(1235) K$	$(\frac{1}{4})^2 + (\frac{\sqrt{2}}{4})^2$	0.55 ± 0.24	0.55 ± 0.24
$K_3^*(1780) \rightarrow \bar{K}_{1,B} \pi$	$(\frac{1}{4})^2 + (\frac{\sqrt{2}}{4})^2$	37 ± 16	37 ± 16
$K_3^*(1780) \rightarrow h_1(1170) \bar{K}$	$[\frac{1}{4} (\cos \beta_{b_1} + \sqrt{2} \sin \beta_{b_1})]^2$	1.61 ± 0.70	0.03 ± 0.01
$\omega_3(1670) \rightarrow b_1(1235) \pi$	$3 (\frac{1}{2} \cos \beta_{w_3})^2$	69 ± 30	69 ± 30
$\phi_3(1850) \rightarrow b_1(1235) \pi$	$3 (\frac{1}{2} \sin \beta_{w_3})^2$	1.17 ± 0.51	1.17 ± 0.51
$\phi_3(1850) \rightarrow \bar{K}_{1,B} K + \text{c.c.}$	$4 [\frac{1}{4} (\sqrt{2} \cos \beta_{w_3} - \sin \beta_{w_3})]^2$	9.1 ± 3.9	9.1 ± 3.9
$\phi_3(1850) \rightarrow h_1(1170) \eta$	$[\frac{1}{2} (-\sin \beta_{w_3} \cos \beta_{b_1} \cos \beta_p + \sqrt{2} \cos \beta_{w_3} \sin \beta_{b_1} \sin \beta_p)]^2$	0.006 ± 0.003	1.1 ± 0.5

Table 5.9: Clebsch-Gordan coefficients and corresponding decay rates for $W_3 \rightarrow B_1 + P$ by using the mixing angle $\beta_{b_1} = 0$ and $\beta_{b_1} = -40^\circ$, respectively. No experimental data is given for this channel in PDG [27] apart from the ‘‘possibly seen’’ decay channel of $\omega_3(1670) \rightarrow b_1(1235) \pi$.

For the purposes of our study, we make use of the theoretical prediction for $\omega_3(1670) \rightarrow \rho(770) \pi$ and the ratio in Eq. (5.41) in order to estimate the coupling constant

$$g_{w_3 b_1 p}^2 \approx (0.008 \pm 0.003) \text{ MeV}^{-2}. \quad (5.43)$$

Even though they are only the first approximate estimations, the coupling and the results in Table 5.9 could still be useful in identifying dominating decay channels. The following factors are also taken into account while determining and interpreting our results:

1. The decay rate $\Gamma_{\phi_3(1850) \rightarrow \bar{K}_{1,B} K}$ is rather small when we take into account $K_{1,B} \approx K_1(1270)$. Yet, the results involving the identification $K_{1,B} \approx K_1(1270)$ may only be treated as a first approximation due to the large mixing between $K_{1,A}$ and $K_{1,B}$. By taking into account the full mixing in Eq. (2.71), $K_{1,B}$ should be written as a superposition of $K_1(1270)$ and $K_1(1400)$ which renders the interaction Lagrangian in Eq. (5.37) insufficient on its own and needs the consideration of the interaction terms for the decays $W_3 \rightarrow A_1 P$ in Eq. (5.44), which includes $K_{1,A}$. For the sake of simplicity, we disregard any potential interference between the two Lagrangians, Eq. (5.37) and Eq. (5.44), via the mixing Eq. (2.71). The dominant assignment $K_{1,B} \approx K_1(1270)$ in this subsection is, although a crude approximation, enough for our goals.
2. We present the results in Table 5.9 for two values of the unknown mixing angle $\beta_{b_1} \approx 0$ and $\beta_{b_1} \approx -40^\circ$, the latter being similar to the mixing angle for the pseudoscalar-isoscalars. According to Table 5.9, the mixing angle β_{b_1} appears in the decay channels $\rho_3(1690) \rightarrow h_1(1170) \pi$, $\rho_3(1690) \rightarrow h_1(1415) \pi$, $K_3^*(1780) \rightarrow h_1(1170) \bar{K}$, and $\phi_3(1850) \rightarrow h_1(1170) \eta$. The decay channel $\omega_3(1670) \rightarrow b_1(1235) \pi$ is the only experimentally "possibly seen" [172], and corresponds to a rather large theoretical partial decay width.
3. The decay channel $\rho_3(1690) \rightarrow h_1(1170) \pi$ is also independent on the mixing β_{b_1} . This decay is the dominant one and thus quite interesting for future investigations. The fact that the remaining decay channels are rather small may be the reason why their experimental observation was not yet possible.

5.3.6 Decay channel $W_3 \rightarrow A_1 + P$

For the decay into an axial-vector and a pseudoscalar meson, the interaction Lagrangian and the corresponding decay formula are given by

$$\mathcal{L}_{w_3 a_1 p} = g_{w_3 a_1 p} \text{tr} [W_3^{\mu\nu\rho} [A_{1,\mu}, (\partial_\nu \partial_\rho P)]_-], \quad (5.44)$$

$$\Gamma_{W_3 \rightarrow A_1 + P}(m_{w_3}, m_{a_1}, m_p) = g_{w_3 a_1 p}^2 \frac{|\vec{k}_{w_3, a_1, p}|^5}{420 m_{w_3}^2} \left(7 + 3 \frac{|\vec{k}_{w_3, a_1, p}|^2}{m_{a_1}^2} \right) \times \kappa_i \ominus(m_{w_3} - m_{a_1} - m_p), \quad (5.45)$$

where κ_i 's are given in Table 5.10. As previously stated, we are assuming that $K_{1,A} \approx K_1(1400)$ in this estimate. Only some predictions for ratios of various decay channels can be made because we lack sufficient experimental data to determine the coupling constant $g_{w_3 a_1 p}$. These predictions are listed in Table 5.10 and are independent of the mixing angle β_{a_1} as can be seen from Table 5.10. In any case, a small mixing is expected [87].

decay ratio	$\frac{\kappa_i}{\kappa_{w_3 a_1 p}}$	theory
$\frac{\Gamma_{K_3^*(1780) \rightarrow K_{1,A} \pi}}{\Gamma_{\rho_3(1690) \rightarrow a_1(1260) \pi}}$	$\frac{\left(\frac{1}{4}\right)^2 + \left(\frac{\sqrt{2}}{4}\right)^2}{2 \left(\frac{1}{2}\right)^2}$	0.12
$\frac{\Gamma_{K_3^*(1780) \rightarrow a_1(1260) K}}{\Gamma_{\rho_3(1690) \rightarrow a_1(1260) \pi}}$	$\frac{\left(\frac{1}{4}\right)^2 + \left(\frac{\sqrt{2}}{4}\right)^2}{2 \left(\frac{1}{2}\right)^2}$	0.01

Table 5.10: Clebsch-Gordan coefficients and corresponding decay ratios for $W_3 \rightarrow A_1 + P$ w.r.t. $\rho_3(1690) \rightarrow a_1(1260) \pi$ decay mode.

Finally, it is intriguing to note that connecting the current model to an underlying chiral model, such as the eLSM, makes it possible to estimate the coupling constant $g_{w_3 a_1 p}$ using Eq. (5.12). This rough estimation leads to

$$g_{w_3 a_1 p}^2 \approx 3 \cdot 10^{-4} \text{ MeV}^{-2} \longrightarrow \Gamma_{\rho_3(1690) \rightarrow a_1(1260) \pi} = 2 \text{ MeV}, \quad (5.46)$$

which implies the suppression of the decays $W_3 \rightarrow A_1 + P$ type.

5.3.7 Decay channel $W_3 \rightarrow V_1^{(1)} + V_1^{(2)}$

The decaying process into two vector mesons is described by

$$\mathcal{L}_{w_3 v_1 v_1} = g_{w_3 v_1 v_1} \text{tr} [W_3^{\mu\nu\rho} [(\partial_\mu V_{1,\nu}), V_{1,\rho}]_-], \quad (5.47)$$

with the corresponding decay rate

$$\begin{aligned} \Gamma_{W_3 \rightarrow V_1^{(1)} + V_1^{(2)}}(m_{w_3}, m_{v^{(1)}}, m_{v^{(2)}}) = & g_{w_3 v_1 v_1}^2 \frac{|\vec{k}_{w_3, v^{(1)}, v^{(2)}}|^3}{840 m_{v^{(1)}}^2 m_{v^{(2)}}^2 m_{w_3}^2} \left[6 |\vec{k}_{w_3, v^{(1)}, v^{(2)}}|^4 + \right. \\ & \left. + 35 m_{v^{(1)}}^2 m_{v^{(2)}}^2 + 14 |\vec{k}_{w_3, v^{(1)}, v^{(2)}}|^2 (m_{v^{(1)}}^2 + m_{v^{(2)}}^2) \right] \kappa_i \Theta(m_{w_3} - m_{v^{(1)}} - m_{v^{(2)}}), \quad (5.48) \end{aligned}$$

where the κ_i are given in Table 5.11. Also here, we are unable to estimate the coupling

decay process	κ_i	theory using (5.49) & (5.50) Γ/MeV	theory using (5.52) & (5.54) Γ/MeV
$\rho_3(1690) \rightarrow \rho(770) \rho(770)$	1	$\lesssim 108.6 \pm 35.3$	$\lesssim 30$
$K_3^*(1780) \rightarrow \rho(770) \bar{K}^*(892)$	$(\frac{1}{2})^2 + (\frac{\sqrt{2}}{2})^2$	$\lesssim 53.6 \pm 17.4$	$\lesssim 15$
$K_3^*(1780) \rightarrow \bar{K}^*(892) \omega(782)$	$[\frac{1}{2} (\cos \beta_{v_1} - \sqrt{2} \sin \beta_{v_1})]^2$	$\lesssim 19.0 \pm 6.2$	$\lesssim 5$
$\phi_3(1850) \rightarrow \bar{K}^*(892) K^*(892)$	$2 [\frac{1}{2} (\sqrt{2} \cos \beta_{w_3} + \sin \beta_{w_3})]^2$	$\lesssim 38.3 \pm 12.5$	$\lesssim 11$

Table 5.11: Estimates of the upper limits for two-vector decay channels.

constant, but we present the decay ratios listed in Table 5.12.

decay ratio	theory
$\frac{\Gamma_{K_3^*(1780) \rightarrow \rho(770) \bar{K}^*(892)}}{\Gamma_{\rho_3(1690) \rightarrow \rho(770) \rho(770)}}$	0.49
$\frac{\Gamma_{K_3^*(1780) \rightarrow \bar{K}^*(892) \omega(782)}}{\Gamma_{\rho_3(1690) \rightarrow \rho(770) \rho(770)}}$	0.17
$\frac{\Gamma_{\phi_3(1850) \rightarrow \bar{K}^*(892) K^*(892)}}{\Gamma_{\rho_3(1690) \rightarrow \rho(770) \rho(770)}}$	0.35

Table 5.12: Decay ratios for $W_3 \rightarrow V_1^{(1)} + V_1^{(2)}$
w.r.t. $\rho_3(1690) \rightarrow \rho \rho$ decay mode.

We also determine an upper bound of the coupling constant via

$$\frac{\Gamma_{\rho_3(1690) \rightarrow \pi \pi}}{\Gamma_{\rho_3(1690) \rightarrow \rho(770) \rho(770)}} \gtrsim \frac{\Gamma_{\rho_3(1690) \rightarrow \pi \pi}}{\Gamma_{\rho_3(1690) \rightarrow \pi^\pm \pi^+ \pi^- \pi^0}} \stackrel{\text{PDG}}{=} 0.35 \pm 0.11, \quad (5.49)$$

which is inferred from the fact that the $\rho_3(1690) \rightarrow \rho(770) \rho(770)$ decay channel is part of the process $\rho_3(1690) \rightarrow \pi^\pm \pi^+ \pi^- \pi^0$, which is one of the dominating channels.

Using the experimental result $\Gamma_{\rho_3(1690) \rightarrow \pi \pi} = (38.0 \pm 3.2)$ MeV we obtain

$$g_{w_3 v_1 v_1}^2 \lesssim 535 \pm 174, \quad (5.50)$$

and calculate upper bounds for the decay rates in Table 5.11.

However, using a value near this upper limit of Eq. (5.50) would suggest that the sum of all the decays of the state $\rho_3(1690)$ would exceed the experimental total width of (161 ± 10) MeV, indicating that the decay width of roughly 108 MeV is undoubtedly too large. This is consistent with the ratio given in PDG [27] where the experimental measurements [173–176],

$$\frac{\Gamma_{\rho_3(1690) \rightarrow \rho(770) \rho(770)}}{\Gamma_{\rho_3(1690) \rightarrow \pi^\pm \pi^+ \pi^- \pi^0}} < 1. \quad (5.51)$$

To get a second, more accurate estimate of these decay channels, we first add up the biggest decay channels:

$$\begin{aligned} \Gamma_{\rho_3}^{\text{tot}} &= 161 \text{ MeV} \approx & (5.52) \\ &= \Gamma_{\rho_3(1690) \rightarrow \pi \pi} + \Gamma_{\rho_3(1690) \rightarrow \bar{K} K} + \Gamma_{\rho_3(1690) \rightarrow \rho(770) \eta} + \\ &\quad + \Gamma_{\rho_3(1690) \rightarrow \bar{K}^*(892) K} + \Gamma_{\rho_3(1690) \rightarrow \omega(782) \pi} + \Gamma_{\rho_3(1690) \rightarrow \phi(1020) \pi} + \\ &\quad + \Gamma_{\rho_3(1690) \rightarrow a_2(1320) \pi} + \Gamma_{\rho_3(1690) \rightarrow a_1(1260) \pi} + \Gamma_{\rho_3(1690) \rightarrow h_1(1170) \pi} + \\ &\quad + \Gamma_{\rho_3(1690) \rightarrow h_1(1415) \pi} + \Gamma_{\rho_3(1690) \rightarrow \rho(770) \rho(770)} + \Gamma_{\rho_3(1690) \rightarrow \text{other}}, \end{aligned}$$

where $\Gamma_{\rho_3 \rightarrow \text{other}}$ is an abbreviation for any other decay channels that are not mentioned above and are expected to be small. We use the smaller value shown in Table 5.9 for $\Gamma_{\rho_3(1690) \rightarrow h_1(1170) \pi}$ while assuming a large mixing angle of $\beta_{b_1} = -40^\circ$. This method

allows us to calculate a reasonable upper limit

$$\Gamma_{\rho_3(1690) \rightarrow \rho(770)\rho(770)} \lesssim 30 \text{ MeV}, \quad (5.53)$$

which implies the following limit for the coupling $g_{w_3 v_1 v_1}$

$$g_{w_3 v_1 v_1}^2 \lesssim 148. \quad (5.54)$$

Table 5.11 contains the predictions for the vector-vector pair decay channels. Next, we add the estimates of the dominant decay channels for the other spin-3 mesons to get the following total decay widths, which are in agreement with the PDG listed in Table 5.3:

$$\Gamma_{K_3^*(1780)}^{\text{sum}} \approx 146 \text{ MeV}, \quad \Gamma_{\omega_3(1670)}^{\text{sum}} \approx 175 \text{ MeV}, \quad \Gamma_{\phi_3(1850)}^{\text{sum}} \approx 80 \text{ MeV}. \quad (5.55)$$

Parameters	Numerical Values	Sections
$g_{w_3 pp}^2$	$(1.5 \pm 0.1) \cdot 10^{-10} \text{ MeV}^{-4}$	Sec. 5.3.1
$g_{w_3 vp}^2$	$(9.2 \pm 1.9) \cdot 10^{-16} \text{ MeV}^{-6}$	Sec. 5.3.2
$g_{w_3 tp}^2$	$(2.8 \pm 1.2) \cdot 10^{-9} \text{ MeV}^{-4}$	Sec. 5.3.4
$g_{w_3 b_1 p}^2$	$(0.008 \pm 0.003) \text{ MeV}^{-2}$	Sec. 5.3.5
$g_{w_3 a_1 p}^2$	$\approx 3 \cdot 10^{-4} \text{ MeV}^{-2}$	Sec. 5.3.6
$g_{w_3 v_1 v_1}^2$	$\lesssim 148$	Sec. 5.3.7

Table 5.13: Parameters of Lagrangians in Table 5.1.

5.4 Spin-3 Glueball

In this section, we extend the model results to a hypothetical glueball with $J^{PC} = 3^{--}$. This glueball has not yet been observed experimentally, just like all the other gluonic bound states, but its mass is predicted to be around 4.13 GeV [131], 4.33 GeV [132], or 4.20 GeV [130] by LQCD calculations using the quenched approximation. General works on glueballs can be found in *e.g.* Refs. [127, 128, 177, 178], and within effective models in Refs. [22, 83, 85, 101, 179]. All decay ratios in this section should be viewed as first indicative results.

5.4.1 Effective Lagrangians for G_3

Each glueball is a flavor singlet object, which is invariant under $SU_V(3)$ transformations. We use this fact to determine the Lagrangian analogous to chapter 4 to describe the decays of the spin-3 glueball. In practise we can obtain the needed interaction terms via the simple replacement

$$W^{\mu\nu\rho} \rightarrow G_3^{\mu\nu\rho} \cdot \mathbb{1}_{3 \times 3}, \quad (5.56)$$

where $G_3^{\mu\nu\rho}$ is the glueball field with $J^{PC} = 3^{--}$ and $\mathbb{1}_{3 \times 3}$ is the 3×3 identity matrix. The interaction terms that go along with a commutator consequently disappear, and the only nonzero contributions to an effective action for the 3^{--} glueball can be obtained from the previous interaction terms involving the anticommutator in Table 5.14.

decay process	Interaction Lagrangians
$G_3 \rightarrow V_1 + P$	$\mathcal{L}_{g_3v_1p} = c_{g_3v_1p} G_{3,\mu\alpha\beta} \varepsilon^{\mu\nu\rho\sigma} \text{tr}[\{(\partial_\nu V_{1,\rho}), (\partial^\alpha \partial^\beta \partial_\sigma P)\}_+]$
$G_3 \rightarrow \gamma + P$	$\mathcal{L}_{g_3\gamma p} = c_{g_3\gamma p} \frac{e}{g_\rho} G_{3,\mu\alpha\beta} (\partial_\nu a_\rho) \varepsilon^{\mu\nu\rho\sigma} \text{tr}[\{Q, (\partial^\alpha \partial^\beta \partial_\sigma P)\}_+]$
$G_3 \rightarrow V_1 + A_1$	$\mathcal{L}_{g_3v_1a_1} = c_{g_3v_1a_1} G_{3,\mu\alpha\beta} \varepsilon^{\mu\nu\rho\sigma} \text{tr}[\{(\partial_\nu V_{1,\rho}), (\partial^\alpha \partial^\beta A_{1,\sigma})\}_+]$
$G_3 \rightarrow B_1 + P$	$\mathcal{L}_{g_3b_1p} = c_{g_3b_1p} G_3^{\mu\nu\rho} \text{tr}[\{B_{1,\mu'}, (\partial_\nu \partial_\rho P)\}_+]$
$G_3 \rightarrow B_1 + A_1$	$\mathcal{L}_{g_3b_1a_1} = c_{g_3b_1a_1} G_3^{\mu\nu\rho} \text{tr}[\{B_{1,\mu'}, (\partial_\nu A_{1,\rho})\}_+]$

Table 5.14: Interaction Lagrangians for the hypothetical glueball state $G_3(4200)$.

Furthermore, there are decays of the types $G_3(4200) \rightarrow V_1 + A_1$ and $G_3(4200) \rightarrow B_1 + A_1$ that were kinematically prohibited and therefore not included in the calculations for the lightest conventional mesons with $J^{PC} = 3^{--}$. Theoretical estimates for decay ratios are provided in the section below and can be computed by using the same procedure as before. The only quantities required to calculate the decay ratios are the particle masses.

decay ratio	theory
$\frac{\Gamma_{G_3(4200) \rightarrow \bar{K}^*(892) K}}{\Gamma_{G_3(4200) \rightarrow \rho(770) \pi}}$	1.11
$\frac{\Gamma_{G_3(4200) \rightarrow \omega(782) \eta}}{\Gamma_{G_3(4200) \rightarrow \rho(770) \pi}}$	0.17
$\frac{\Gamma_{G_3(4200) \rightarrow \omega(782) \eta'(958)}}{\Gamma_{G_3(4200) \rightarrow \rho(770) \pi}}$	0.089
$\frac{\Gamma_{G_3(4200) \rightarrow \phi(1020) \eta}}{\Gamma_{G_3(4200) \rightarrow \rho(770) \pi}}$	0.098
$\frac{\Gamma_{G_3(4200) \rightarrow \phi(1020) \eta'(958)}}{\Gamma_{G_3(4200) \rightarrow \rho(770) \pi}}$	0.11

Table 5.15: Decay ratios of $G_3(4200)$ w.r.t. $\rho \pi$.

5.4.2 Decay channel $G_3 \rightarrow V_1 + P$

The decay of a spin-3 tensor glueball into a vector and a pseudoscalar meson is represented by the following interaction Lagrangian:

$$\mathcal{L}_{g_3 v_1 p} = c_{g_3 v_1 p} G_{3, \mu \alpha \beta} \varepsilon^{\mu \nu \rho \sigma} \text{tr} \left[\{ (\partial_\nu V_{1, \rho}), (\partial^\alpha \partial^\beta \partial_\sigma P) \}_+ \right], \quad (5.57)$$

and the decay rate formula:

$$\Gamma_{G_3 \rightarrow V_1 + P}(m_{g_3}, m_v, m_p) = c_{g_3 v_1 p}^2 \frac{|\vec{k}_{g_3, v, p}|^7}{105} \kappa_i \Theta(m_{g_3} - m_v - m_p), \quad (5.58)$$

where κ_i are given in Table 5.20. Throughout the remaining of the chapter, we use the glueball mass $m_{g_3} = 4200$ MeV in Table 5.2 to calculate the momenta of the outgoing particles. Since we do not know the coupling constant $c_{g_3 v_1 p}$, we compute the nonzero ratios in Table 5.15. This channel will eventually appear in the experiments (ones G_3 will be found) as a decay into three (or four) pseudoscalar mesons, because the vector mesons further decay into two (or three) pseudoscalar mesons.

5.4.3 Decay channel $G_3 \rightarrow \gamma + P$

We can also study radiative decay terms for the spin-3 glueball using vector meson dominance via the shift of Eq. (3.15):

$$\mathcal{L}_{g_3\gamma p} = c_{g_3\gamma p} \frac{e}{g_\rho} G_{3,\mu\alpha\beta} (\partial_\nu a_\rho) \varepsilon^{\mu\nu\rho\sigma} \text{tr}[\{Q, (\partial^\alpha \partial^\beta \partial_\sigma P)\}_+],$$

leading to the κ_i^γ are summarized in Table 5.20, which are used in the following decay rate formula to obtain the results in Table 5.16

$$\Gamma_{G_3 \rightarrow \gamma + P}(m_{g_3}, m_p) = c_{g_3 v_1 p}^2 \left(\frac{e}{g_\rho}\right)^2 \frac{|\vec{k}_{g_3\gamma,p}|^7}{105\pi} \kappa_i^\gamma.$$

We present the decays $\Gamma_{G_3 \rightarrow \gamma P}$ w.r.t. the strong decay channel $\Gamma_{G_3(4200) \rightarrow \rho(770) \pi}$ in Table 5.16.

decay ratio	theory
$\frac{\Gamma_{G_3(4200) \rightarrow \gamma \pi^0}}{\Gamma_{G_3(4200) \rightarrow \rho(770) \pi}}$	$129 \cdot 10^{-5}$
$\frac{\Gamma_{G_3(4200) \rightarrow \gamma \eta}}{\Gamma_{G_3(4200) \rightarrow \rho(770) \pi}}$	$37 \cdot 10^{-5}$
$\frac{\Gamma_{G_3(4200) \rightarrow \gamma \eta'(958)}}{\Gamma_{G_3(4200) \rightarrow \rho(770) \pi}}$	$1 \cdot 10^{-5}$

Table 5.16: Decay ratios of $G_3(4200)$ w.r.t. $G_3(4200) \rightarrow \rho \pi$.

5.4.4 Decay channel $G_3 \rightarrow V_1 + A_1$

By taking into account the Lagrangian in which G_3 couples to $V_1 A_1$, we provide the glueball decay ratios into one vector and one axial-vector

$$\mathcal{L}_{g_3 v_1 a_1} = c_{g_3 v_1 a_1} G_{3,\mu\alpha\beta} \varepsilon^{\mu\nu\rho\sigma} \text{tr}[\{(\partial_\nu V_{1,\rho}), (\partial^\alpha \partial^\beta A_{1,\sigma})\}_+],$$

which leads to the tree-level decay formula given by

$$\begin{aligned} \Gamma_{G_3 \rightarrow V_1 + A_1}(m_{g_3}, m_v, m_{a_1}) &= \quad (5.59) \\ &= c_{g_3 v_1 a_1}^2 \frac{|\vec{k}_{g_3, v, a_1}|^5}{210 m_{g_3}^2} \left[|\vec{k}_{g_3, v, a_1}|^2 \left(3 + 2 \frac{m_{g_3}^2}{m_{a_1}^2} \right) + 7 m_v^2 \right] \kappa_i \Theta(m_{g_3} - m_v - m_{a_1}), \end{aligned}$$

where the coefficients κ_i are presented in Table 5.20 and the outcomes are shown in Table 5.17.

decay ratio	theory
$\frac{\Gamma_{G_3(4200) \rightarrow \bar{K}^*(892) K_{1,A}}}{\Gamma_{G_3(4200) \rightarrow \rho(770) a_1(1260)}}$	0.78
$\frac{\Gamma_{G_3(4200) \rightarrow \omega(782) f_1(1285)}}{\Gamma_{G_3(4200) \rightarrow \rho(770) a_1(1260)}}$	0.29
$\frac{\Gamma_{G_3(4200) \rightarrow \omega(782) f_1(1420)}}{\Gamma_{G_3(4200) \rightarrow \rho(770) a_1(1260)}}$	0.0009
$\frac{\Gamma_{G_3(4200) \rightarrow \phi(1020) f_1(1285)}}{\Gamma_{G_3(4200) \rightarrow \rho(770) a_1(1260)}}$	0.0011
$\frac{\Gamma_{G_3(4200) \rightarrow \phi(1020) f_1(1420)}}{\Gamma_{G_3(4200) \rightarrow \rho(770) a_1(1260)}}$	0.16

Table 5.17: Decay ratios of $G_3(4200)$ w.r.t. $G_3(4200) \rightarrow \rho a_1$.

5.4.5 Decay channel $G_3 \rightarrow B_1 + P$

The decay of the $J^{PC} = 3^{--}$ glueball into a pseudovector and a pseudoscalar meson is given by the interaction Lagrangian

$$\mathcal{L}_{g_3 b_1 p} = c_{g_3 b_1 p} G_3^{\mu\nu\rho} \text{tr}[\{B_{1,\mu'} (\partial_\nu \partial_\rho P)\}_+], \quad (5.60)$$

which leads to the decay rate formula

$$\Gamma_{G_3 \rightarrow B_1 + P}(m_{g_3}, m_{b_1}, m_p) = c_{g_3 b_1 p}^2 \frac{|\vec{k}_{g_3 b_1 p}|^5}{420 m_{g_3}^2} \left(7 + 3 \frac{|\vec{k}_{g_3 b_1 p}|^2}{m_{b_1}^2} \right) \kappa_i \Theta(m_{g_3} - m_{b_1} - m_p). \quad (5.61)$$

We consider two mixing angle options ($\beta_{b_1} \approx 0^\circ$ and $\beta_{b_1} \approx -40^\circ$) and report the decay rates in Table 5.18 using $m_{K_{1,B}} \approx m_{K_1(1270)}$.

decay ratio	theory for	theory for
	$\beta_{b_1} = 0^\circ$	$\beta_{b_1} = -40^\circ$
$\frac{\Gamma_{G_3(4200) \rightarrow K_{1,B} K}}{\Gamma_{G_3(4200) \rightarrow b_1(1235) \pi}}$	1.15	1.15
$\frac{\Gamma_{G_3(4200) \rightarrow h_1(1170) \eta}}{\Gamma_{G_3(4200) \rightarrow b_1(1235) \pi}}$	0.17	0.33
$\frac{\Gamma_{G_3(4200) \rightarrow h_1(1170) \eta'(958)}}{\Gamma_{G_3(4200) \rightarrow b_1(1235) \pi}}$	0.12	0.001
$\frac{\Gamma_{G_3(4200) \rightarrow h_1(1415) \eta}}{\Gamma_{G_3(4200) \rightarrow b_1(1235) \pi}}$	0.10	0.001
$\frac{\Gamma_{G_3(4200) \rightarrow h_1(1415) \eta'(958)}}{\Gamma_{G_3(4200) \rightarrow b_1(1235) \pi}}$	0.08	0.16

Table 5.18: Decay ratios of $G_3(4200)$ w.r.t. $G_3(4200) \rightarrow b_1 \pi$.

5.4.6 Decay channel $G_3 \rightarrow B_1 + A_1$

Additionally, for $\beta_{a_1} \approx 0^\circ$, we show in Table 5.19 the results for the decay of the spin-3 glueball into a pseudovector and an axial-vector using the following Lagrangian

$$\mathcal{L}_{g_3 b_1 a_1} = c_{g_3 b_1 a_1} G_3^{\mu\nu\rho} \text{tr}[\{B_{1,\mu'} (\partial_\nu A_{1,\rho})\}_+], \quad (5.62)$$

with the resulting decay formula

$$\begin{aligned}
\Gamma_{G_3 \rightarrow B_1 + A_1}(m_{g_3}, m_{b_1}, m_{a_1}) &= \tag{5.63} \\
&= c_{g_3 b_1 a_1}^2 \frac{|\vec{k}_{g_3, b_1, a_1}|^3}{840 m_{b_1}^2 m_{a_1}^2 m_{g_3}^2} \left[6 |\vec{k}_{g_3, b_1, a_1}|^4 + \right. \\
&\quad \left. + 35 m_{b_1}^2 m_{a_1}^2 + 14 |\vec{k}_{g_3, b_1, a_1}|^2 (m_{b_1}^2 + m_{a_1}^2) \right] \kappa_i \Theta(m_{g_3} - m_{b_1} - m_{a_1}),
\end{aligned}$$

where the κ_i are listed in Table 5.20.

decay ratio	theory for $\beta_{b_1} = 0^\circ$	theory for $\beta_{b_1} = -40^\circ$
$\frac{\Gamma_{G_3(4200) \rightarrow K_{1,B} K_{1,A}}}{\Gamma_{G_3(4200) \rightarrow b_1(1235) a_1(1260)}}$	0.96	0.96
$\frac{\Gamma_{G_3(4200) \rightarrow h_1(1170) f_1(1285)}}{\Gamma_{G_3(4200) \rightarrow b_1(1235) a_1(1260)}}$	0.34	0.20
$\frac{\Gamma_{G_3(4200) \rightarrow h_1(1170) f_1(1420)}}{\Gamma_{G_3(4200) \rightarrow b_1(1235) a_1(1260)}}$	0	0.11
$\frac{\Gamma_{G_3(4200) \rightarrow h_1(1415) f_1(1285)}}{\Gamma_{G_3(4200) \rightarrow b_1(1235) a_1(1260)}}$	0	0.092
$\frac{\Gamma_{G_3(4200) \rightarrow h_1(1415) f_1(1420)}}{\Gamma_{G_3(4200) \rightarrow b_1(1235) a_1(1260)}}$	0.17	0.10

Table 5.19: Decay ratios of $G_3(4200)$ w.r.t. $G_3(4200) \rightarrow b_1 a_1$.

5.5 Conclusions

In this chapter, we used an effective QFT model based on flavor symmetry to study the decays of the lightest mesonic $\bar{q}q$ nonet with $J^{PC} = 3^{--}$. Only the dominant terms in the large- N_c expansion and the lowest derivatives were kept in our model. We come to the conclusion that the $\bar{q}q$ assignment for decay widths and some known branching ratios, which are listed in PDG [27], works quite well, as the comparison of theoretical

decay process	κ_i
$G_3(4200) \rightarrow \rho(770) \pi$	3
$G_3(4200) \rightarrow \bar{K}^*(892) K$	4
$G_3(4200) \rightarrow \omega(782) \eta$	$[\cos(\beta_p - \beta_{v_1})]^2$
$G_3(4200) \rightarrow \omega(782) \eta'(958)$	$[\sin(\beta_p - \beta_{v_1})]^2$
$G_3(4200) \rightarrow \phi(1020) \eta$	$[\sin(\beta_p - \beta_{v_1})]^2$
$G_3(4200) \rightarrow \phi(1020) \eta'(958)$	$[\cos(\beta_p - \beta_{v_1})]^2$
$G_3(4200) \rightarrow \gamma \pi^0$	1
$G_3(4200) \rightarrow \gamma \eta$	$[\frac{1}{3} (\cos \beta_p - \sqrt{2} \sin \beta_p)]^2$
$G_3(4200) \rightarrow \gamma \eta'(958)$	$[\frac{1}{3} (\sin \beta_p + \sqrt{2} \cos \beta_p)]^2$
$G_3(4200) \rightarrow \rho(770) a_1(1260)$	3
$G_3(4200) \rightarrow \bar{K}^*(892) K_{1,A}$	4
$G_3(4200) \rightarrow \omega(782) f_1(1285)$	$[\cos(\beta_{a_1} - \beta_{v_1})]^2$
$G_3(4200) \rightarrow \omega(782) f_1'(1420)$	$[\sin(\beta_{a_1} - \beta_{v_1})]^2$
$G_3(4200) \rightarrow \phi(1020) f_1(1285)$	$[\sin(\beta_{a_1} - \beta_{v_1})]^2$
$G_3(4200) \rightarrow \phi(1020) f_1'(1420)$	$[\cos(\beta_{a_1} - \beta_{v_1})]^2$
$G_3(4200) \rightarrow b_1(1235) \pi$	3
$G_3(4200) \rightarrow K_{1,B} K$	4
$G_3(4200) \rightarrow h_1(1170) \eta$	$[\cos(\beta_p - \beta_{b_1})]^2$
$G_3(4200) \rightarrow h_1(1170) \eta'(958)$	$[\sin(\beta_p - \beta_{b_1})]^2$
$G_3(4200) \rightarrow h_1(1415) \eta$	$[\sin(\beta_p - \beta_{b_1})]^2$
$G_3(4200) \rightarrow h_1(1415) \eta'(958)$	$[\cos(\beta_p - \beta_{b_1})]^2$
$G_3(4200) \rightarrow b_1(1235) a_1(1260)$	3
$G_3(4200) \rightarrow K_{1,B} K_{1,A}$	4
$G_3(4200) \rightarrow h_1(1170) f_1(1285)$	$[\cos(\beta_{a_1} - \beta_{b_1})]^2$
$G_3(4200) \rightarrow h_1(1170) f_1'(1420)$	$[\sin(\beta_{a_1} - \beta_{b_1})]^2$
$G_3(4200) \rightarrow h_1(1415) f_1(1285)$	$[\sin(\beta_{a_1} - \beta_{b_1})]^2$
$G_3(4200) \rightarrow h_1(1415) f_1'(1420)$	$[\cos(\beta_{a_1} - \beta_{b_1})]^2$

Table 5.20: Clebsch-Gordan coefficients κ_i for the decay channels of $G_3(4200)$.

outcomes with the current state of experimental data shows. However, some of the decay channels in our study also merit more in-depth theoretical and experimental work in the future. Moreover, we presented a variety of predictions for strong and radiative decays of conventional $J^{PC} = 3^{--}$ mesons, eventually useful for upcoming experimental tests. Figure 5.1 and Figure 5.2 summarize the comparison between our model results and PDG as well as LQCD predictions.

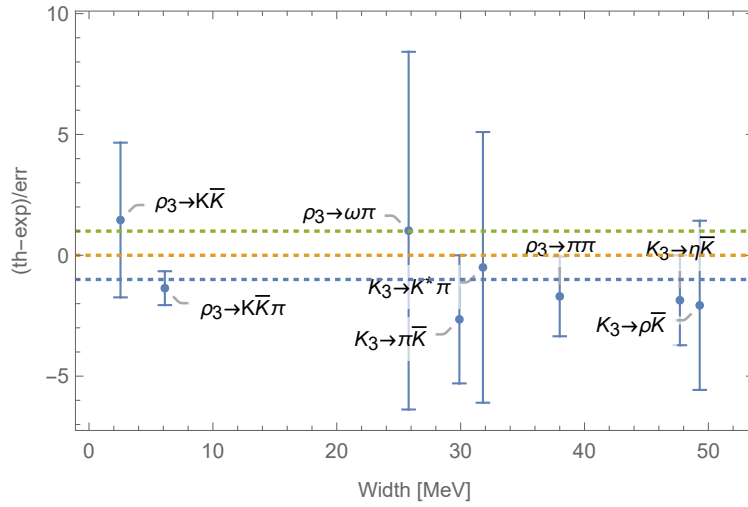


Figure 5.1: Model results compared to PDG [27].

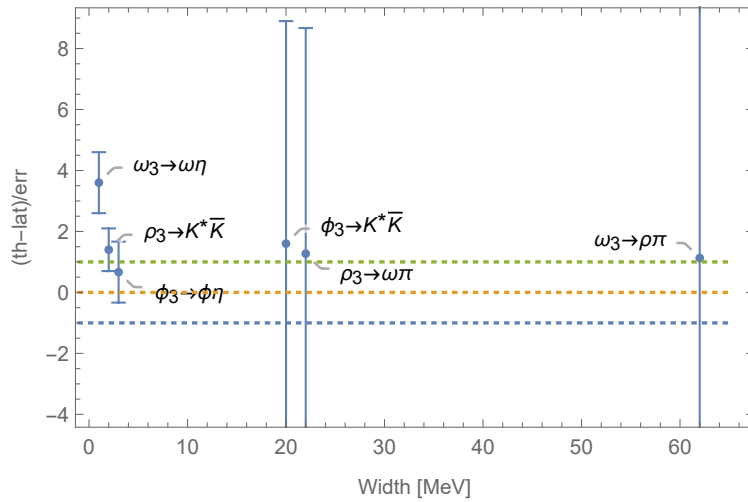


Figure 5.2: Model results compared to LQCD [28].

We have then extended the effective model for spin-3 mesons to the case of a glueball. Because of the unknown coupling, we presented only the strong and radiative decay ratios.

Chapter 6

Glueball Resonance Gas model

This chapter is about the effect of the glueball spectrum on the pure YM part of the QCD Equation of State (EoS) at nonzero temperature.

6.1 Introduction

Some experiments at the RHIC and LHC are devoted to the formation of extremely hot and dense QCD matter through the collision of heavy nuclei. Intriguing non-perturbative characteristics of QCD are realized in the QCD in the medium, which are explored through these experiments. That is why the understanding of the QCD phase diagram is the subject of extensive theoretical studies [180–182]. Theoretical methods for studying the QCD phase diagram are divided into two parts:

1. From first principles:

- Lattice QCD (see e.g. Refs. [30, 183–188]);
- Functional methods (functional renormalization group - FRG (see e.g. Refs. [45, 189–191]);
- Dyson-Schwinger equation (see e.g. Refs. [192, 193]);
- Perturbative approach (see e.g. [194] and Refs therein).

2. Model-based approaches:

- Nambu-Jona-Lasinio (NJL)-type models [112, 113];
- Hadronic models (see e.g. eLSM [195, 196]);

- Hadron Resonance Gas (HRG) model (see e.g. [197–202]).

At zero quark chemical potential, LQCD shows a smooth cross-over phase transition between high-temperature regime quark-gluon plasma (QGP) and HRG at low temperature.

As we have mentioned in the previous chapters, glueballs are the predictions of the pure YM sector of QCD. They have been investigated using a variety of techniques, such as LQCD, where their spectrum is analyzed; in spite of that, they need a final experimental confirmation (although certain candidates do exist) [29, 132, 203, 204]. They have been investigated in various models [67, 205–208]. Studies on the pomeron and odderon trajectories support the existence of glueballs. [209].

One can use glueballs to construct the so-called Glueball Resonance Gas (GRG) in order to study the properties of the YM Equation of State at low temperatures. Lattice simulations show a first-order phase transition between the gluonic bound states at low temperature (the glueballs) and a gas of gluons at high temperature [30, 210–215]. The inclusion of the Hagedorn contribution (see the original work in [216]) to the GRG with the mass spectrum Ref. [203] is proposed in order to fill the gap between the lattice thermodynamic simulations for the pressure close to the critical temperature T_c [217].

There are other methods to study the thermal properties of QCD, including the T-Matrix approach [218], the Polyakov-loop potential [219], functional methods [220], holographic QCD [221], quasi-particle models [222, 223], bag model [224, 225], hard-thermal-loop perturbation theory [198] and a gas of gluons at high temperature [226–228].

In this chapter, we revisit the role of the glueball spectrum, taken from Refs. [29, 132, 203] within the low-temperature phase diagram of the pure YM sector of QCD by comparing the results to the lattice thermodynamic outcomes of Ref. [30]. The physical masses of the glueball spectrum depend on the lattice parameters, which eventually lead to different T_c for three different glueball gases. The best agreement of the GRG and with thermal LQCD simulation in [30] is obtained by using the masses of Ref. [29]. This agreement implies $T_c \sim 320 \pm 20$ MeV which is somewhat larger than the commonly used value of $T_c \sim 260$ MeV [30]. It is interesting to note that Ref [229] estimates T_c around 300 MeV for pure YM using functional techniques. Furthermore, assuming the Regge trajectories for the glueball states, contributions from radially

excited glueballs are also taken into account. Also, the role of the interaction between glueballs will be investigated.

6.2 Thermodynamics of the GRG

The energy density ϵ_i and pressure p_i of the i -th glueball with the total spin J_i are used to explain the thermodynamic properties of the GRG and have the following forms (see Ref. [180] for more details about QCD thermodynamics):

$$\epsilon_i = (2J_i + 1) \int_0^\infty \frac{k^2}{2\pi^2} \frac{\sqrt{k^2 + m_i^2}}{\exp\left[\frac{\sqrt{k^2 + m_i^2}}{T}\right] - 1} dk, \quad (6.1)$$

and

$$p_i = -(2J_i + 1)T \int_0^\infty \frac{k^2}{2\pi^2} \ln\left(1 - e^{-\frac{\sqrt{k^2 + m_i^2}}{T}}\right) dk. \quad (6.2)$$

The total energy density and the total pressure of the GRG are calculated by taking into account N glueballs as follows:

$$\epsilon^{\text{GRG}} \equiv \epsilon = \sum_{i=1}^N \epsilon_i, \quad p^{\text{GRG}} \equiv p = \sum_{i=1}^N p_i. \quad (6.3)$$

Information regarding the trace anomaly I and the entropy density s is provided

$$I = \epsilon - 3p, \quad s = \frac{p + \epsilon}{T}. \quad (6.4)$$

In the following, it is practical to work with the dimensionless pressure \hat{p} , energy density $\hat{\epsilon}$, trace anomaly \hat{I} and entropy \hat{s}

$$\hat{p} = p/T^4, \quad \hat{\epsilon} = \epsilon/T^4, \quad \hat{I} = \hat{\epsilon} - 3\hat{p}, \quad \hat{s} = s/T^3. \quad (6.5)$$

Using the masses from the lattice simulations provided in Table 6.1 and Table 6.2, we compute the GRG pressure and energy density using the aforementioned equations and compare the results to the relevant lattice calculations below the critical

temperature in the continuum limit of Ref. [30]. The thermodynamic quantities are functions of the ratio T/T_c in Ref. [30]. Thus, it is crucial to take into account the value of the critical temperature independently for each given lattice glueball spectrum. To this end, we call that the critical temperature T_c is connected to both the QCD string tension σ and the so-called Lambda parameter Λ_{MS} as follows [210,230,231]:

$$T_c = 0.629(3) \cdot \sqrt{\sigma}, \quad (6.6)$$

$$T_c = 1.26(7) \cdot \Lambda_{MS} = 1.26(7) \cdot 0.614(2) \cdot r_0^{-1}. \quad (6.7)$$

By using the formulas above, we determine the relevant critical temperature (along with an estimation of its error) for each simulation of the glueball mass spectrum, which is summarized in Table 6.1 (only statistical errors are given in [29]).

LQCD papers	Number of glueballs	Lattice Parameter	T_c (using Eqs. (6.6)-(6.7))
Chen et.al [203]	12	$r_0^{-1} = 410(20)$ MeV	317 ± 23 MeV
Meyer [132]	22	$\sqrt{\sigma} = 440(20)$ MeV	277 ± 13 MeV
Athenodorou and Teper [29]	20	$r_0^{-1} = 418(5)$ MeV	323 ± 18 MeV

Table 6.1: The LQCD parameters that have been used to get the glueball mass spectrum.

In Ref. [29], inspired by [232], a new scale $r_0 = 0.472(5)$ fm (corresponding to $r_0^{-1} = 418(5)$ MeV) is used, which results in slightly different glueball masses compared to Ref. [203]. Yet the results are compatible within errors. In contrast, masses and corresponding T_c in Ref. [132] are slightly smaller than Refs. [29,132].

In Ref. [135] for $N_c = 6$, a new approach is used to determine the masses of the glueballs with quantum numbers $J^{PC} = 0^{++}, 2^{++}, 0^{-+}, 2^{-+}, 1^{+-}$. The results match the values of Ref. [29] with an error of 2 – 5%, validating both the large- N_c limit and the masses in that reference. Moreover, it is intriguing that recent developments in functional techniques and Bethe-Salpeter approaches provide a spectrum that is similar to that found from lattice simulations [35,36,233].

We contrast LQCD simulations for the pure YM sector in Ref. [30] to the GRG results for pressure in Fig. 6.1, the trace anomaly in Fig. 6.2 and the entropy density in Fig. 6.3 using the parameters given in Table 6.1. As we see from the plots, the most recent lattice study, [29], generates a GRG that closely resembles the results in Ref. [30]

$n J^{PC}$	M[MeV]			$n J^{PC}$	M[MeV]		
	Chen et.al. [203]	Meyer [132]	A & T [29]		Chen et.al. [203]	Meyer [132]	A & T [29]
$1 0^{++}$	1710(50)(80)	1475(30)(65)	1653(26)	11^{--}	3830(40)(190)	3240(330)(150)	4030(70)
$2 0^{++}$		2755(30)(120)	2842(40)	12^{--}	4010(45)(200)	3660(130)(170)	3920(90)
$3 0^{++}$		3370(100)(150)		22^{--}		3740(200)(170)	
$4 0^{++}$		3990(210)(180)		13^{--}	4200(45)(200)	4330(260)(200)	
12^{++}	2390(30)(120)	2150(30)(100)	2376(32)	10^{+-}	4780(60)(230)		
22^{++}		2880(100)(130)	3300(50)	11^{+-}	2980(30)(140)	2670(65)(120)	2944(42)
13^{++}	3670(50)(180)	3385(90)(150)	3740(70)	21^{+-}			3800(60)
14^{++}		3640(90)(160)	3690(80)	12^{+-}	4230(50)(200)		4240(80)
16^{++}		4360(260)(200)		13^{+-}	3600(40)(170)	3270(90)(150)	3530(80)
10^{-+}	2560(35)(120)	2250(60)(100)	2561(40)	23^{+-}		3630(140)(160)	
20^{-+}		3370(150)(150)	3540(80)	14^{+-}			4380(80)
12^{-+}	3040(40)(150)	2780(50)(130)	3070(60)	15^{+-}		4110(170)(190)	
22^{-+}		3480(140)(160)	3970(70)				
15^{-+}		3942(160)(180)					
11^{-+}			4120(80)				
21^{-+}			4160(80)				
31^{-+}			4200(90)				

Table 6.2: The list of the glueball masses in Refs. [29, 132, 203].

for temperatures less than $0.9T_c$. The critical temperature $T_c \approx 323 \pm 18$ MeV turns out to be a larger than the reference value 260-270 MeV estimated in Ref. [30], but is consistent with the FRG result of Ref. [229].

In particular, we see from Figs. (6.1-6.3) that the GRG based on the mass spectrum in Ref. [29] (green dashed line) explains the data of Ref. [30] (blue thick line) better than the mass spectrum in Refs [132, 203] (black dotted and orange dashed lines). The fact that the pressure determined in Ref. [30] agrees with the free GRG with glueballs from [29] also suggests that the additional contribution from Hagedorn spectrum may not be necessary, at least up to $0.9T_c$.

The agreement is not spoiled by the contribution of further states as well as the interaction between the glueballs, see the next sections. Having a negligible contribution from the interaction is consistent with predictions by the large- N_c limit of the YM theory, which implies the glueballs can be seen, in first approximation, as non-interacting bosons since the interaction among glueballs scales as N_c^{-2} [119, 120, 234].

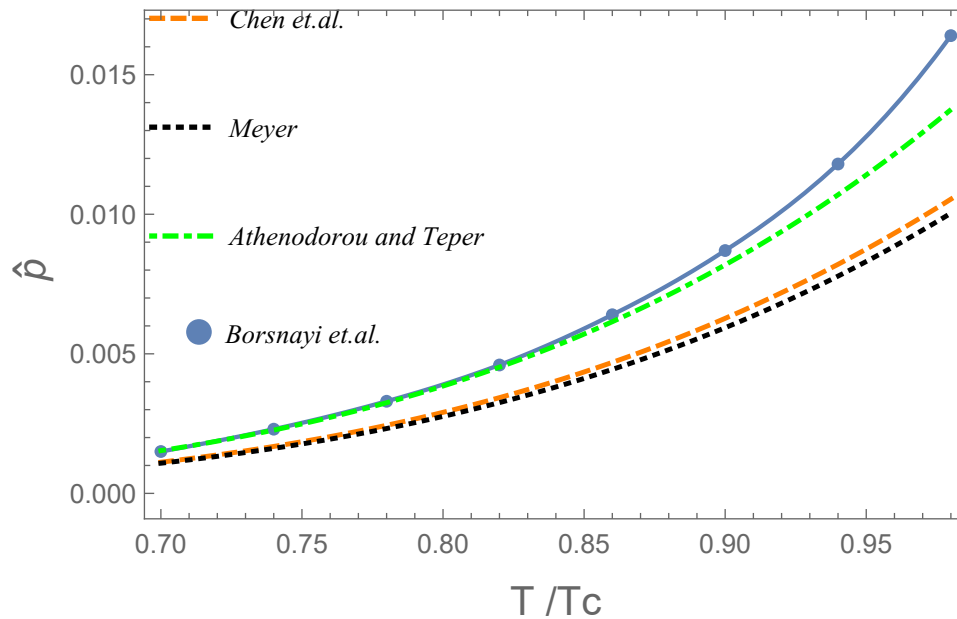


Figure 6.1: Comparison of the pressure (continuous limit) calculated in Ref. [30] to the GRG pressures for three different sets of lattice masses [29, 132, 203].

6.3 Contribution of heavier glueballs

In this section, we study the contribution to the thermodynamical quantities of further heavier excited glueball states, which have not been observed in lattice simulations yet. Namely, for each J^{PC} , an infinite tower of glueball states is believed to exist [119].

Light conventional quark-antiquark states can be analyzed quantitatively in a three-dimensional space including the mass M , the radial quantum number n , and the total spin J , as indicated in various publications (e.g., Refs. [235, 236]). Masses of the conventional mesons fulfill the relation and lie in the so-called Regge trajectories:

$$M^2(n, J^{PC}) = a(n + J) + b_{J^{PC}}. \quad (6.8)$$

We extend the Regge trajectories for the conventional mesons to the unconventional ones, such as glueballs. This approximation is limited because of the lack of experimental data. There are other elements that must be taken into account, such as the number of gluons included in a particular J^{PC} glueball, in order to group the states into various planes [132]. Also, despite the remark of Chen et. al. [237] about the ground-state glueballs with the quantum numbers $J^{PC} = 1^{++}$ and 1^{-+} that do not exist in the relativistic framework because their corresponding currents disappear, the

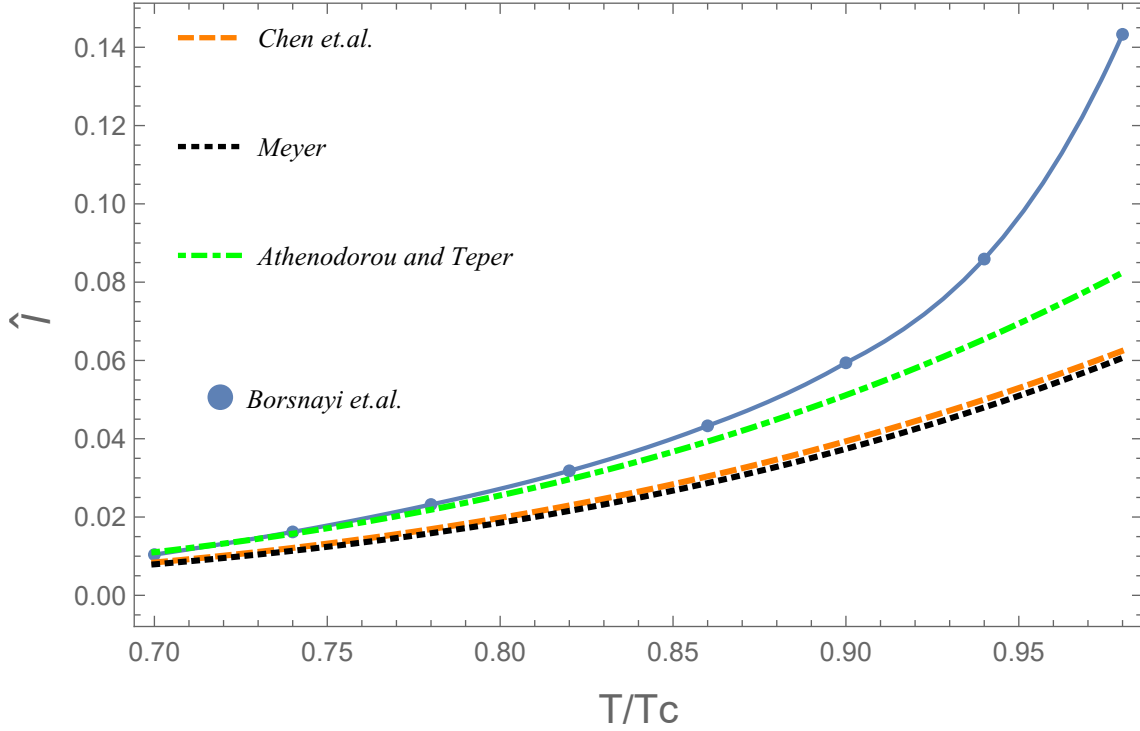


Figure 6.2: Comparison of the trace anomaly (continuous limit) calculated in Ref. [30] to the GRG trace anomalies for three different sets of lattice masses [29, 132, 203].

authors of Ref. [204] obtain the masses for these glueballs. This discrepancy implies that, eventually, not all J^{PC} may be formed in LQCD.

One can approximately construct a Regge trajectory for the glueball states in Ref. [29] by considering the ground states with physical masses lighter than 3 GeV. There are five such states with quantum numbers: $J^{PC} = 0^{++}, 2^{++}, 0^{-+}, 2^{-+}, 1^{+-}$ (Note that these ground states are observed in Refs. [132, 203] as well.) We define the χ^2 as follows:

$$\chi^2(a, b_{0^{++}}, b_{2^{++}}, b_{0^{-+}}, b_{2^{-+}}, b_{1^{+-}}) = \sum_{n=1}^2 \sum_{J^{PC}} \left(\frac{M(n, J^{PC}) - M^{\text{lat}}(n, J^{PC})}{\delta M^{\text{lat}}(n, J^{PC})} \right)^2, \quad (6.9)$$

where the parameters of the Regge trajectories are a and $b_{J^{PC}}$; the masses of the glueballs and their errors on them are M^{lat} and δM^{lat} as shown in the “AT” columns of Table 6.2. Table 6.3 shows the numerical values of the parameters from the fit, along with the masses that were employed. Interestingly, as a result of the fit for the masses in Ref. [29], we obtain a unique slope with $a = 5.49 \pm 0.17 \text{ GeV}^2$ and $\chi_{\text{d.o.f.}}^2 = 0.84$.

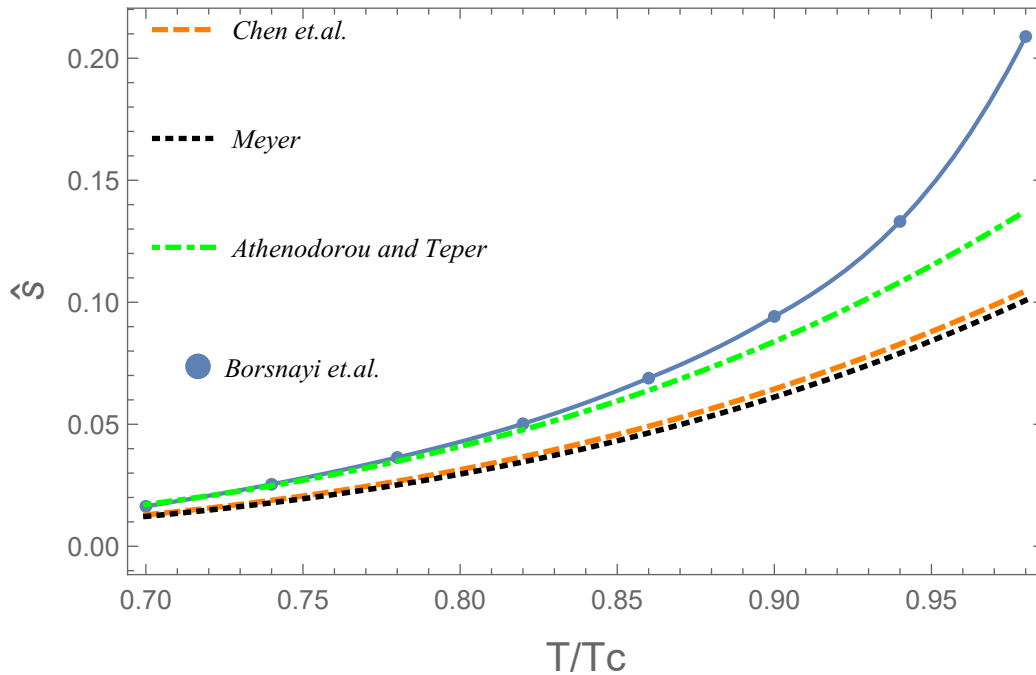


Figure 6.3: Comparison of the entropy (continuous limit) calculated in Ref. [30] to the GRG entropies for three different sets of lattice masses [29, 132, 203].

The pressure and trace anomaly of the GRG are then calculated using these Regge trajectories by including glueball states up to $n = 10$ for each quantum number specified in Table 6.2 (i.e., assuming the same slope a for all observed ground states in Ref. [29], not only those used in the fit of Eq. (6.9)). From Fig. 6.4, we see that the effect of further radially excited glueball states on the pressure and trace anomaly (red full lines) becomes visible very near T_c , but it is still very small¹.

It should be stressed that, the technique used in this section may be considered as a way to estimate the magnitude of the impact of heavy glueballs on the thermodynamic variables, but it does not provide a precise way to predict the masses of further radially excited glueballs.

Before finishing this section, we present the pressure of GRG in Fig. 6.5, in which the substantial impact of pomeron ($C=+1$) states becomes evident when compared to odderon ($C=-1$) states. The pomeron states dominate, but the odderon ones are non-negligible. For studies of pomeron/odderon, see Refs. [209, 238, 239].

¹If we take into account an infinite number of glueballs with Hagedorn-like properties, the picture could eventually alter and improve the agreement around T_c .

Glueball spectrum compared to the fit in Eq. (6.9)				Parameters [GeV ²]
$n J^{PC}$	m [GeV] (from [29])	Fit [GeV]	χ_i^2	
1 0^{++}	1.653(26)	1.647(25)	0.04	$b_{0^{++}} = -2.78 \pm 0.21$
2 0^{++}	2.842(40)	2.865(30)	0.3	
1 2^{++}	2.376(32)	2.367(30)	0.08	$b_{2^{++}} = -10.87 \pm 0.57$
2 2^{++}	3.30(5)	3.33(3)	0.38	
1 0^{-+}	2.561(40)	2.572(38)	0.08	$b_{0^{-+}} = 1.12 \pm 0.27$
2 0^{-+}	3.54(8)	3.48(4)	0.57	
1 2^{-+}	3.07(6)	3.11(5)	0.52	$b_{2^{-+}} = -6.79 \pm 0.66$
2 2^{-+}	3.97(7)	3.90(4)	1.10	
1 1^{+-}	2.944(42)	2.955(37)	0.07	$b_{1^{+-}} = -2.25 \pm 0.45$
2 1^{+-}	3.80(6)	3.77(3)	0.23	
			$\chi_{tot}^2=3.38$	$a = 5.49 \pm 0.17$

Table 6.3: Fit summary obtained from Eq. (6.9) by assuming Eq. (6.8).

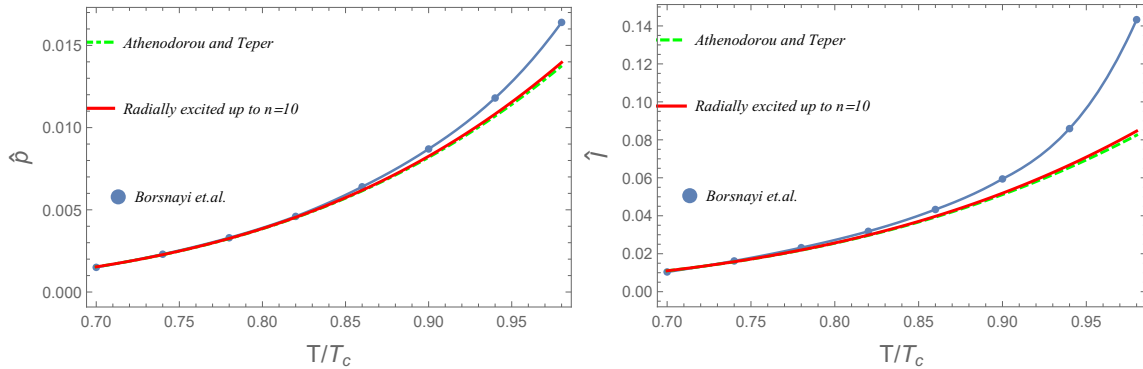


Figure 6.4: The effect of the radially excited glueball states up to $n = 10$ within GRG on the pressure (left) and trace anomaly (right).

6.4 Glueball-glueball interactions

The GRG was approximated as a free gas in the previous section, which is a valid approximation at lowest order. This section is devoted to studying the role of the interaction between glueballs in GRG. Importantly, the interactions of two lightest states in the glueball spectrum, scalar and tensor glueball, are investigated.

One of the common methods is the so-called S-matrix or phase-space formalism [240] applied to the investigation of the nonzero properties of hadrons (see e.g. Refs. [241–253]). The derivative of the scattering phase shift, which is proportional to

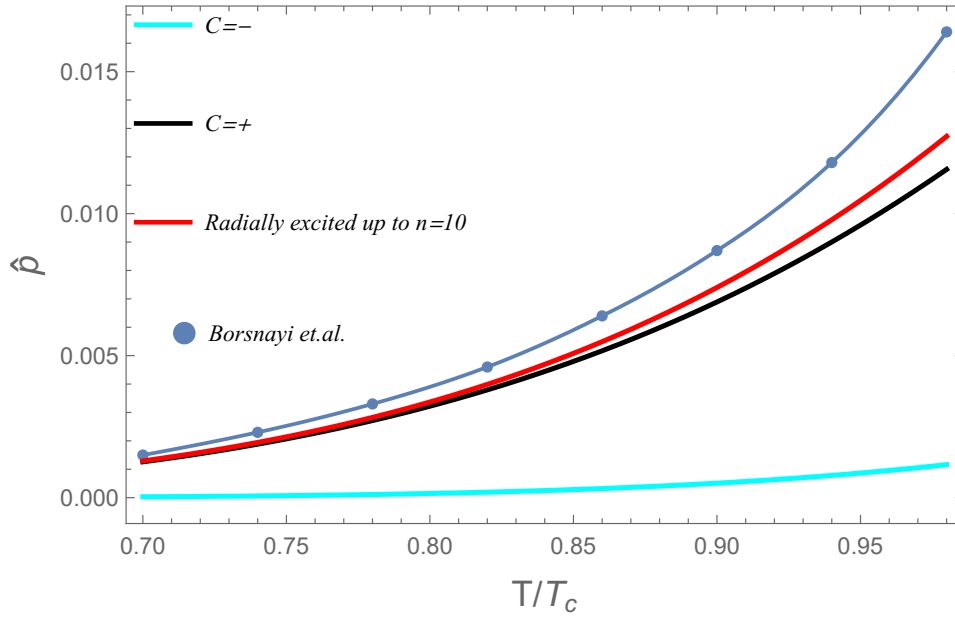


Figure 6.5: The GRG pressure depending on the negative and positive charge conjugation of the glueball spectrum compared to Ref. [30].

the density of states, enables us to determine how the interaction affects the pressure. Hence, it is possible to properly consider both attraction or repulsion. The corresponding pressure within this approach is equivalent to the free gas in the small interaction limit. The GRG free gas in the YM sector of QCD is therefore justified by this method, which also gives the possibility of going beyond the free gas approximation.

Considering the two lightest glueballs, the scalar glueball G and the tensor glueball $G_2 \equiv G_2^{\mu\nu}$ within the following potential

$$V_{\text{eff}}(G, G_2) = V_{\text{dil}}(G) - \frac{\alpha}{2} G^2 G_{2,\mu\nu} G_2^{\mu\nu}, \quad (6.10)$$

where the dilaton potential $V_{\text{dil}}(G)$ describes the scalar glueball (see Eq. (6.13)). Recall the scale $G_0 \sim 0.4$ GeV, which resembles the trace anomaly of the YM theory, is the only dimensional parameter present in the effective potential. There are two dimensionless parameters λ and α which are fixed by using the LQCD predictions for $m_G \sim 1.7$ GeV and $m_{G_2} \sim 2.4$ GeV. As a result of the following shift

$$G \longrightarrow G + G_0, \quad (6.11)$$

we obtain the relation between the parameters of the potential and masses of the scalar and the tensor glueball fields in the following forms:

$$m_{0^{++}}^2 = m_G^2 = \lambda G_0^2, \quad m_{2^{++}}^2 = m_{G_2}^2 = \alpha G_0^2. \quad (6.12)$$

The expansion of the dilaton potential around its minimum G_0 :

$$V_{dil}(G) = -\frac{1}{16}G_0^4 + \frac{1}{2}m_G^2 G^2 + \frac{1}{3!} \left(5\frac{m_G^2}{G_0}\right) G^3 + \frac{1}{4!} \left(11\frac{m_G^2}{G_0^2}\right) G^4 + \dots \quad (6.13)$$

leads to the tree-level scattering amplitude based on the three-leg and four-leg interactions. The corresponding amplitude has the following form:

$$A(s, t, u) = -11\frac{m_G^2}{G_0^2} - \left(5\frac{m_G^2}{G_0}\right)^2 \frac{1}{s - m_G^2} - \left(5\frac{m_G^2}{G_0}\right)^2 \frac{1}{t - m_G^2} - \left(5\frac{m_G^2}{G_0}\right)^2 \frac{1}{u - m_G^2}. \quad (6.14)$$

The l -th amplitude, therefore, reads as follows after being rewritten as a function of the channel s and the scattering angle θ :

$$A_l(s) = \frac{1}{2} \int_{-1}^1 d \cos \theta A(s, \cos \theta) P_l(\cos \theta), \quad (6.15)$$

which is related to the phase shift $\delta_l(s)$ using the 3-momentum k of any particle in the center of mass frame as:

$$\delta_l(s) = \frac{1}{2} \arg \left[1 + 2i \frac{k}{16\pi\sqrt{s}} A_l(s) \right]. \quad (6.16)$$

Two unitarization procedures (on-shell and N/D) are used to determine the phase shift in Refs. [253–256]. We consider these results within the following expression for pressure:

$$\hat{p}_{0^{++}0^{++}}^{\text{int}} = -\frac{1}{T^3} \sum_{l=0}^{\infty} \int_{2m_{0^{++}}}^{\infty} dx \frac{2l+1}{\pi} \frac{d\delta_l^{0^{++}0^{++}}(x)}{dx} \int \frac{d^3k}{(2\pi)^3} \ln \left(1 - e^{-\frac{\sqrt{k^2+x^2}}{T}} \right) + \hat{p}_B, \quad (6.17)$$

where the summation is over the angular momentum l , the integration variable x is the square root of the Mandelstam variable s , and k is the length of the three-momentum

of the scalar glueball. The phase shift of l -th wave $\delta_l^{0^{++}0^{++}}(x)$ describes the scattering of two scalar glueballs with the quantum number $J^{PC} = 0^{++}$.

The pressure of a bound state of two scalar glueballs \hat{p}_B that can eventually exist is also considered in Eq. (6.17). Using the dilaton potential to represent the interaction of scalar glueballs, as suggested by Ref. [254, 255, 257], a bound state of two scalar glueballs known as glueballonium does in fact exist, even though the pressure is not significantly affected by this state. This is because the pressure is a continuous function of the interaction strength; as a result, when a bound state emerges, there is no abrupt change in the pressure. The jump in the phase-shift contribution above the threshold is correlated with the jump in pressure that results from the formation of a bound state. This partial cancellation occurs whenever a bound state forms [252, 253, 258].

The phase shifts computed in Ref. [254] are implemented in Figure 6.6, which depicts the $l = 0, 2, 4$ pressure terms resulting from the interaction of two scalar glueballs. We use $m_{0^{++}} = 1.7$ GeV, which is consistent with Refs. [29, 203] and $G_0 = 0.4$ GeV, which delivers a glueballonium with a mass of 3.34 GeV (for further information see Ref. [254]). Namely, the critical value to form a bound state with a mass of $2m_G$ is $G_{0,crit} = 0.504$ GeV. The mass of the bound state is decreasing for decreasing G_0 and exceeds $m_B = 3.34$ GeV for $G_0 = 0.4$ GeV. On the other hand, no glueballonium exists for $G_0 > G_{0,crit}$. This fact is included in the following expression of the pressure for the bound state:

$$\hat{p}_B = -\theta(\Lambda_{G,crit} - G_0) \frac{1}{T^3} \int \frac{d^3k}{(2\pi)^3} \ln \left(1 - e^{-\beta \frac{\sqrt{k^2 + m_B^2}}{T}} \right). \quad (6.18)$$

The results for the s-wave ($l = 0$) are evidently the dominating ones. When increasing the value of l , the contribution rapidly becomes smaller and smaller, allowing us to approximate the total interaction with only the s-wave. While significantly greater than the other waves, the $l = 0$ wave contribution is still negligible when compared to the pressure of the 0^{++} non-interacting glueballs.

In order to describe the interaction between two tensor glueballs, we use an analogous method to two-pion scattering in Ref. [259]. A schematic description of the s-channel scattering is given below:

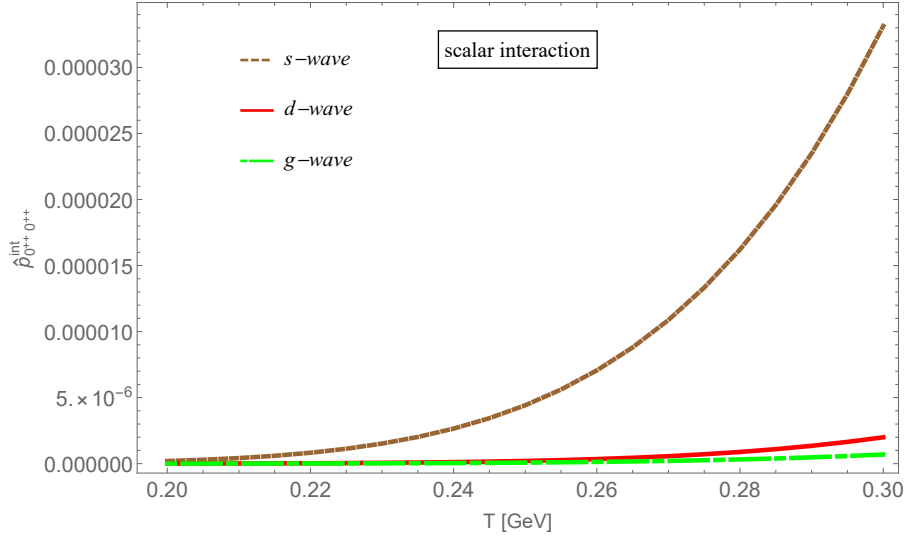
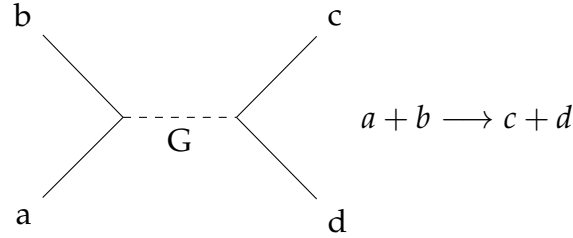


Figure 6.6: Contributions of three different waves to the pressure from scalar-scalar glueball interactions.



where the third component of the spin J of the incoming and outgoing tensor glueballs is denoted by a, b, c, d . To be more specific, four particles can each have a unique value for the third spin component, m_J , provided that

$$m_J^{ab} \equiv m_J^a + m_J^b = m_J^{cd}. \quad (6.19)$$

There are analogous diagrams for the t and u channels.

A general expression for the total amplitude with the transition matrix T reads:

$$\langle cd|T|ab\rangle = A\delta^{ab}\delta^{cd} + B\delta^{ac}\delta^{bd} + C\delta^{ad}\delta^{bc}, \quad (6.20)$$

and

$$A := \frac{-4(\alpha G_0)^2}{s - m_G^2}, \quad B := \frac{-4(\alpha G_0)^2}{t - m_G^2}, \quad C := \frac{-4(\alpha G_0)^2}{u - m_G^2}. \quad (6.21)$$

We obtain the expression for the initial state using the Clebsh-Gordan coefficients

$$|J^{ab}, m_J^{ab}\rangle = \sum_{m_J^a, m_J^b} \langle J^a m_J^a J^b m_J^b | J^{ab} m_J^{ab} \rangle |J^a, m_J^a\rangle \otimes |J^b, m_J^b\rangle. \quad (6.22)$$

Considering $J^a = J^b = 2$ and $m_J^a \in [-2, +2]$, $m_J^b \in [-2, +2]$ leads to

$$J^{ab} \in [0, 4], \quad m_J^{ab} \in [-J^{ab}, +J^{ab}]. \quad (6.23)$$

Similarly, the outgoing state is expressed in the same compact form.

There are 25 nonzero amplitudes $\langle J^{cd}, m_J^{cd} | T | J^{ab}, m_J^{ab} \rangle$, for which $J^{cd} = J^{ab}$ and $m_J^{cd} = m_J^{ab}$ are satisfied. We introduce T^q , where the total incoming (and outgoing) spin $q \equiv J^{cd} = J^{ab} = 0, 1, 2, 3, 4$ in Eq. (6.20) as:

$$T^q = \sum_{i_a, i_b, i_c, i_d} \rho_{abcd} \langle i_c | \langle i_d | T | i_a \rangle | i_b \rangle, \quad \text{where } i_a, i_b, i_c, i_d \equiv (I, II, III, IV, V). \quad (6.24)$$

Here ρ_{abcd} is defined in terms of the Clebsh-Gordan coefficients

$$\rho_{abcd} := \langle 2 m_J^a 2 m_J^b | J^{ab} m_J^{ab} \rangle \cdot \langle 2 m_J^c 2 m_J^d | J^{cd} m_J^{cd} \rangle. \quad (6.25)$$

Note that we have used the short-hand notation

$$|i_a\rangle \otimes |i_b\rangle = |i_a\rangle |i_b\rangle, \quad (6.26)$$

where the value of any $\langle i_c | \langle i_d | T | i_a \rangle | i_b \rangle$ are represented in terms of the parameters A , B and C , given in Eq. (6.21), and the relations between two basis read:

$$\begin{aligned} |2, +1\rangle &= -\sqrt{\frac{1}{2}} (|I\rangle - i|II\rangle), \\ |2, -1\rangle &= \sqrt{\frac{1}{2}} (|I\rangle + i|II\rangle), \\ |2, +2\rangle &= -\sqrt{\frac{1}{2}} (|III\rangle - i|IV\rangle), \\ |2, -2\rangle &= -\sqrt{\frac{1}{2}} (|III\rangle + i|IV\rangle), \\ |2, 0\rangle &= |V\rangle. \end{aligned} \quad (6.27)$$

We obtain the following results, which will be used to describe the interaction pressure between the tensor glueballs:

$$\boxed{T^4 = T^2 = B + C, \quad T^3 = T^1 = B - C, \quad T^0 = 5A + B + C}.$$

For tensor glueballs, we use the the analogous expression to Eq. (6.17):

$$\hat{p}_{2^{++}2^{++}}^{\text{int}} = -\frac{1}{T^3} \sum_{J=0}^4 \sum_{l=0}^2 \int_{2m_{2^{++}}}^{\infty} dx (2J+1) \frac{2l+1}{\pi} \frac{d\delta_l^{2^{++}2^{++},J}(x)}{dx} \int \frac{d^3k}{(2\pi)^3} \ln \left(1 - e^{-\frac{\sqrt{k^2+x^2}}{T}} \right), \quad (6.28)$$

where the total spin J of the system varies between 0 and 4 and $m_{2^{++}} = 2.4$ GeV istaken from Ref. [29, 203].

The phase shifts $\delta_l^{2^{++}2^{++},J}(x)$ are calculated by utilizing the effective theory for the tensor glueball we discussed above. Similar to the scalar glueball case, the result for the s -channel is larger than the others (see Fig. 6.7). We expect a small contribution in the case of interaction terms between tensor glueballs (e.g., a four-leg interaction).

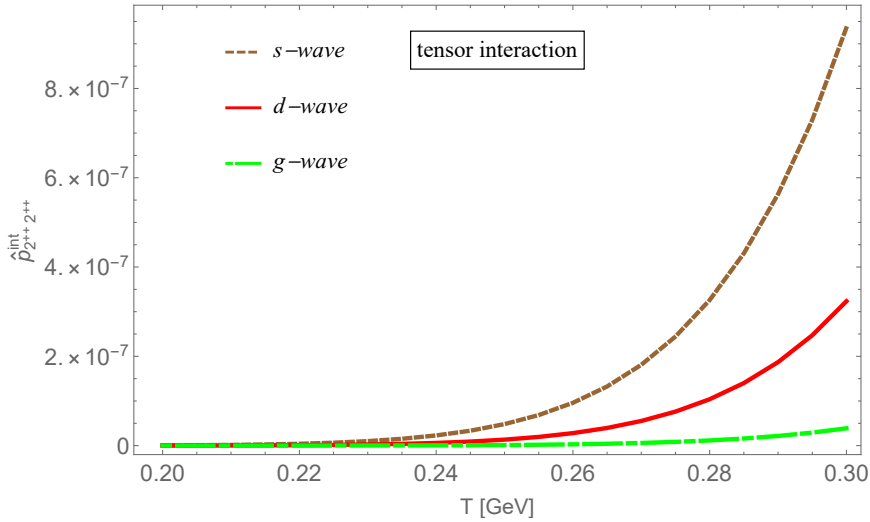


Figure 6.7: Contributions of three different waves to the pressure from tensor-tensor glueball interactions.

By adding together all possible terms, it is possible to determine the entire contribution to the pressure of interacting glueballs:

$$\hat{p}^{\text{int}} \approx \hat{p}_{0^{++}0^{++}}^{\text{int}} + \hat{p}_{2^{++}2^{++}}^{\text{int}} + \dots, \quad (6.29)$$

where the first two terms are related to the interactions between the two lightest glueballs, while the additional terms are denoted by the dots referring to smaller contributions from interaction terms of heavier glueballs. We have seen that the tensor-tensor contribution is considerably smaller than that of the scalar-scalar one. By making use of the proper treatment of inelasticities and instability of the states (see Refs. [245,251,253,260]), one could extend the results to the scattering of any glueball states with J_1 and J_2 .

In summary, the plots for the pressure and energy density would essentially show no impact from the combined effects of the scalar and tensor interaction components. In light of this, it appears that the free gas approximation (together with the eventual small contribution of heavy glueball states) is a reliable approach to the YM pressure for temperatures below T_c .

6.5 Conclusion

In this chapter, we revisited the GRG model by considering the recent glueball mass spectrum in Ref. [29] (as well as the previous results in Refs. [132,203]). Including the further glueball states from Regge trajectories as well as the interaction between two light glueball states led to a small change in the thermodynamic quantities. We observe that the lattice data of Ref. [30] below the critical temperature (predicted to be around $T_c = 323 \pm 18$ MeV) is well explained by the GRG model.

Chapter 7

Conclusions and discussions

In this thesis, I have mainly explored two aspects of QCD: high-spin mesons within the low-energy mesonic spectrum and the thermodynamics of the Yang-Mills (YM) theory.

For the first part, I used an effective model based on chiral symmetry, called the extended Linear Sigma Model (eLSM). This model, previously used for lower spin mesons, was extended to spin-2 conventional $\bar{q}q$ mesons (tensor and axial-tensor mesons, linked by chiral transformations) and a tensor glueball. Finally, the eLSM applies also to $J = 3$ mesons, but the lack of information about $J^{PC} = 3^{++}$ implies that only flavor symmetry is implemented in this case.

Results for the ground state tensor mesons (with $J^{PC} = 2^{++}, 3^{--}$) confirm their quark-anti-quark structure. Qualitative agreement with PDG as well as LQCD results is obtained. Further interesting hadronic and radiative decay channels could be predicted and need to be tested in ongoing experiments (e.g., GlueX and CLAS12) and compared with LQCD simulation results.

Thanks to the eLSM, we were able to estimate the masses and decay widths of the axial tensor mesons (with $J^{PC} = 2^{--}$). Our model outcomes, as well as the LQCD results, predict that they are broad. The main decay channels are:

- decay widths of ρ_2 with the mass $m_{\rho_2} = 1663$ MeV

$$\begin{aligned}\Gamma(\rho_2 \rightarrow \rho(770) \eta) &= 99 \pm 50 \text{ MeV}, \\ \Gamma(\rho_2 \rightarrow \bar{K}^*(892) K + \text{c.c.}) &= 85 \pm 43 \text{ MeV}, \\ \Gamma(\rho_2 \rightarrow \omega(782) \pi) &= 419 \pm 210 \text{ MeV};\end{aligned}$$

- decay widths of ω_2 with the mass $m_{\omega_2} = 1663$ MeV

$$\begin{aligned}\Gamma(\omega_2 \rightarrow \rho(770) \pi) &= 1314 \pm 657 \text{ MeV}, \\ \Gamma(\omega_2 \rightarrow \bar{K}^*(892) K + \text{c.c.}) &= 85 \pm 43 \text{ MeV}, \\ \Gamma(\omega_2 \rightarrow \omega(782) \eta) &= 93 \pm 47 \text{ MeV};\end{aligned}$$

- decay widths of ϕ_2 with the mass $m_{\phi_2} = 1971$ MeV

$$\begin{aligned}\Gamma(\phi_2 \rightarrow \bar{K}^*(892) K + \text{c.c.}) &= 510 \pm 255 \text{ MeV}, \\ \Gamma(\phi_2 \rightarrow \phi(782) \eta) &= 101 \pm 51 \text{ MeV}.\end{aligned}$$

Next, we estimated the decay ratios for the spin-2 tensor glueball, which shows that the dominant decay channels are the ones into two vector mesons. Various spin-2 resonances listed in PDG are tested as possible tensor glueball candidates. Despite the large decay width, our model estimations agree with PDG for the resonance $f_2(1950)$. These outcomes could be interesting for experiments such as BESIII, and LHCb searching for the tensor glueball.

For what concerns the thermodynamics of the YM theory, we revisit the Glueball Resonance Gas (GRG) model by using the glueball spectrum obtained in 3 different LQCD simulations. We have compared the model results for the pressure (and other thermodynamic quantities) with the corresponding LQCD results of the pressure for pure YM theory below the critical temperature of deconfinement (glueballs \rightarrow gluons). The GRG model was improved by including the contribution from further excited states and from the interaction between the two lightest glueballs (scalar and tensor ones). These additional contributions turned out to be negligible, which supports the validity of the free gas description of the glueball states as a valid approximation.

As an outlook of this thesis, one can go beyond the hadronic degrees of freedom. Namely, one can study the effect of quarks (quark zero modes) to investigate some interesting problems for mesons. For instance, we know that the large mixing between η and $\eta'(958)$ is related to the instantons. Analogously, one can study the role of the instanton in the mixing between the spin-2 mesons ($J^{PC} = 2^{-+}$) $\eta_2(1645)$ and $\eta_2(1870)$. In this case, the instanton-induced interactions will lead to hadronic effective Lagrangians of the type considered in this thesis. Yet, the coupling constant could be computed by using a microscopic instanton-based calculation. This approach can be

useful to estimate the size and signature of the mixing angle between the isoscalar mesons with $J^{PC} = 1^{+-}, 2^{-+}$, as well as to evaluate novel decay modes.

Bibliography

- [1] Shahriyar Jafarzade, Adrian Koenigstein, and Francesco Giacosa. Phenomenology of $J^{PC} = 3^{--}$ tensor mesons. *Phys. Rev. D*, 103(9):096027, 2021.
- [2] Shahriyar Jafarzade, Arthur Vereijken, Milena Piotrowska, and Francesco Giacosa. From well-known tensor mesons to yet unknown axial-tensor mesons. *Phys. Rev. D*, 106(3):036008, 2022.
- [3] Arthur Vereijken, Shahriyar Jafarzade, Milena Piotrowska, and Francesco Giacosa. Is $f_2(1950)$ the tensor glueball? *Phys. Rev. D*, 108(1):014023, 2023.
- [4] Enrico Trozzi, Shahriyar Jafarzade, and Francesco Giacosa. Thermodynamics of the Glueball Resonance Gas. *Eur. Phys. J. C*, 83(5):390, 2023.
- [5] Murray Gell-Mann. A Schematic Model of Baryons and Mesons. *Phys. Lett.*, 8:214–215, 1964.
- [6] G. Zweig. *An $SU(3)$ model for strong interaction symmetry and its breaking. Version 2*, pages 22–101. 1964.
- [7] Jürg Gasser and Heinrich Leutwyler. Chiral Perturbation Theory to one loop. *Annals Phys.*, 158(1):142–210, 1984.
- [8] Jürg Gasser and Heinrich Leutwyler. Chiral Perturbation Theory: Expansions in the mass of the strange quark. *Nucl. Phys. B*, 250(1–4):465–516, 1985.
- [9] Stefan Scherer. Introduction to Chiral Perturbation Theory. *Adv. Nucl. Phys.*, 27:277–538, 2003.
- [10] H. Leutwyler. On the foundations of Chiral Perturbation Theory. *Annals Phys.*, 235(1):165–203, 1994.
- [11] Antonio Pich. Chiral Perturbation Theory. *Rept. Prog. Phys.*, 58(6):563–610, 1995.
- [12] Veronique Bernard and Ulf-G. Meissner. Chiral Perturbation Theory. *Ann. Rev.*

- Nucl. Part. Sci.*, 57:33–60, 2007.
- [13] Matthias R. Schindler, Jambul Gegelia, and Stefan Scherer. Electromagnetic form factors of the nucleon in Chiral Perturbation Theory including vector mesons. *Eur. Phys. J. A*, 26:1–5, 2005.
- [14] Elizabeth Ellen Jenkins, Aneesh V. Manohar, and Mark B. Wise. Chiral Perturbation Theory for vector mesons. *Phys. Rev. Lett.*, 75:2272–2275, 1995.
- [15] Michael Booth, George Chiladze, and Adam F. Falk. Quenched Chiral Perturbation Theory for vector mesons. *Phys. Rev. D*, 55:3092–3100, 1997.
- [16] Carla Terschläusen and Stefan Leupold. Renormalization of the low-energy constants of Chiral Perturbation Theory from loops with dynamical vector mesons. *Phys. Rev. D*, 94(1):014021, 2016.
- [17] Vincenzo Cirigliano, Gerhard Ecker, Helmut Neufeld, and Antonio Pich. Meson resonances, large N_c and chiral symmetry. *JHEP*, 6:1–12, 2003.
- [18] Murray Gell-Mann and Maurice M. Levy. The axial vector current in beta decay. *Nuovo Cim.*, 16(3):705–726, 1960.
- [19] Denis Parganlija, Peter Kovacs, Gyorgy Wolf, Francesco Giacosa, and Dirk H. Rischke. Meson vacuum phenomenology in a three-flavor linear sigma model with (axial-)vector mesons. *Phys. Rev. D*, 87(1):014011, 2013.
- [20] Pyungwon Ko and Serge L. Rudaz. Phenomenology of scalar and vector mesons in the linear σ model. *Phys. Rev. D*, 50:6877–6894, 12 1994.
- [21] Gregory W. Carter, Paul J. Ellis, and Serge L. Rudaz. An effective Lagrangian with broken scale and chiral symmetry II: pion phenomenology. *Nucl. Phys. A*, 603(3-4):367–386, 6 1996. [Erratum: *Nucl.Phys.A* 608, 514–514 (1996)].
- [22] Stanislaus Janowski, Francesco Giacosa, and Dirk H. Rischke. Is $f_0(1710)$ a glueball? *Phys. Rev. D*, 90(11):114005, 2014.
- [23] Volker Koch. Aspects of chiral symmetry. *Int. J. Mod. Phys. E*, 6(2):203–250, 1997.
- [24] Eberhard Klempt. Meson spectroscopy: Glueballs, hybrids and Q anti- Q mesons. In *Zuo Summer School on Phenomenology of Gauge Interactions*, pages 61–126, 8 2000.
- [25] Vanamali Shastry, Christian S. Fischer, and Francesco Giacosa. The phenomenol-

- ogy of the exotic hybrid nonet with $\pi_1(1600)$ and $\eta_1(1855)$. *Phys. Lett. B*, 834:137478, 2022.
- [26] Vanamali Shastry and Francesco Giacosa. Radiative production and decays of the exotic $\eta_1'(1855)$ and its siblings. *arXiv*, 2302.07687, 2023.
- [27] R. L. Workman and Others. Review of Particle Physics. *PTEP*, 2022:083C01, 2022.
- [28] Christopher T. Johnson and Jozef J. Dudek. Excited J^{--} meson resonances at the SU(3) flavor point from lattice QCD. *Phys. Rev. D*, 103(7):074502, 2021.
- [29] Andreas Athenodorou and Michael Teper. The glueball spectrum of SU(3) gauge theory in 3 + 1 dimensions. *JHEP*, 11:172, 2020.
- [30] Sz. Borsanyi, G. Endrodi, Z. Fodor, S. D. Katz, and K. K. Szabo. Precision SU(3) lattice thermodynamics for a large temperature range. *JHEP*, 07:056, 2012.
- [31] Jozef J. Dudek, Robert G. Edwards, Peng Guo, and Christopher E. Thomas. Toward the excited isoscalar meson spectrum from lattice QCD. *Phys. Rev. D*, 88(9):094505, 2013.
- [32] Emanuel Katz, Adam Lewandowski, and Matthew D. Schwartz. Tensor mesons in AdS/QCD. *Phys. Rev. D*, 74:086004, 2006.
- [33] Frederic Brünner, Denis Parganlija, and Anton Rebhan. Glueball Decay Rates in the Witten-Sakai-Sugimoto Model. *Phys. Rev. D*, 91(10):106002, 2015. [Erratum: *Phys.Rev.D* 93, 109903 (2016)].
- [34] J. Y. Süngü, A. Türkan, E. Sertbakan, and E. Veli Veliev. Axial-tensor Meson family at $T \neq 0$. *Eur. Phys. J. C*, 80(10):943, 2020.
- [35] Markus Q. Huber, Christian S. Fischer, and Hèlios Sanchis-Alepuz. Spectrum of scalar and pseudoscalar glueballs from functional methods. *Eur. Phys. J. C*, 80(11):1077, 2020.
- [36] Markus Q. Huber, Christian S. Fischer, and Helios Sanchis-Alepuz. Higher spin glueballs from functional methods. *Eur. Phys. J. C*, 81(12):1083, 2021.
- [37] Christian S. Fischer, Stanislav Kubrak, and Richard Williams. Mass spectra and Regge trajectories of light mesons in the Bethe-Salpeter approach. *Eur. Phys. J. A*, 50:126, 2014.

- [38] Chi-Keung Chow and Soo-Jong Rey. Chiral perturbation theory for tensor mesons. *JHEP*, 05:010, 1998.
- [39] Shahriyar Jafarzade. A phenomenological note on the missing ρ_2 meson. *PoS, ICHEP2022:903*, 2022.
- [40] Holger Gies. Introduction to the Functional RG and applications to gauge theories. *Lect. Notes Phys.*, 852:287–348, 2012.
- [41] Janos Polonyi. Lectures on the Functional Renormalization Group method. *Central Eur. J. Phys.*, 1(1):1–71, 2003.
- [42] Christof Wetterich. Exact evolution equation for the effective potential. *Phys. Lett. B*, 301:90–94, 1993.
- [43] Tim R. Morris. The Exact Renormalization Group and approximate solutions. *Int. J. Mod. Phys. A*, 9(14):2411–2450, 1994.
- [44] Nicolas Dupuis, Leonie Canet, Astrid Eichhorn, Walter Metzner, Jan M. Pawłowski, Matthieu Tissier, and Nicolas Wschebor. The nonperturbative functional renormalization group and its applications. *arXiv*, 2006.04853, 2020.
- [45] Jan M. Pawłowski. Aspects of the functional renormalisation group. *Annals Phys.*, 322:2831–2915, 2007.
- [46] Mara Grahl and Dirk H. Rischke. Functional Renormalization Group study of the two-flavor linear sigma model in the presence of the axial anomaly. *Phys. Rev. D*, 88(5):056014, 2013.
- [47] Jürgen Eser, Mara Grahl, and Dirk H. Rischke. Functional Renormalization Group study of the chiral phase transition including vector and axial-vector mesons. *Phys. Rev. D*, 92(9):096008, 2015.
- [48] Fabian Rennecke and Bernd-Jochen Schaefer. Fluctuation-induced modifications of the phase structure in $(2 + 1)$ -flavor QCD. *Phys. Rev. D*, 96(1):016009, 2017.
- [49] Jan M. Pawłowski and Fabian Rennecke. Higher order quark-mesonic scattering processes and the phase structure of QCD. *Phys. Rev. D*, 90(7):076002, 2014.
- [50] Jürgen Eser, Florian Divotgey, Mario Mitter, and Dirk H. Rischke. Low-energy limit of the $O(4)$ quark-meson model from the functional renormalization group approach. *Phys. Rev. D*, 98(1):014024, 2018.

- [51] Florian Divotgey, Jürgen Eser, and Mario Mitter. Dynamical generation of low-energy couplings from quark-meson fluctuations. *Phys. Rev. D*, 99(5):054023, 3 2019.
- [52] Jürgen Eser, Florian Divotgey, and Mario Mitter. Low-energy limit of the $O(4)$ quark-meson model. *PoS*, CD2018:060, 2 2020.
- [53] Niklas Cichutek, Florian Divotgey, and Jürgen Eser. Fluctuation-induced higher-derivative couplings and infrared dynamics of the Quark-Meson-Diquark Model. *Phys. Rev. D*, 102(3):034030, 2020.
- [54] Konstantin Otto, Micaela Oertel, and Bernd-Jochen Schaefer. Hybrid and quark star matter based on a nonperturbative equation of state. *Phys. Rev. D*, 101(10):103021, 5 2020.
- [55] Konstantin Otto, Micaela Oertel, and Bernd-Jochen Schaefer. Nonperturbative quark matter equations of state with vector interactions. *Eur. Phys. J. ST*, 229(22-23):3629–3649, 7 2020.
- [56] Christopher Jung and Lorenz von Smekal. Fluctuating vector mesons in analytically continued functional RG flow equations. *Phys. Rev. D*, 100(11):116009, 12 2019.
- [57] Markus Heller and Mario Mitter. Pion and η -meson mass splitting at the two-flavour chiral crossover. *Phys. Rev. D*, 94(7):074002, 2016.
- [58] Masako Bando, Taichiro Kugo, and Koichi Yamawaki. Nonlinear Realization and Hidden Local Symmetries. *Phys. Rept.*, 164:217–314, 1988.
- [59] Denis Parganlija, Francesco Giacosa, and Dirk H. Rischke. Vacuum Properties of Mesons in a Linear Sigma Model with Vector Mesons and Global Chiral Invariance. *Phys. Rev. D*, 82:054024, 2010.
- [60] Ta-Pei Cheng and Ling-Fong Li. *Gauge Theory of Elementary Particle Physics*. Oxford University Press, Oxford, UK, 1984.
- [61] Giovanni Amelino-Camelia et al. Physics with the KLOE-2 experiment at the upgraded DAΦNE. *Eur. Phys. J. C*, 68:619–681, 2010.
- [62] Thorsten Feldmann, Peter Kroll, and Berthold Stech. Mixing and decay constants of pseudoscalar mesons. *Phys. Rev. D*, 58:114006, 10 1998.

- [63] Gerardus 't Hooft. How instantons solve the $U(1)$ problem. *Phys. Rept.*, 142(6):357–387, 9 1986.
- [64] Felipe J. Llanes-Estrada. Glueballs as the Ithaca of meson spectroscopy: From simple theory to challenging detection. *Eur. Phys. J. ST*, 230(6):1575–1592, 2021.
- [65] Hai-Yang Cheng, Chun-Khiang Chua, and Keh-Fei Liu. Scalar glueball, scalar quarkonia, and their mixing. *Phys. Rev. D*, 74:094005, 2006.
- [66] Francesco Giacosa, Thomas Gutsche, Valery E. Lyubovitskij, and Amand Faessler. Scalar nonet quarkonia and the scalar glueball: Mixing and decays in an effective chiral approach. *Phys. Rev. D*, 72:094006, 11 2005.
- [67] Claude Amsler and Frank E. Close. Is $f_0(1500)$ a scalar glueball? *Phys. Rev. D*, 53:295–311, 1996.
- [68] Claude Amsler and Frank E. Close. Evidence for a scalar glueball. *Phys. Lett. B*, 353(2–3):385–390, 1995.
- [69] J. R. Pelaez. From controversy to precision on the sigma meson: a review on the status of the non-ordinary $f_0(500)$ resonance. *Phys. Rept.*, 658:1, 2016.
- [70] A. V. Sarantsev, I. Denisenko, U. Thoma, and E. Klempt. Scalar isoscalar mesons and the scalar glueball from radiative J/ψ decays. *Phys. Lett. B*, 816:136227, 2021.
- [71] A. Rodas, A. Pilloni, M. Albaladejo, C. Fernandez-Ramirez, V. Mathieu, and A. P. Szczepaniak. Scalar and tensor resonances in J/ψ radiative decays. *Eur. Phys. J. C*, 82(1):80, 2022.
- [72] Daniele Binosi, Alessandro Pilloni, and Ralf-Arno Tripolt. Study for a model-independent pole determination of overlapping resonances. *arXiv*, 2205.02690, 2022.
- [73] E. Klempt, A. V. Sarantsev, I. Denisenko, and K. V. Nikonov. Search for the tensor glueball. *Phys. Lett. B*, 830:137171, 2022.
- [74] Eberhard Klempt. Scalar mesons and the fragmented glueball. *Phys. Lett. B*, 820:136512, 2021.
- [75] Eberhard Klempt and Andrey V. Sarantsev. Singlet-octet-glueball mixing of scalar mesons. *Phys. Lett. B*, 826:136906, 2022.
- [76] Dan Guo, Wei Chen, Hua-Xing Chen, Xiang Liu, and Shi-Lin Zhu. Newly

- observed $a_0(1817)$ as the scaling point of constructing the scalar meson spectroscopy. *Phys. Rev. D*, 105(11):114014, 2022.
- [77] Stephen Godfrey and Nathan Isgur. Mesons in a relativized quark model with chromodynamics. *Phys. Rev. D*, 32:189–231, Jul 1985.
- [78] Kwei-Chou Yang. Light-cone distribution amplitudes of axial-vector mesons. *Nucl. Phys. B*, 776:187–257, 2007.
- [79] Hisaki Hatanaka and Kwei-Chou Yang. $K_1(1270) - K_1(1400)$ mixing angle and new-physics effects in $B \rightarrow K_1 l^+ l^-$ decays. *Phys. Rev. D*, 78:074007, 10 2008.
- [80] Hai-Yang Cheng. Revisiting axial-vector meson mixing. *Phys. Lett. B*, 707(1):116–120, 2012.
- [81] Milena Piotrowska, Christian Reisinger, and Francesco Giacosa. Strong and radiative decays of excited vector mesons and predictions for a new $\phi(1930)$ resonance. *Phys. Rev. D*, 96(5):054033, 9 2017.
- [82] Leonid Burakovsky and Terrance J. Goldman. Regarding the enigmas of P -wave meson spectroscopy. *Phys. Rev. D*, 57:2879–2888, 1998.
- [83] F. Giacosa, Th. Gutsche, V. E. Lyubovitskij, and Amand Faessler. Decays of tensor mesons and the tensor glueball in an effective field approach. *Phys. Rev. D*, 72:114021, 2005.
- [84] Adrian Koenigstein, Francesco Giacosa, and Dirk H. Rischke. Classical and quantum theory of the massive spin-two field. *Annals Phys.*, 368:16–55, 2016.
- [85] Adrian Koenigstein and Francesco Giacosa. Phenomenology of pseudotensor mesons and the pseudotensor glueball. *Eur. Phys. J. A*, 52(12):356, 12 2016.
- [86] Vanamali Shastry, Enrico Trotti, and Francesco Giacosa. Constraints imposed by the partial wave amplitudes on the decays of $J=1, 2$ mesons. *Phys. Rev. D*, 105(5):054022, 2022.
- [87] Francesco Giacosa, Adrian Koenigstein, and Robert D. Pisarski. How the axial anomaly controls flavor mixing among mesons. *Phys. Rev. D*, 97(9):091901, 2018.
- [88] Dan Guo, Cheng-Qun Pang, Zhan-Wei Liu, and Xiang Liu. Study of unflavored light mesons with $J^{PC} = 2^{--}$. *Phys. Rev. D*, 99(5):056001, 2019.
- [89] L. M. Abreu, F. M. da Costa Júnior, and A. G. Favero. Revisiting the tensor

- $J^{PC} = 2^{--}$ meson spectrum. *Phys. Rev. D*, 101(11):116016, 2020.
- [90] Xue Chao Feng, Ke Wei Wei, Jie Wu, Xue Zhen Zhai, and ShiZhuo Wang. Towards the Assignments for 1^1D_2 and 1^3D_2 Meson Nonets. *Acta Phys. Polon. B*, 53(10):4, 2022.
- [91] A. Türkan, H. Dağ, J. Y. Süngü, and E. Veli Veliev. Hot medium effects on pseudoscalar $K_2(1820)$ meson. *EPJ Web Conf.*, 199:03007, 2019.
- [92] Stephen Godfrey and Nathan Isgur. Mesons in a relativized quark model with chromodynamics. *Phys. Rev. D*, 32:189–231, 1985.
- [93] Tianhong Wang, Zhi-Hui Wang, Yue Jiang, Libo Jiang, and Guo-Li Wang. Strong decays of $D_3^*(2760)$, $D_{s3}^*(2860)$, B_3^* , and B_{s3}^* . *Eur. Phys. J. C*, 77:38, 2017.
- [94] Tianhong Wang, Hui-Feng Fu, Yue Jiang, Qiang Li, and Guo-Li Wang. Annihilation rates of $^3D_2(2^{--})$ and $^3D_3(3^{--})$ heavy quarkonia. *Int. J. Mod. Phys. A*, 32(06n07):1750035, 2017.
- [95] Lars Bergstrom, Howard Grotch, and Richard W. Robinett. D -wave quarkonium production and annihilation decays: Formalism and applications. *Phys. Rev. D*, 43:2157–2160, 1991.
- [96] John P. Harnad. Lorentz poles in a particle exchange model. *Nucl. Phys. B*, 38(2):350–364, 1972.
- [97] Cheng-Qun Pang, Bo Wang, Xiang Liu, and Takayuki Matsuki. High-spin mesons below 3 GeV. *Phys. Rev. D*, 92(1):014012, 2015.
- [98] Francesco Caporale and Igor P. Ivanov. Production of spin-3 mesons in diffractive DIS. *Eur. Phys. J. C*, 44:505–514, 2005.
- [99] T. Barnes, N. Black, and P. R. Page. Strong decays of strange quarkonia. *Phys. Rev. D*, 68:054014, 2003.
- [100] Denis Parganlija and Francesco Giacosa. Excited Scalar and Pseudoscalar Mesons in the Extended Linear Sigma Model. *Eur. Phys. J. C*, 77(7):450, 2017.
- [101] Francesco Giacosa, Julia Sammet, and Stanislaus Janowski. Decays of the vector glueball. *Phys. Rev. D*, 95(11):114004, 2017.
- [102] Walaa I. Eshraim, Christian S. Fischer, Francesco Giacosa, and Denis Parganlija. Hybrid phenomenology in a chiral approach. *Eur. Phys. J. Plus*, 135(12):945, 2020.

- [103] Giulio Mezzadri. Light hadron spectroscopy at BESIII. *PoS*, 234:423, 2015. The European Physical Society Conference on High Energy Physics (EPS-HEP2015).
- [104] Simonetta Marcello. Hadron Physics from BESIII. *JPS Conf. Proc.*, 10:010009, 2016. Proceedings of the 10th International Workshop on the Physics of Excited Nucleons (NSTAR2015).
- [105] Alessandro Rizzo. The meson spectroscopy program with CLAS12 at Jefferson Laboratory. *PoS*, 253:8, 2016. The 8th International Workshop on Chiral Dynamics.
- [106] Dmitry Ryabchikov. Meson spectroscopy at VES and COMPASS. *EPJ Web Conf.*, 212:03010, 6 2019. The 12th International Workshop on $e^+ e^-$ Collisions from Phi to Psi (PhiPsi 2019).
- [107] Hussein Al Ghouli et al. First results from the GlueX experiment. *AIP Conf. Proc.*, 1735(1):020001, 2016.
- [108] Benny Zihlmann. GlueX a new facility to search for gluonic degrees of freedom in mesons. *AIP Conf. Proc.*, 1257(1):116–120, 2010.
- [109] Matthew Shepherd. GlueX at Jefferson Lab: a search for exotic states of matter in photon-proton collisions. *PoS*, 212:12, 2014. 52nd International Winter Meeting on Nuclear Physics.
- [110] Ivan B. Logashenko et al. CMD-3 Overview. *EPJ Web Conf.*, 218:02001, 2019.
- [111] Matthias F. M. Lutz et al. Physics Performance Report for PANDA: Strong Interaction Studies with Antiprotons. *arXiv*, 0903.3905, 2009.
- [112] Yoichiro Nambu and Giovanni Jona-Lasinio. Dynamical model of elementary particles based on an analogy with superconductivity. I. *Phys. Rev.*, 122:345–358, 1961.
- [113] Yoichiro Nambu and Giovanni Jona-Lasinio. Dynamical model of elementary particles based on an analogy with superconductivity. II. *Phys. Rev.*, 124:246–254, 1961.
- [114] Murray Gell-Mann. The Eightfold Way: A theory of strong interaction symmetry. *CTSL-20, TID-12608*, 1961.
- [115] Yuval Ne'eman. Derivation of strong interactions from a gauge invariance. *Nucl.*

- Phys.*, 26:222–229, 1961.
- [116] Walter Greiner and Berndt Müller. *Symmetries*. Springer-Verlag Berlin Heidelberg, 2 edition, 1994.
- [117] Alexander A. Migdal and Mikhail A. Shifman. Dilaton Effective Lagrangian in Gluodynamics. *Phys. Lett. B*, 114:445–449, 1982.
- [118] A. Salomone, J. Schechter, and T. Tudron. Properties of Scalar Gluonium. *Phys. Rev. D*, 23:1143, 1981.
- [119] Edward Witten. Baryons in the $1/N$ expansion. *Nucl. Phys. B*, 160(1):57–115, 1979.
- [120] Richard F. Lebed. Phenomenology of large N_c QCD. *Czech. J. Phys.*, 49:1273–1306, 1999.
- [121] Dietmar Ebert and Mikhail K. Volkov. Composite-meson model with vector dominance based on $U(2)$ invariant four-quark interactions. *Z. Phys. C*, 16:205, 1983.
- [122] Heath B. O’Connell, Bruce C. Pearce, Anthony W. Thomas, and Anthony G. Williams. $\rho - \omega$ mixing, vector meson dominance and the pion form-factor. *Prog. Part. Nucl. Phys.*, 39:201–252, 1997.
- [123] Jae K. Kim, Pyungwon Ko, Kang Y. Lee, and Serge Rudaz. $a_1(1260)$ contribution to photon and dilepton productions from hot hadronic matter reexamined. *Phys. Rev. D*, 53:4787–4792, 1996.
- [124] Michael E. Peskin and Daniel V. Schroeder. *An Introduction to quantum field theory*. Addison-Wesley, Reading, USA, 1995.
- [125] L. Kopke and N. Wermes. J/psi Decays. *Phys. Rept.*, 174:67, 1989.
- [126] Francesco Giacosa, Anna Okopińska, and Vanamali Shastry. A simple alternative to the relativistic Breit–Wigner distribution. *Eur. Phys. J. A*, 57(12):336, 2021.
- [127] Vincent Mathieu, Nikolai Kochelev, and Vicente Vento. The physics of glueballs. *Int. J. Mod. Phys. E*, 18(1):1–49, 2009.
- [128] Volker Crede and Curtis A. Meyer. The experimental status of glueballs. *Prog. Part. Nucl. Phys.*, 63(1):74–116, 2009.

- [129] Hua-Xing Chen, Wei Chen, Xiang Liu, Yan-Rui Liu, and Shi-Lin Zhu. An updated review of the new hadron states. 2022.
- [130] Ying Chen et al. Glueball spectrum and matrix elements on anisotropic lattices. *Phys. Rev. D*, 73:014516, 2006.
- [131] Colin J. Morningstar and Mike J. Peardon. The glueball spectrum from an anisotropic lattice study. *Phys. Rev. D*, 60:034509, 1999.
- [132] Harvey B. Meyer. Glueball Regge trajectories. Phd thesis, University of Oxford, 2004.
- [133] Keita Sakai and Shoichi Sasaki. Glueball spectroscopy in lattice QCD using gradient flow. *arXiv*, 2211.15176, 2022.
- [134] Feiyu Chen, Xiangyu Jiang, Ying Chen, Keh-Fei Liu, Wei Sun, and Yi-Bo Yang. Glueballs at Physical Pion Mass. *arXiv*, 2111.11929, 2021.
- [135] Claudio Bonanno, Massimo D’Elia, Biagio Lucini, and Davide Vadacchino. Towards glueball masses of large- N $SU(N)$ pure-gauge theories without topological freezing. *Phys. Lett. B*, 833:137281, 2022.
- [136] A. V. Sarantsev and E. Klempt. Scalar and tensor mesons in $d\bar{d}$, $s\bar{s}$ and $gg \rightarrow f_0, f_2$. *arXiv*, 2211.08791, 2022.
- [137] Eberhard Klempt. Glueballs, a fulfilled promise of QCD? *arXiv*, 2211.12901, 2022.
- [138] Stephan Narison. Masses, decays and mixings of gluonia in QCD. *Nucl. Phys. B*, 509:312–356, 1998.
- [139] Stephan Narison. QCD spectral sum rules 2022. In *12th High-Energy International Conference in Madagascar*, 2022.
- [140] Yidian Chen, Danning Li, and Mei Huang. The dynamical holographic QCD method for hadron physics and QCD matter. *Commun. Theor. Phys.*, 74(9):097201, 2022.
- [141] Frederic Brünner and Anton Rebhan. Nonchiral enhancement of scalar glueball decay in the Witten-Sakai-Sugimoto model. *Phys. Rev. Lett.*, 115(13):131601, 2015.
- [142] Richard C. Brower, Samir D. Mathur, and Chung-I Tan. Glueball spectrum for QCD from AdS supergravity duality. *Nucl. Phys. B*, 587:249–276, 2000.

- [143] Yidian Chen and Mei Huang. Two-gluon and trigluon glueballs from dynamical holography QCD. *Chin. Phys. C*, 40(12):123101, 2016.
- [144] Matteo Rinaldi and Vicente Vento. Glueballs at high temperature within the hard-wall holographic model. *Eur. Phys. J. C*, 82(2):140, 2022.
- [145] Matteo Rinaldi. Meson and glueball spectroscopy within the graviton soft-wall model. *Rev. Mex. Fis. Suppl.*, 3(3):0308019, 2022.
- [146] Daniel Elander, Maurizio Piai, and John Roughley. Holographic glueballs from the circle reduction of Romans supergravity. *JHEP*, 02:101, 2019.
- [147] Bing An Li. 2^{++} Glueball. *Phys. Rev. D*, 86:017501, 2012.
- [148] Stanislaus Janowski, Denis Parganlija, Francesco Giacosa, and Dirk H. Rischke. The Glueball in a Chiral Linear Sigma Model with Vector Mesons. *Phys. Rev. D*, 84:054007, 2011.
- [149] Alexey A. Petrov. Glueball molecules. *arXiv*, 2204.11269, 2022.
- [150] S. Okubo. ρ -meson and unitary symmetry model. *Physics Letters*, 5(2):165–168, 1963.
- [151] Jugoro Iizuka, Kunihiko Okada, and Okiyasu Shito. Systematics and phenomenology of boson mass levels. 3. *Prog. Theor. Phys.*, 35:1061–1073, 1966.
- [152] Walter Toki. Search for Glueballs. In *24th Annual SLAC Summer Institute on Particle Physics: The Strong Interaction, From Hadrons to Protons*, pages 141–169, 1996.
- [153] Francesco Giacosa. Heavy Glueballs: Status and Large- N_c Widths Estimate. *Acta Phys. Polon. Suppl.*, 10:1021–1027, 2017.
- [154] V. V. Anisovich. Systematization of tensor mesons and the determination of the 2^{++} glueball. *JETP Lett.*, 80:715–720, 2004.
- [155] V. V. Anisovich and A. V. Sarantsev. Observation of tensor glueball in the reactions $p \text{ anti-}p \rightarrow \pi \pi, \eta \eta, \eta \eta'$. *JETP Lett.*, 81:417–423, 2005.
- [156] Zao-Chen Ye, Xiao Wang, Xiang Liu, and Qiang Zhao. Mass spectrum and strong decays of isoscalar tensor mesons. *Phys. Rev. D*, 86:054025, Sep 2012.
- [157] Francesco Giacosa, Thomas Gutsche, Valery E. Lyubovitskij, and Amand Faessler.

- Scalar meson and glueball decays within a effective chiral approach. *Phys. Lett. B*, 622:277–285, 2005.
- [158] Florian Divotgey, Lisa Olbrich, and Francesco Giacosa. Phenomenology of axial-vector and pseudovector mesons: decays and mixing in the kaonic sector. *Eur. Phys. J. A*, 49:135, 10 2013.
- [159] Gerardus 't Hooft. A planar diagram theory for strong interactions. *Nucl. Phys. B*, 72(3):461–473, 1974.
- [160] Mitja Strohmeier-Presicek, Thomas Gutsche, Robert Vinh Mau, and Amand Faessler. Glueball-quarkonia content and decay of scalar-isoscalar mesons. *Phys. Rev. D*, 60:054010, 1999.
- [161] Weon-Jong Lee and Don Weingarten. Scalar quarkonium masses and mixing with the lightest scalar glueball. *Phys. Rev. D*, 61:014015, 1999.
- [162] Thomas Gutsche, Serguei Kuleshov, Valery E. Lyubovitskij, and Igor T. Obukhovskiy. Search for the glueball content of hadrons in γp interactions at GlueX. *Phys. Rev. D*, 94(3):034010, 2016.
- [163] John C. Collins, Anthony Duncan, and Satish D. Joglekar. Trace and dilatation anomalies in gauge theories. *Phys. Rev. D*, 16:438–449, 1977.
- [164] Walter Greiner, Stefan Schramm, and Eckart Stein. *Quantum Chromodynamics*. Springer-Verlag Berlin Heidelberg, 3 edition, 2007.
- [165] Francesco Giacosa and Giuseppe Pagliara. Spectral functions of scalar mesons. *Phys. Rev. C*, 76:065204, 2007.
- [166] Jonas Schneitzer, Thomas Wolkanowski, and Francesco Giacosa. The role of the next-to-leading order triangle-shaped diagram in two-body hadronic decays. *Nucl. Phys. B*, 888:287–299, 2014.
- [167] David Aston et al. Spin-parity determination of the $\phi_J(1850)$ from $K^- p$ interactions at 11 GeV/c. *Phys. Lett. B*, 208:324–330, 1988.
- [168] S. Al-Harran et al. Observation of a $K \bar{K}$ enhancement at 1.85 GeV in the reaction $K^- p \rightarrow K \bar{K} \Lambda$ at 8.25 GeV/c. *Phys. Lett. B*, 101:357–360, 1981.
- [169] Dmitry V. Amelin et al. Natural parity resonances in $\eta \pi^+ \pi^-$. *Nucl. Phys. A*, 668:83–96, 2000.

- [170] David Aston et al. The strange meson resonances observed in the reaction $K^- p \rightarrow \bar{K}^0 \pi^+ \pi^- n$ at 11 GeV/c. *Nucl. Phys. B*, 292:693–713, 1987.
- [171] Michel Baubillier et al. Evidence for the $B \pi$ decay mode of the $\omega(1670)$. *Phys. Lett. B*, 89(1):131–135, 1979.
- [172] Jose. Diaz et al. Evidence for the omega $\omega \pi \pi$ decay modes of the A_2 and $\omega(1675)$. *Phys. Rev. Lett.*, 32:260–264, 1974.
- [173] Charles Baltay, Victor C. Cautis, Daniel H. Cohen, Steven E. Csorna, Mohan Kalelkar, Daniel Pisello, William D. Smith, and Noel Yeh. Meson resonance production in $\pi^+ p$ interactions at 15 GeV/c. *Phys. Rev. D*, 17:62, 1978.
- [174] Joachim Bartsch et al. The g -meson. *Nucl. Phys. B*, 22(1):109–130, 9 1970.
- [175] G.K. Kliger et al. Investigation of a four π system in the $\rho'(1710)$ -meson mass region in the reaction $\pi^- \rho \rightarrow \rho \pi^+ \pi^- \pi^- \pi^0$ at 4.5 GeV/c. *Sov. J. Nucl. Phys.*, 19:428–432, 1974.
- [176] Graham Thompson et al. Study of the R Meson Produced in 13 GeV/c $\pi^+ p$ Interactions. *Nucl. Phys. B*, 69:220–236, 1974.
- [177] Eric B. Gregory, Alan C. Irving, Biagio Lucini, Craig C. McNeile, Antonio Rago, Chris Richards, and Enrico Rinaldi. Towards the glueball spectrum from unquenched lattice QCD. *JHEP*, 10:170, 2012.
- [178] Wolfgang Ochs. The status of glueballs. *J. Phys. G*, 40:043001, 2013.
- [179] Walaa I. Eshraim, Stanislaus Janowski, Francesco Giacosa, and Dirk H. Rischke. Decay of the pseudoscalar glueball into scalar and pseudoscalar mesons. *Phys. Rev. D*, 87(5):054036, 2013.
- [180] Claudia Ratti and Rene Bellwied. *The Deconfinement Transition of QCD; Theory Meets Experiment*. 2021.
- [181] Dirk H. Rischke. The Quark gluon plasma in equilibrium. *Prog. Part. Nucl. Phys.*, 52:197–296, 2004.
- [182] N. Brambilla et al. QCD and Strongly Coupled Gauge Theories: Challenges and Perspectives. *Eur. Phys. J. C*, 74(10):2981, 2014.
- [183] Szabolcs Borsanyi, Gergely Endrodi, Zoltan Fodor, Antal Jakovac, Sandor D. Katz, Stefan Krieg, Claudia Ratti, and Kalman K. Szabo. The QCD equation of

- state with dynamical quarks. *JHEP*, 11:077, 2010.
- [184] Szabocs Borsanyi, Zoltan Fodor, Christian Hoelbling, Sandor D. Katz, Stefan Krieg, and Kalman K. Szabo. Full result for the QCD equation of state with 2+1 flavors. *Phys. Lett. B*, 730:99–104, 2014.
- [185] F. Karsch and E. Laermann. Thermodynamics and in medium hadron properties from lattice QCD. *arXiv*, hep-lat/0305025.
- [186] David E. Miller. Lattice QCD Calculation for the Physical Equation of State. *Phys. Rept.*, 443:55–96, 2007.
- [187] Sayantan Sharma. QCD Thermodynamics on the Lattice. *Adv. High Energy Phys.*, 2013:452978, 2013.
- [188] A. Bazavov et al. Equation of state in (2+1)-flavor QCD. *Phys. Rev. D*, 90:094503, 2014.
- [189] Reinhard Alkofer, Axel Maas, Walid Ahmed Mian, Mario Mitter, Jordi París-López, Jan M. Pawłowski, and Nicolas Wink. Bound state properties from the functional renormalization group. *Phys. Rev. D*, 99(5):054029, 2019.
- [190] Wei-jie Fu. QCD at finite temperature and density within the fRG approach: an overview. *Commun. Theor. Phys.*, 74(9):097304, 2022.
- [191] Adrian Koenigstein, Martin J. Steil, Nicolas Wink, Eduardo Grossi, Jens Braun, Michael Buballa, and Dirk H. Rischke. Numerical fluid dynamics for FRG flow equations: Zero-dimensional QFTs as numerical test cases. I. The O(N) model. *Phys. Rev. D*, 106(6):065012, 2022.
- [192] Christian S. Fischer and Jens A. Mueller. Chiral and deconfinement transition from Dyson-Schwinger equations. *Phys. Rev. D*, 80:074029, 2009.
- [193] Jens A. Mueller, Christian S. Fischer, and Dominik Nickel. Quark spectral properties above T_c from Dyson-Schwinger equations. *Eur. Phys. J. C*, 70:1037–1049, 2010.
- [194] Jacopo Ghiglieri, Aleksi Kurkela, Michael Strickland, and Aleksi Vuorinen. Perturbative Thermal QCD: Formalism and Applications. *Phys. Rept.*, 880:1–73, 2020.
- [195] Peter Kovács, Zsolt Szép, and György Wolf. Existence of the critical endpoint

- in the vector meson extended linear sigma model. *Phys. Rev. D*, 93(11):114014, 2016.
- [196] Péter Kovács, Győző Kovács, and Francesco Giacosa. Fate of the critical endpoint at large N_c . *Phys. Rev. D*, 106(11):116016, 2022.
- [197] A. Andronic, P. Braun-Munzinger, and J. Stachel. Thermal hadron production in relativistic nuclear collisions: The Hadron mass spectrum, the horn, and the QCD phase transition. *Phys. Lett. B*, 673:142–145, 2009. [Erratum: *Phys.Lett.B* 678, 516 (2009)].
- [198] Jens O. Andersen, Lars E. Leganger, Michael Strickland, and Nan Su. The QCD trace anomaly. *Phys. Rev. D*, 84:087703, 2011.
- [199] A. Andronic, P. Braun-Munzinger, K. Redlich, and J. Stachel. The statistical model in Pb-Pb collisions at the LHC. *Nucl. Phys. A*, 904-905:535c–538c, 2013.
- [200] Anton Andronic, Peter Braun-Munzinger, Markus K. Köhler, Aleksas Mazeliauskas, Krzysztof Redlich, Johanna Stachel, and Vytautas Vislavicius. The multiple-charm hierarchy in the statistical hadronization model. *JHEP*, 07:035, 2021.
- [201] Paolo Alba, Wanda Alberico, Rene Bellwied, Marcus Bluhm, Valentina Mantovani Sarti, Marlene Nahrgang, and Claudia Ratti. Freeze-out conditions from net-proton and net-charge fluctuations at RHIC. *Phys. Lett. B*, 738:305–310, 2014.
- [202] Giorgio Torrieri, S. Steinke, Wojciech Broniowski, Wojciech Florkowski, Jean Letessier, and Johann Rafelski. SHARE: Statistical hadronization with resonances. *Comput. Phys. Commun.*, 167:229–251, 2005.
- [203] Y. Chen et al. Glueball spectrum and matrix elements on anisotropic lattices. *Phys. Rev. D*, 73:014516, 2006.
- [204] Jian-Xing Chen and Jun-Chen Su. Glueball spectrum based on a rigorous three-dimensional relativistic equation for two gluon bound states. II. Calculation of the glueball spectrum. *Phys. Rev. D*, 69:076003, 2004.
- [205] Wolfgang Ochs. The Status of Glueballs. *J. Phys. G*, 40:043001, 2013.
- [206] Vincent Mathieu, Nikolai Kochelev, and Vicente Vento. The Physics of Glueballs. *Int. J. Mod. Phys. E*, 18:1–49, 2009.

- [207] Stanislaus Janowski, Francesco Giacosa, and Dirk H. Rischke. Is $f_0(1710)$ a glueball? *Phys. Rev. D*, 90(11):114005, 2014.
- [208] Francesco Giacosa. Modelling glueballs. *EPJ Web of Conferences*, 130:01009, 2016.
- [209] István Szanyi, László Jenkovszky, Rainer Schicker, and Volodymyr Svintozelskyi. Pomeron/glueball and odderon/oddball trajectories. *Nucl. Phys. A*, 998:121728, 2020.
- [210] G. Boyd, J. Engels, F. Karsch, E. Laermann, C. Legeland, M. Lutgemeier, and B. Petersson. Thermodynamics of SU(3) lattice gauge theory. *Nucl. Phys. B*, 469:419–444, 1996.
- [211] Marco Panero. Thermodynamics of the QCD plasma and the large-N limit. *Phys. Rev. Lett.*, 103:232001, 2009.
- [212] Biagio Lucini and Marco Panero. SU(N) gauge theories at large N. *Phys. Rept.*, 526:93–163, 2013.
- [213] Michele Caselle, Luca Castagnini, Alessandra Feo, Ferdinando Gliozzi, and Marco Panero. Thermodynamics of SU(N) Yang-Mills theories in 2+1 dimensions I - The confining phase. *JHEP*, 06:142, 2011.
- [214] Michele Caselle, Alessandro Nada, and Marco Panero. Hagedorn spectrum and thermodynamics of SU(2) and SU(3) Yang-Mills theories. *JHEP*, 07:143, 2015. [Erratum: JHEP 11, 016 (2017)].
- [215] Paolo Alba, Wanda Maria Alberico, Alessandro Nada, Marco Panero, and Horst Stöcker. Excluded-volume effects for a hadron gas in Yang-Mills theory. *Phys. Rev. D*, 95(9):094511, 2017.
- [216] R. Hagedorn. Statistical thermodynamics of strong interactions at high-energies. *Nuovo Cim. Suppl.*, 3:147–186, 1965.
- [217] Harvey B. Meyer. High-Precision Thermodynamics and Hagedorn Density of States. *Phys. Rev. D*, 80:051502, 2009.
- [218] Gwendolyn Lacroix, Claude Semay, Daniel Cabrera, and Fabien Buisseret. Glueballs and the Yang-Mills plasma in a T -matrix approach. *Phys. Rev. D*, 87(5):054025, 2013.
- [219] Robert D. Pisarski. Finite-temperature qcd at large n . *Phys. Rev. D*, 29:1222–1227,

Mar 1984.

- [220] Kei-Ichi Kondo. Confinement–deconfinement phase transition and gauge-invariant gluonic mass in Yang-Mills theory. *arXiv*, 1508.02656, 2015.
- [221] Lin Zhang, Chutian Chen, Yidian Chen, and Mei Huang. Spectra of glueballs and oddballs and the equation of state from holographic QCD. *Phys. Rev. D*, 105(2):026020, 2022.
- [222] Valeriya Mykhaylova, Marcus Bluhm, Krzysztof Redlich, and Chihiro Sasaki. Quark-flavor dependence of the shear viscosity in a quasiparticle model. *Phys. Rev. D*, 100(3):034002, 2019.
- [223] Valeriya Mykhaylova and Chihiro Sasaki. Impact of quark quasiparticles on transport coefficients in hot QCD. *Phys. Rev. D*, 103(1):014007, 2021.
- [224] Francesco Giacosa. Dynamical generation and dynamical reconstruction. *Phys. Rev. D*, 80:074028, 2009.
- [225] Robert D. Pisarski. Fuzzy Bags and Wilson Lines. *Prog. Theor. Phys. Suppl.*, 168:276–284, 2007.
- [226] Peter Levai and Ulrich W. Heinz. Massive gluons and quarks and the equation of state obtained from SU(3) lattice QCD. *Phys. Rev. C*, 57:1879–1890, 1998.
- [227] A. Peshier, Burkhard Kampfer, O. P. Pavlenko, and G. Soff. A Massive quasiparticle model of the SU(3) gluon plasma. *Phys. Rev. D*, 54:2399–2402, 1996.
- [228] Francesco Giacosa. Analytical study of a gas of gluonic quasiparticles at high temperature: Effective mass, pressure and trace anomaly. *Phys. Rev. D*, 83:114002, 2011.
- [229] Jens Braun, Astrid Eichhorn, Holger Gies, and Jan M. Pawłowski. On the Nature of the Phase Transition in SU(N), Sp(2) and E(7) Yang-Mills theory. *Eur. Phys. J. C*, 70:689–702, 2010.
- [230] M. Gockeler, R. Horsley, A. C. Irving, D. Pleiter, P. E. L. Rakow, G. Schierholz, and H. Stuben. A Determination of the Lambda parameter from full lattice QCD. *Phys. Rev. D*, 73:014513, 2006.
- [231] Marco Guagnelli, Rainer Sommer, and Hartmut Wittig. Precision computation of a low-energy reference scale in quenched lattice QCD. *Nucl. Phys. B*, 535:389–402,

- 1998.
- [232] Rainer Sommer. Scale setting in lattice QCD. *PoS, LATTICE2013:015*, 2014.
- [233] Helios Sanchis-Alepuz, Christian S. Fischer, Christian Kellermann, and Lorenz von Smekal. Glueballs from the Bethe-Salpeter equation. *Phys. Rev. D*, 92:034001, 2015.
- [234] Gerard 't Hooft. A Two-Dimensional Model for Mesons. *Nucl. Phys. B*, 75:461–470, 1974.
- [235] Pere Masjuan, Enrique Ruiz Arriola, and Wojciech Broniowski. Systematics of radial and angular-momentum Regge trajectories of light non-strange $q\bar{q}$ states. *Phys. Rev. D*, 85:094006, 2012.
- [236] A. V. Anisovich, V. V. Anisovich, and A. V. Sarantsev. Systematics of q anti- q states in the (n, M^2) and (J, M^2) planes. *Phys. Rev. D*, 62:051502, 2000.
- [237] Hua-Xing Chen, Wei Chen, and Shi-Lin Zhu. Two- and three-gluon glueballs of $C=+$. *Phys. Rev. D*, 104(9):094050, 2021.
- [238] Andras Ster, Laszlo Jenkovszky, and Tamas Csorgo. Extracting the Odderon from pp and $\bar{p}p$ scattering data. *Phys. Rev. D*, 91(7):074018, 2015.
- [239] I. Szanyi and T. Csörgő. The ReBB model and its $H(x)$ scaling version at 8 TeV: Odderon exchange is a certainty. *Eur. Phys. J. C*, 82(9):827, 2022.
- [240] Roger Dashen, Shang-Keng Ma, and Herbert J. Bernstein. S Matrix formulation of statistical mechanics. *Phys. Rev.*, 187:345–370, 1969.
- [241] R. Venugopalan and M. Prakash. Thermal properties of interacting hadrons. *Nucl. Phys. A*, 546:718–760, 1992.
- [242] W. Weinhold, B. L. Friman, and W. Noerenberg. Thermodynamics of an interacting πN system. *Acta Phys. Polon. B*, 27:3249–3253, 1996.
- [243] W. Weinhold, B. Friman, and W. Norenberg. Thermodynamics of Delta resonances. *Phys. Lett. B*, 433:236–242, 1998.
- [244] Wojciech Broniowski, Wojciech Florkowski, and Brigitte Hiller. Thermal analysis of production of resonances in relativistic heavy ion collisions. *Phys. Rev. C*, 68:034911, 2003.

- [245] Wojciech Broniowski, Francesco Giacosa, and Viktor Begun. Cancellation of the σ meson in thermal models. *Phys. Rev. C*, 92(3):034905, 2015.
- [246] Pok Man Lo, Bengt Friman, Michal Marczenko, Krzysztof Redlich, and Chihiro Sasaki. Repulsive interactions and their effects on the thermodynamics of a hadron gas. *Phys. Rev. C*, 96(1):015207, 2017.
- [247] Pok Man Lo. S-matrix formulation of thermodynamics with N-body scatterings. *Eur. Phys. J. C*, 77(8):533, 2017.
- [248] Pok Man Lo, Bengt Friman, Krzysztof Redlich, and Chihiro Sasaki. S-matrix analysis of the baryon electric charge correlation. *Phys. Lett. B*, 778:454–458, 2018.
- [249] Ashutosh Dash, Subhasis Samanta, and Bedangadas Mohanty. Interacting hadron resonance gas model in the K -matrix formalism. *Phys. Rev. C*, 97(5):055208, 2018.
- [250] Ashutosh Dash, Subhasis Samanta, and Bedangadas Mohanty. Thermodynamics of a gas of hadrons with attractive and repulsive interactions within an S -matrix formalism. *Phys. Rev. C*, 99(4):044919, 2019.
- [251] Pok Man Lo and Francesco Giacosa. Thermal contribution of unstable states. *Eur. Phys. J. C*, 79(4):336, 2019.
- [252] Subhasis Samanta and Francesco Giacosa. QFT treatment of a bound state in a thermal gas. *Phys. Rev. D*, 102:116023, 2020.
- [253] Subhasis Samanta and Francesco Giacosa. Role of bound states and resonances in scalar QFT at nonzero temperature. *Phys. Rev. D*, 107(3):036001, 2023.
- [254] Francesco Giacosa, Alessandro Pilloni, and Enrico Trotti. Glueball–glueball scattering and the glueballonium. *Eur. Phys. J. C*, 82(5):487, 2022.
- [255] Enrico Trotti and Francesco Giacosa. On the mass of the glueballonium. *Rev. Mex. Fis. Suppl.*, 3(3):0308014, 2022.
- [256] Vanamali Shastry and Francesco Giacosa. Higgs-Higgs scattering and the (non-)existence of the Higgsonium. *arXiv*, 2212.01272, 2022.
- [257] Enrico Trotti. Emergence of ghost in once-subtracted on-shell unitarization in glueball-glueball scattering. *EPJ Web Conf.*, 274:03005, 2022.
- [258] Pablo G. Ortega, David R. Entem, Francisco Fernandez, and Enrique Ruiz Ar-

- riola. Counting states and the Hadron Resonance Gas: Does X(3872) count? *Phys. Lett. B*, 781:678–683, 2018.
- [259] J. L. Petersen. Meson-meson scattering. *Phys. Rept.*, 2:155–252, 1971.
- [260] Pok Man Lo. Thermal study of a coupled-channel system: a brief review. *Eur. Phys. J. A*, 57(2):60, 2021.

List of figures

1.1	List of conventional mesons with $2 \leq J \leq 3$	7
1.2	List of spin-2 resonances with a mass above 1.9 GeV.	7
1.3	Ground-state light mesons with $2 \leq J \leq 3$	9
2.1	Mexican hat potential with minima along the chiral circle (left) and the explicit breaking of the chiral symmetry (right).	18
3.1	χ^2 dependence on Λ for $g_2^{\text{ten}} = 0$	45
3.2	Comparison of the eLSM results to PDG [27].	57
4.1	Decay ratios for different values of tensor glueball mass.	64
5.1	Model results compared to PDG [27].	101
5.2	Model results compared to LQCD [28].	101
6.1	Comparison of the pressure (continuous limit) calculated in Ref. [30] to the GRG pressures for three different sets of lattice masses [29, 132, 203].	108
6.2	Comparison of the trace anomaly (continuous limit) calculated in Ref. [30] to the GRG trace anomalies for three different sets of lattice masses [29, 132, 203].	109
6.3	Comparison of the entropy (continuous limit) calculated in Ref. [30] to the GRG entropies for three different sets of lattice masses [29, 132, 203].	110
6.4	The effect of the radially excited glueball states up to $n = 10$ within GRG on the pressure (left) and trace anomaly (right).	111

- 6.5 The GRG pressure depending on the negative and positive charge conjugation of the glueball spectrum compared to Ref. [30]. 112
- 6.6 Contributions of three different waves to the pressure from scalar-scalar glueball interactions. 115
- 6.7 Contributions of three different waves to the pressure from tensor-tensor glueball interactions. 117

List of tables

1.1	Quantum numbers for the light (anti-)quarks.	4
1.2	List of conventional $q\bar{q}$ mesons following the quark model review of Ref. [27] up to $J = 3$ and for the lowest radial excitation ($n=1$). Bold entries with question marks have not been assigned to known resonances yet.	6
2.1	Mesonic nonets under P, C and $U_V(3)$ transformations.	28
3.1	Chiral nonets under P, C , and $U_L(3) \times U_R(3)$ transformations.	31
3.2	Fit results for the parameters of the basic version of the eLSM. They will be used in this and the next chapter (see for details in Ref. [19]). Note, these values are one specific solution of the fit. For instance, in the case of $Z_{\pi'}$, an uncertainty of about 20% was estimated.	34
3.3	Amplitude squares for the decay of spin-2 resonances.	37
3.4	Fit results to known experimental data of PDG fixes the parameters of the eLSM associated with the (axial-)tensor mesons (the details are given in the upcoming section). It should be noted that the suffix "lat" in $g_{2\text{lat}}^{\text{ten}}$ denotes that the data has been obtained through comparison to lattice reports in [31].	39
3.5	Masses of the spin-2 mesons within eLSM where the small mixing angle in the tensor sector and no mixing in the axial-tensor are considered. The PDG values are shown as bold numbers.	41
3.6	Clebsch-Gordan coefficients for $T \rightarrow P^{(1)} + P^{(2)}$	43
3.7	Decay rates for $T \rightarrow P^{(1)} + P^{(2)}$ compared to PDG [27].	44

3.8	Clebsch-Gordan coefficients and corresponding decay rates for $T \rightarrow P + V$ compared to PDG [27].	46
3.9	Clebsch-Gordan coefficients and corresponding decay rates for $T \rightarrow \gamma + P$ compared to PDG [27].	47
3.10	Clebsch-Gordan coefficients and corresponding decay rates for $T \rightarrow \gamma\gamma$ compared to PDG [27].	48
3.11	Clebsch-Gordan coefficients for $T \rightarrow \gamma + V_1$	49
3.12	Radiative decay rates for $T \rightarrow \gamma + V_1$	50
3.13	Decay rates for $A_2 \rightarrow V_1 + P$ compared to LQCD results [28].	53
3.14	Clebsch-Gordan coefficients and corresponding decay rates for $A_2 \rightarrow V_1 + P$	54
3.15	Clebsch-Gordan coefficients and corresponding decay rates for $A_2 \rightarrow A_1 + P$. We recall that $c^{\text{ten}} := c_1^{\text{ten}} + c_2^{\text{ten}}$ and $c'^{\text{ten}} := c_1^{\text{ten}} - c_2^{\text{ten}}$	55
3.16	Clebsch-Gordan coefficients and corresponding decay rates for $A_2 \rightarrow T + P$	56
4.1	Spin 2 resonances with masses around 2 GeV in PDG [27].	60
4.2	Clebsch-Gordan coefficients for the decays of G_2	63
4.3	Decay ratios of G_2 w.r.t. $\pi\pi$	64
4.4	Decay ratios for the tensor-pseudoscalar pair compared to PDG [27].	65
4.5	Results for the $f_2(1910)$ mass.	65
4.6	Results for the $f_2(1950)$ mass.	65
4.7	Results for the $f_2(2150)$ mass.	65
4.8	Results for the $f_2(2300)$ and $f_2(2340)$ masses.	65
4.9	Two pseudoscalar decay estimations of the tensor glueball.	68
4.10	Status of spin-2 resonances within eLSM-based analyses.	70
5.1	Interaction Lagrangians describing the decay of spin-3 mesons.	74

5.2	Amplitude squares for the decay of spin-3 resonances.	75
5.3	Total decay widths and masses of $J^{PC} = 3^{--}$ mesons [27].	79
5.4	Clebsch-Gordan coefficients and corresponding decay rates for $W_3 \rightarrow P^{(1)} + P^{(1)}$ compared to PDG [27].	81
5.5	Clebsch-Gordan coefficients and corresponding decay rates for $W_3 \rightarrow V + P$ compared to PDG [27].	82
5.6	Decay rates for $W_3 \rightarrow V_1 + P$ compared to LQCD [28].	83
5.7	Clebsch-Gordan coefficients and corresponding decay rates for $W_3 \rightarrow \gamma + P$	85
5.8	Clebsch-Gordan coefficients and corresponding decay rates for $W_3 \rightarrow T + P$ compared to PDG [27].	87
5.9	Clebsch-Gordan coefficients and corresponding decay rates for $W_3 \rightarrow B_1 + P$ by using the mixing angle $\beta_{b_1} = 0$ and $\beta_{b_1} = -40^\circ$, respectively. No experimental data is given for this channel in PDG [27] apart from the “possibly seen” decay channel of $\omega_3(1670) \rightarrow b_1(1235) \pi$	88
5.10	Clebsch-Gordan coefficients and corresponding decay ratios for $W_3 \rightarrow A_1 + P$ w.r.t. $\rho_3(1690) \rightarrow a_1(1260) \pi$ decay mode.	90
5.11	Estimates of the upper limits for two-vector decay channels.	91
5.12	Decay ratios for $W_3 \rightarrow V_1^{(1)} + V_1^{(2)}$ w.r.t. $\rho_3(1690) \rightarrow \rho \rho$ decay mode.	91
5.13	Parameters of Lagrangians in Table 5.1.	93
5.14	Interaction Lagrangians for the hypothetical glueball state $G_3(4200)$	94
5.15	Decay ratios of $G_3(4200)$ w.r.t. $\rho \pi$	95
5.16	Decay ratios of $G_3(4200)$ w.r.t. $G_3(4200) \rightarrow \rho \pi$	96
5.17	Decay ratios of $G_3(4200)$ w.r.t. $G_3(4200) \rightarrow \rho a_1$	97
5.18	Decay ratios of $G_3(4200)$ w.r.t. $G_3(4200) \rightarrow b_1 \pi$	98
5.19	Decay ratios of $G_3(4200)$ w.r.t. $G_3(4200) \rightarrow b_1 a_1$	99
5.20	Clebsch-Gordan coefficients κ_i for the decay channels of $G_3(4200)$	100

6.1	The LQCD parameters that have been used to get the glueball mass spectrum.	106
6.2	The list of the glueball masses in Refs. [29, 132, 203].	107
6.3	Fit summary obtained from Eq. (6.9) by assuming Eq. (6.8).	111